UNIVERSITÀ DI PARMA

UNIVERSITA' DEGLI STUDI DI PARMA

DOTTORATO DI RICERCA IN
"*Scienza e Tecnologia dei Materiali*"

CICLO XXXIII

OECT-based *in-vivo* monitoring for plant science and smart agriculture

Coordinatore:
Chiar.mo Prof. Enrico Dalcanale

Tutori:
Dr. Michela Janni
Dr. Andrea Zappettini

Dottorando: Filippo Vurro

Anni Accademici 2017/2018 – 2019/2020

Acknowledgements

First of all, I would like to thank ALSIA-Agrobios Metapontum for the financial support, especially, giving me the opportunity to get an insight into a real frontier context. A special mention goes to Francesco Cellini, Angelo Petrozza, Filomena Carriero, Nunzio Briglia and Angelo Mossuto for introducing me in a "green world" making me feel at home.

I would like to express my grateful thanks to my research group: my supervisors Michela Janni and Andrea Zappettini, who have show great faith in my qualities stimulating me to do better and better and teaching me the scientific rigour, as well as for having supported me after some fall. A sincere and heartfelt thanks goes to Michela Janni for her help in writing this thesis work.

A special thanks goes to Manuele Bettelli whose patience, versatility and competence made me a better researcher and as a person. I would also like to thank my Ph.D. "buddies" Nicola Sarzi Amadé and Riccardo Manfredi. I am genuinely happy that I met people with whome I shared experiences, concerns, uncertainties and ideas.

Thanks also to the rest of the old "SIGNAL" group, with a special mention for Nicola Coppedè and Marco Villani for productive scientific debates and the inevitable "philosophical break".

Moreover, I would like to thank all research group and companies who helped me in my research activity including Professor Nelson Marmiroli of University of Parma, Professor Luigi Manfrini of University of Bologna, the Canale Emiliano Romagnolo (CER) and all participants in the PORFESR POSITIVE project.

The list is indeed long but a special mention goes to: Michele Croci, Giorgio Impollonia, Alessandra Fracasso and Giulia Antonucci of the Professor Amaducci's group of Catholic University in Piacenza; Sandro Cornali of the Podere Stuard in Parma for his valuable help in 2018 and 2019 open field trial; Ugo Peruch and Franco Dameno of Mutti S.p.A. for being the first to believe in the Bioristor giving us the opportunity to try it in open field; Claudio Lucchi of Apofruit and the Severi Farm for the opportunity to test our sensor on a kiwi plantation.

Finally, thanks to my parents, Vincenzo, Veronica and all the special people in my life for their whole hearted support.

Parma,

December 31, 2020 Filippo Vurro

Summary

Motivation & Outline

Agriculture has accompanied humanity since the beginning of its civilization by stimulating enormous social and technological changes, and water use has been a fundamental factor in this symbiotic path[1].

In fact, the history of humanity could be described through its epic relationship with water and agriculture. Man's life has always been inextricably linked to the presence of water resources. The greatest civilizations of the past have flourished along the rivers: the Nile in Egypt (3000 BC), the Yellow River in China (3000 BC), the Tigris-Euphrates in Mesopotamia (2400 BC) and the Indus in northern India (2500 BC). Civilizations fell when water resources were lacking or were poorly administered. Still today, the quality of life of every person depends on this precious resource[1,2].

Climate change has been dominating the global agenda for the last few years. Greenhouse gas emissions are showing no signs of falling, in spite of the fact they must meet the goals of the Paris Agreement and the 2030 Agenda for Sustainable Development. The world is in danger of missing the target of limiting global warming to 1.5 °C this century, set out in the Paris Agreement. FAO's State of the World's Biodiversity for Food and Agriculture and the report from the world's top biodiversity body, IPBES, laid out how climate change will accelerate the loss of the ecosystems and biodiversity that provide foundations for human existence, including food production[3]. With these premises, the most important challenge that humanity is facing today is climate change with all its consequences. Among these, the most dramatic is the scarcity of water resources with a strong impact on agricultural production up to 83% of the yield loss. It should be underlined that 70% of all water withdrawals are employed in agriculture[4] and global demand for water could increase by 50% by 2030[5]: as an indication of the intensive use of water, consider that 180 liters of water are needed to produce 1 kg of tomatoes[6]. Moreover, the exponential increase in the world population of the recent decades, together with the impact of climate change, poses a serious threat to food security since the demand for food is increasing and will further increase in the coming years, while at the same time the arable land will decrease. Starting from 1980 until 2000, the total global population grew from 4.4 billion to 6.1 billion, with a 50% increase in the world food production[5]. Since 2000, the world population has increased by about 2% each year, reaching a total of 7.3 billion in 2014[7]. It is estimated that the world population should reach 9.7 billion[8] by 2050 and this will have a significant impact on the environment, which in turn will affects food production capacity through changes in arable land availability.

For all these reasons, the focus of the recent years is reducing water consumption, without decreasing yield and the quality of crops by means of something that accompanies man symbiotically since the dawn of civilization: technology.

In the last few years, scientists have been involved in thinking, developing and engineering devices to monitor crop health status indirectly and directly. These included: proximal sensors that measure soil humidity, temperature, and air humidity; remote sensors, in particular image sensors integrated on drones and satellites[9–12].

In this frame, a new sensor called Bioristor has been developed in the laboratories of the CNR-IMEM, able to collect biophysical and biochemical information from the inside of the plant *in-vivo*, in real-time and continuously. The Bioristor is a textile - Organic Electrochemical Transistor (tex-OECT), belonging to the class of electrolyte-gated transistors, whose organic semiconductor channel and gate are immersed into an electrolyte. The main advantages of the OECT are the high local amplification, the low voltage operation, the easiness of manufacture, and its excellent biocompatibility [13,14]. The OECT has lent itself to a wide range of promising applications, ranging from the recording of neural activity of organs to the detection of ions, analytes and metabolites[15].

In light of these considerations, the overall goal of this work was to exploit the Bioristor to monitor the physiological changes that occur in the plant following abiotic stress and environmental changes both in controlled conditions and in the open field. Moreover, since plant performance can be strongly improved by agriculture practices, the effect on plants of biostimulants as enhancer for the plant defence response was monitored.

The thesis is organized as follows: in **Chapter 1** the theoretical background regarding the main issues of PEDOT:PSS and OECTs is presented. The second part of Chapter 1 describes Bioristor state of the art, as well as basic guidance on plant response to abiotic stress. In **Chapter 2** the materials and methods of Bioristor preparation as well as the settings of the measurements of each experiment are described. **Chapter 3** presents the application of Bioristor in the study of water stress in a controlled environment on different types of plants, and the comparison of these results with the data simultaneously registering from the Italian phenotyping platform in ALISA-Metapontum. The second part of the chapter focuses on the promising use of Bioristor to study the effect of biostimulants on plants under water stress and as a tool to select varieties of mutant plants resistant to water deprivation. With a different approach but with the same objective as the previous chapters, **Chapter 4** is dedicated to exploring the response of Bioristor in plants under changes of environmental Vapor Pressure Deficit (VPD), in greenhouse to increase water use efficiency. Following the excellent results obtained in a controlled environment, **Chapter 5** is focused on the application of Bioristor on

tomato and kiwi plants in open fields subjected to different irrigation regimes during the harvest seasons of 2018, 2019 and 2020. This step was mandatory to ground validating Bioristor as tool for precision agriculture, managing the hydric resources in a sustainable way. Finally, **Chapter 6** reported the application of Bioristor in saline soil condition as strictly related to water scarcity and use efficiency.

Chapter 1

Introduction

This chapter is dedicated to give the basis of bioelectronic sensors, involving the general concept and the state-of-the-art technologies. Organic electrochemical transistor (OECT) will be the main focus of this thesis and will be discussed in more details. The second part of the chapter focuses on an accurate description of the Bioristor, and on a short introduction in essential physiological response of plants to abiotic stresses.

1.1 Bioelectronics

Bioelectronics is a rapidly growing interdisciplinary field in which organic electronics interfaces with the living world, both animal and vegetable, in order to i)study biochemical and biophysical mechanisms directly inside the organism in real time thanks to the use of biocompatible materials[16]; ii) interact directly with biological systems and regulate their physiological mechanisms[17].

However, bioelectronics is strongly limited by materials used, as it enables these two fields, that seem apparently distant, to interact. In particular, devices based[18] on conventional materials, such as metals or metal oxides, can show low compatibility towards biological systems. It should be considered that the classical electronics is based on electrons as dominant charge carriers, which rarely happens in biology as ions and small molecules are exploited much more frequently in inter- and intra-cellular communications[18].

The polymers can strongly affect direct interfacing with biological materials; in addition, the similarity between structural and functional properties, such as the "soft" nature of conductive polymers, ideally mimics the biological tissues[19]. In fact, several types of standard cell viability tests were carried out to assess the biocompatibility of conjugated polymers for biological applications[20] , showing that materials such as poly(3,4-ethyldiphenoxythiophene) (PEDOT), doped with

poly(styrene sulfonic acid) (PSS), were extremely suitable and efficient in operating in biological environments[19].

Due to the electronic and ionic mixed conductivity of conductive polymers, these materials provide highly efficient signal transduction and amplification between the device and the biological environment. The growing updates in organic electronics offered new and improved electro-active characteristics compared to inorganic oxides. In particular, the organic oxide-free interface, together with the efficiency of ionic transport between the biological environment and the entire volume of organic film, allowed the development of powerful biosensors to pacemakers, neural implants and biomedical or precision agricultural devices[21,22].

As a result the development of low-cost and easy to use devices as fabrication and fine-tuning electrodes, organic field effect transistors (OFETs) and electrolyte-gated field-effect transistors (EGOFETs), organic electronic ion pumps (OEIPs), ionic diodes and circuits have shortened the gap between electronics and biology.

One of the most promising devices emerging from this field is the organic electrochemical transistor (OECT) based on the conductive polymer PEDOT:PSS. This device will be accurately described in the next two sections[15].

1.2 Conductive Polymers

The invention of conductive polymers dates to 1977 when Shirikawa, Heeger and Macdiarmid discovered that it was possible to dope polyacetylene (Figure 2) with arsenic pentafluoride (Asf5) to obtain an organic material with a conductivity value comparable to the metal semiconductor. The basic skeleton of a conducting polymer is a carbon chain consisting of conjugated double bonds in which each carbon atom is hybridized sp2. Three of the electrons in the carbon's sp2 hybrid orbital will form three σ bonds, while the remaining electrons in the p_z orbitals will form a π bond, which permits the electrons relocation along the polymer spine.

Because of their properties, semiconductors are conventionally described as materials with intermediate characteristics between conductors and insulators[23]. As shown in Figure 1, the gap energy in the insulators is relatively high preventing electrons from passing from the valence band to the conduction band, hence leading to a lack of conductibility in this type of materials.

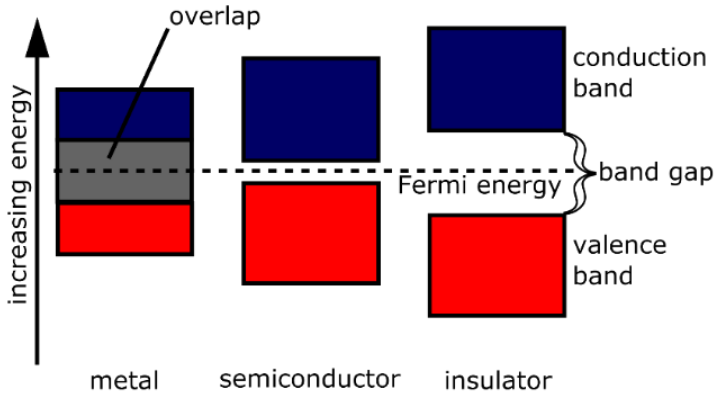

Figure 1: Energy gap in conductor, semiconductor and insulator[24]

In contrast, in metals the conduction and valence bands are superimposed. This allows the electrons to pass freely between the two bands, causing the material to lead. The peculiarity of semiconductor materials is the lack of the two overlapping bands, that are separated by a gap although smaller than that of insulators. The smaller width of the gap band allows that, at temperatures which are higher than 0 K, some electrons can still pass from the valence band to the conduction one, leaving in the first of the gaps. Electrons in the conduction band and gaps in the valence band are responsible for the conductivity of the material.

The conductivity of neutral conjugated polymers is closer to insulators than to semiconductors. To increase the conductivity polymers doping is essential and, unlike metal semiconductors, it must affect a greater fraction of the material. In the doping of crystalline semiconductors (ex. silicon and germanium) the doping atom replaces an atom of the crystalline lattice, establishing with the surrounding atoms a covalent bond. On the contrary, in conjugated polymers, the interaction between the polymer chain leads to an ionic bond. In addition, polymer doping may be caused either by the oxidation of the polymer chain due to the substitution of electrons by the π system (p-type); or to the reduction of the π system leading to negatively charged units in the conjugated system (n-type).

The most used methods for doping conjugated polymers are:

- ***Chemical doping*** It occurs through redox reactions between the polymer to be doped and the doping species, in case of oxidation doping it is type p, in case of reduction it is type n. This doping, however, leads to the formation of a non-homogeneous material.

- ***Electrochemical doping.*** An electrode is polarized to produce an ion flow from the polymer to dope that tends to maintain neutrality in the polymer itself. The difference in potential applied to the electrode determines the level of doping.
- ***Photodoping*** The polymer is oxidized and reduced by photo-absorption and consequent separation of charges, to produce electron-gap pairs and thus free carriers.
- ***Charge injection*** Electrons and gaps are injected through a metal contact, resulting in a state of oxidation or reduction of the polymer. It does not need any counter-ion, unlike chemical or electrochemical drugs.

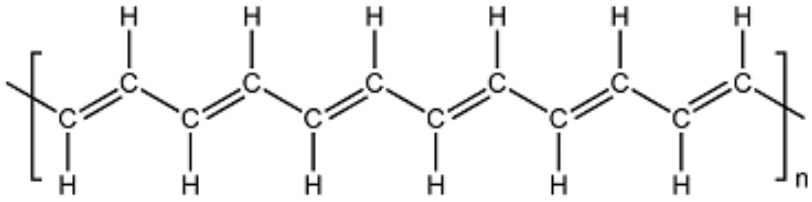

Figure 2: Chemical structure of polyacetylene

More precisely, its conductivity could vary from 103 S/m to 1011 S/m, which means that the polymer was able to assume, based on the treatment used, the conductivity of an insulator, a semiconductor, or a metal.

These studies lead to the development of the so-called "synthetic metals" called intrinsically conductive polymers (ICPs), as well as the attribution of the Nobel prize for chemistry to the three scientists in 2000. Since the 80s, the excellent processing properties, lightness, and versatility in addition to the electronic ones described, have led to an in-depth study of ICPs, including polyparafenilene (PPP), polyparafenilensulfide (PPS), polyparafenilenvinilene (PPV), polyaniline (PANI), polypyrrole (Ppy), polyethylene (PT), polyisotianafene (PITN) and polyethylenenediossitiophene (PEDOT).

1.3 PEDOT:PSS

One of the most studied and characterized conjugated polymers is the p-doped poly(3,4-ethylenedioxythiophene) (PEDOT)[25].

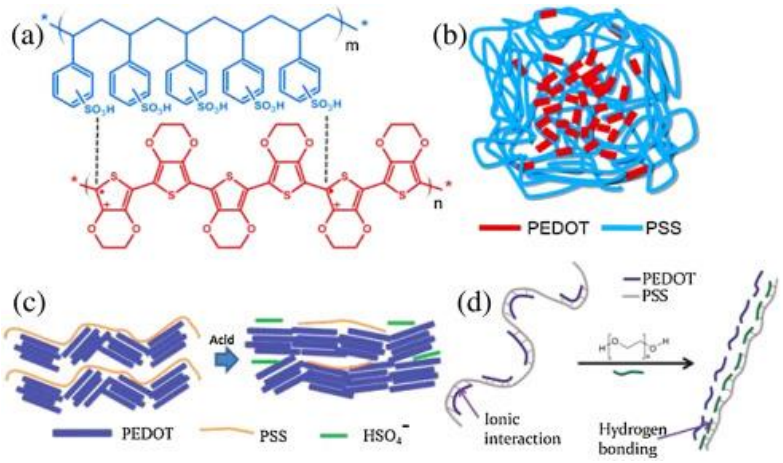

Figure 3[26]: Chemical structure of PEDOT:PSS (a); Molecular arrangement of pristine (b), Acid-treated (c) and PEG-treated (d) PEDOT:PSS[27–29]

Main properties that distinguish this ICP and make it one of the most used to date are[30–32].

- ***High conductivity***. PEDOT is characterized by a band gap of about 1.5 1.6 eV that can fall below the eV if subjected to doping. This results in a high electrical conductivity of about 550 S/cm.
- ***Reversibility of the drug state***. PEDOT can return to the initial state after undergoing a drug and be drugged again. In addition, the PEDOT, normally dark blue and opaque, if doped becomes light blue and transparent: it is this change of color and opacity to make it exploitable in some optical devices.
- ***Regularity of the structure***. Being composed of chains of reduced length of the alcoholic group, the PEDOT has in the space a regular structure.
- ***Stability***.PEDOT has excellent thermal and chemical stability and its electrical conductivity properties seem to remain almost unchanged over time.
- ***Electrochemical stability***. Electrochemically synthesized PEDOT films present not only low reduction and oxidation potentials, but also excellent stability in their doped state.

Some properties, as for example conductivity, can be implemented depending on the dopant used. Traditionally, a water-dispersible polyelectrolyte poly(styrene sulfonic acid) (PSS) is the most used dopant in increasing conductivity (1 - 100 S/cm) and, at the same time, in overcoming the insolubility problems of PEDOT[25,31]. The PSS is a polyanion which compensates the gaps in the PEDOT backbone with its negative charges.

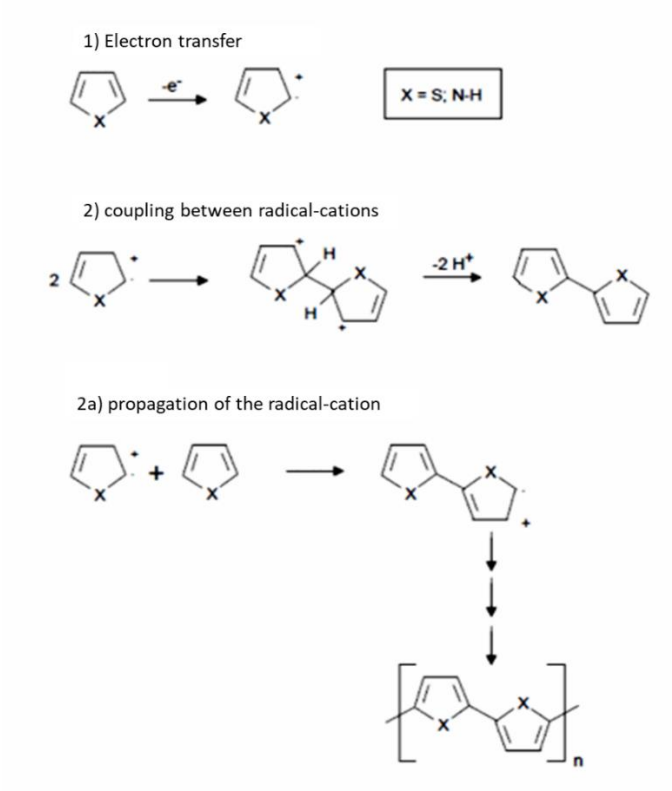

Figure 4: PEDOT polymerization mechanisms[33]

Other properties related to the use of PSS worth to be mentioned are:

- transparency,
- good film forming,
- wide commercial availability.

PEDOT:PSS can be prepared with standard chemical or electrochemical polymerization (Figure 4). During electrochemical polymerization, in a three-electrode electrochemical cell, the metal electrode oxidizes the monomer solution of 3,4-ethylenedioxythiophene (EDOT) in presence of sodium salt PSS. The resulting cations will combine into chains that eventually fall on the electrode. In the chemical approach, the oxidation of EDOT monomers is carried by oxidizing agents such as iron (III) chloride or nitride and peroxodisulfates. In both methodologies, the PSS is the key factor to stabilise the process and solvate the PEDOT. An excess of PSS is also required to form shells around the highly conductive PEDOT:PSS particles and prevent aggregation.

PEDOT characteristics and its degree of doping can also be regulated through the variation of some additional components, which perform different functions in the mixture. Ethylene glycol (EG) was used to increase conduction of PEDOT and a surfactant like dodecylbenzenesulfonic acid (DBSA) to change the viscosity of the polymer mixture and improve substrate adhesion[34].

Main deposition techniques of PEDOT:PSS are here described[35]. Different deposition methods can be identified: the coating technique and the printing technique. The coating technique consists in covering all the available surface of the substrate, while in the printing techniques a solution (called ink) is printed on the substrate. Considering as selection criteria the viscosity of the solution used, the shape, the homogeneity and the adhesion of the substrate, the waste of solution and the speed of the process, the best deposition technique to employ can be determined.

- ***Drop casting:*** is the simplest deposition method. It consists in depositing a drop of solution on a substrate, and wait for the evaporation of the solvent, which leaves a thin solid polymer film. It is a very fast and chip method but has the defect of producing uneven substrates.
- ***Spin coating:*** a quantity of liquid ink is deposited on the substrate that is sufficient to cover it all, then the spin coater specifies the angular velocity and acceleration chosen for spinning. Based on these parameters the thickness of the film on the substrate is adjusted, which remains within 100μm, and can be calculated with a relation of the type: $d = k\omega\alpha$, in which ω is the angular velocity of spinning, k and α are constants that depend on the solvent and the substrate chosen. By spin coating a homogeneous film over large areas (even up to about 30 cm^2) and highly reproducible is obtained. In fact, its main characteristics are determined by the parameters chosen for spinning and the type of solution used, rather than the amount of ink initially deposited. Because of the working principle of this technique, a certain amount of solution will be certainly wasted. However, this does not cause problems, at least in a laboratory, since the process requires a small amount of ink.
- ***Ink-jet printing:*** the use of this technique prevents the waste of solution, at the cost, however, of putting appropriate measures during its preparation. In fact, the ink-jet printing consists in the injection of ink onto the substrate accelerating the solution droplets through an electric field. In order to accelerate them, they must be electrically charged, whereas to form them, a needle is used, and the solution is heated. The solution must therefore dispose of a high surface tension and a low viscosity.
- ***Electro-deposition***: unlike the first two techniques described, electrodeposition has a different nature. *In situ*, that is directly on a conductive substrate, EDOT is polymerized with doping

PSS. This method takes place in an aqueous electrolytic solution, containing EDOT and PSS in right quantities. The deposition takes place by applying a potential difference of a few volts, constant or variable, between two electrodes: one that makes the substrate and the other, the counter electrode, which polarizes the solution. However the electrodeposition requires that the layer on which the PEDOT:PSS is deposited is conductive. One solution is therefore able to perform electro-deposition on a layer of PEDOT:PSS already deposited by means of other techniques.

1.4 Organic Electrochemical Transistor

Organic electrochemical transistors (OECTs) belong to the class of electrode-gated transistors (EGTs)[32] with electrode-gated organic field effect transistors (EGOFETs). Due to their nature all ECD are suitable to be used in aqueous environment, allowing to exploit their potential even in biological environment[32]. In the OECTs, the main difference to the EGOFETs is that the ions are injected from the electrolyte into the conducting polymer, modifying its doping state, and thereby its bulk conductivity[32]. This latter feature allows OECTs to generate large amplifications, while working with potential differences of less than 1 volt.

In recent years, OECTs have aroused considerable interest. The characteristics that make these devices interesting technology in the scientific research and for sensory applications are:

- low costs of production;
- ease of use;
- possibility of miniaturization;
- low voltage operation;
- selectivity towards ions and molecules through functionalization;
- high sensitivity with high trans-conductance ratio.

Among the different applications of this kind of sensors, their use in the biomedical and agricultural field is particularly interesting, for analysis of biological matrices such as saliva, sweat, plasma and sap[36–39].

A scheme of an Organic Electro Chemical Transistor (OECT) is shown in Figure 5. It is a device composed of three terminals namely source, drain and gate. The source and drain terminals are connected by a layer of organic conductive material called channel. The gate, on which the third terminal is placed, can be formed by another layer of organic conductive material or by a metal electrode. The essential and integral part of the transistor is the electrolyte (solid, liquid or gel), which contacts the channel and the gate, otherwise separated.

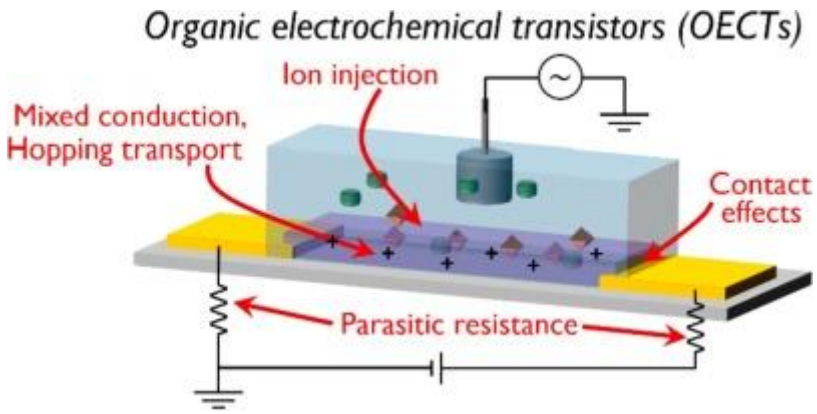

Figure 5: Schematic representation of the OECT operation[40]

An OECT can work in two modes. When a positive gate voltage is applied (depletion-mode), cations from the electrolyte are injected into the channel, resulting in a decreasing of the number of holes in the channel (de-doping by electrochemical point of view), which leads to a drop in the drain current[15]. By contrast, in accumulation-mode, the application of a negative gate bias causes injection of anions into the channel and a corresponding accumulation of holes (doping)[15].

The following discussion concerns the depletion-mode, because of its greater interest in the following chapters compared to the second mode. Furthermore, p-doped organic conductive materials are considered, in which holes are responsible for the current transport, since this is the case of PEDOT:PSS. According to the depicted transistor, V_{ds} potential difference is applied to drain and source terminals (the letter connected to ground) and V_g is applied to the gate terminal. V_g is set to 0: if a positive V_{ds} is applied, the holes in the channel will flow from drain to source, generating an I_{ds} current in the channel. Turning on the V_g with a positive value, the cations of the electrolyte are pushed into the channel, where they interact with the organic semiconductor, causing an alteration of the doping level of the same and a consequent decrease in I_{ds}.

To give a quantitative view, a physical model of the transistor is required to explain the dependence of I_{ds} on V_g. The model developed by D.A. Bernards and G.G. Malliaras[41] considered the combination of an electronic model and an ionic one. The electronic model accounts for the transport of holes that takes place in the channel, while the second illustrates the transport of charged ions in the electrolyte.

- ***Electronic circuit***. The electronic circuit of an OECT is ruled by the generalized Ohm's law:

$$J(x) = q\mu\rho(x)\frac{dV(x)}{dx}$$

where μ indicates the mobility of holes and $\rho(x)$ their concentration in the semiconductor, while x is the coordinate of the axis on which the channel is placed longitudinally. The cation migration into the polymer film is a process that maintains the neutrality of the polymer and decreases its doping, because each cation that is added balances the charge of a hole extracted from the source electrode. In this way the number of holes and then the doping decreases, but the electroneutrality of the material is guaranteed. The expression that describes this process is:

$$\rho = \rho_0(1 - \frac{Q}{qV\rho_0})$$

where ρ_0 indicates the holes concentration for $V_g = 0$, V is the semiconductor volume and Q is the electrical charge of the cations injected into the polymer film. As expected, as Q increases, ρ decreases.

- ***Ion circuit*** the ion circuit concerns the transport of the cations present in the electrolyte in the direction of the channel and can be modeled as a capacitor and a resistance placed in series between them. The resistance describes the conductivity of the electrolyte and measures its ionic force, while the polarization at channel-electrolyte and gate-electrolyte interfaces is expressed by the capacitor.

Measurements through the transistor can be made according to two methodologies.

- Static behavior: situation in which the transistor is applied a constant V_g voltage over time and the current Ids is evaluated according to the source-drain potential (V_{ds}).
- Dynamic behavior: it involves working under constant V_{ds} conditions, varying V_g between zero and a constant value for a finite time and then returning to $V_g = 0V$.

The static method allows a uniform de-doping process throughout the polymer film. The equation that governs the behavior of the organic electrochemical transistor is:

$$J(x) = q\mu\rho[1 - \frac{V_g - V}{V_{ds}}]\frac{dV(x)}{dx}$$

The result of this equation changes with V_{ds} (for $V_g > 0$)

- $V_{ds} > 0$, $V_{ds} < V_g$: de-doping occurs throughout the film;
- $V_{ds} > 0$, $V_{ds} > V_g$: is called emptying condition (de-doping) and occurs when $V(x) < V_g$;
- V_{ds} 0, $V_{ds} \leq V_{dsat}$: saturation voltage V_{dsat} is the critical drain voltage. Upon reaching the V_{dsat} the polymer doping can be undone. The local density of injected cations is equal to that of the semiconductor's intrinsic doping. The current saturation will then be observed.

The resulting curve through this system is called a "*Characteristics*" (Figure 6).

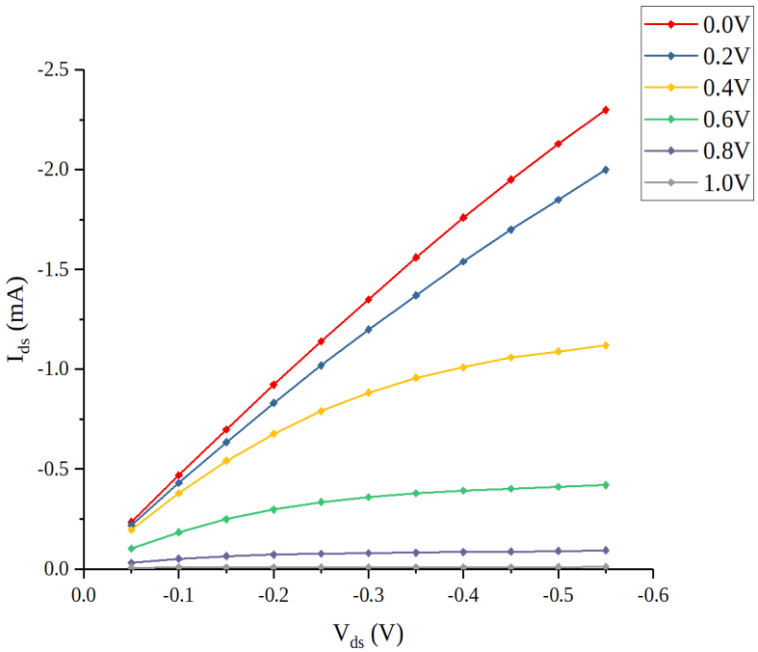

Figure 6: Characteristic curve of a transistor sensor. The curves are obtained at constant V_g while V_{ds} is being varied.

During dynamic behavior, the application of a positive gate potential allows the de-doping phase of the polymer, this is followed by a doping phase when V_g is returned to zero. The "trans-characteristic" curve (Figure 7a) depicts the system response to different electrolytic solutions[13]. A signal variation can be observed by changing the composition of the solution, as the presence of ions alters the electrochemical processes at the base of the transistor's operation.

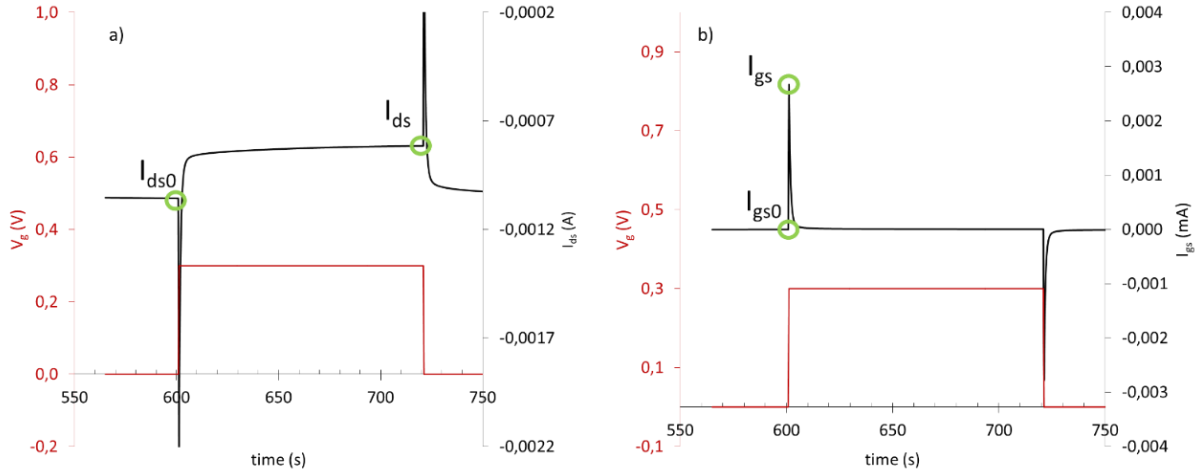

Figure 7: a) I_{ds} modulation when gate voltage is applied in OECT. Green circles indicate the drain-source current when V_g=0 (I_{ds0}), and the drain source-current when $V_g > 0$ (I_{ds}); b) I_{gs} behavior when gate voltage is applied in OECT. Green circles indicate the gate-source current when V_g=0 (I_{gs0}), and the gate-source current when $V_g > 0$ (I_{gs})

The device response, called modulation, is a dimensionless value obtained from the ratio of source and drain currents.

The application of positive gate potential results in a decrease of the current flowing into the channel, caused by the entry of positive ionic charges into the polymer. The modulation of the current between on and off state is called response (R) calculated by the following formula for each potential applied to the gate:

$$R = \frac{|I_{ds} - I_{ds0}|}{I_{ds0}}$$

Once a positive gate bias is applied, a current starts flowing also through the solution from the gate to the main channel (I_{gs}). Then, according to Gentile et al 2020[42] the variation observed may be proportional to the OECT wettability status. The difference of the gate-source current between on and off state is calculated by the following formula:

$$\Delta I_{gs} = I_{gs} - I_{gs0}$$

where I_{gs0} is the current across the electrolyte when $V_g = 0$.

Another parameter considered in the analysis of the data is the time constant (τ), which is calculated by fitting the curves of the current I_{ds} as a function of time, as shown in Figure 8a.

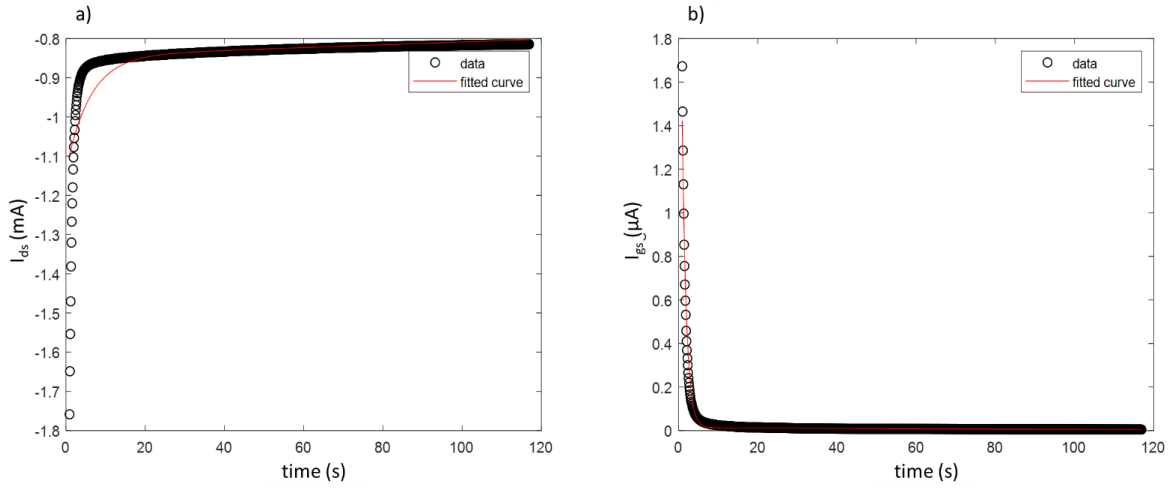

Figure 8: a) I_{ds} curve fitted with an exponential model; b) I_{gs} curve fitted with an exponential model

The value of the constant τ is derived from the formula: $A\left(1-\mathrm{e}^{(-t/\tau)}\right)$which represents how fast the curve reaches a plateau situation. Therefore, the presence of different ionic species that may have overlapping trends is not taken into consideration. The change of τ as well as the composition of the effect of all ionic species will be assessed. With the same approach τ_{gs} is calculated by fitting the curves of the current I_{gs} as a function of time (Figure 8b) resulting from the formula: $A(\mathrm{e}^{(-t/\tau)})$.

The conductor polymer, used in its doped state (PEDOT:PSS), forms the main channel of the transistor. Applying a suitable potential difference to the heads of the channel the current I_{ds} is obtained. Thanks to the presence of electrolyte ions the current of the device channel can be modulated, obtaining a current characteristic of transistors.

1.5 Climate change and Smart farming

The agricultural sector will face enormous challenges due to the sever impact of climate change on the planet. For centuries, man has exerted an increasing influence on the climate and on the variation of temperatures.

Climate change affects all regions of the world, albeit in different ways and in different forms with dramatic consequences: from the melting of polar ice sheets and perennial ice to rising sea levels; from the change in the annual distribution of rainfall to the increase in drought and fire risk; not to

mention the extinction of some species and the change in agricultural productivity and quality/nutritional capacity. In addition, the United Nations predicts that the world population will reach 9.7 billion by 2050, leading to the necessity to increase the global agricultural production of 69% between 2010 and 2050[8].

Food and agriculture are the larger water consumers, it is estimated that 70% of the fresh water available in the planet goes into irrigation[43] of this only a part of the water withdrawals are effectively used in the production of food since a large proportion of water does not even not reach the crop plants being evaporated from the soil in the field, or is used by non-productive growth such as weeds. Thus, new agriculture practice and new technology is needed to overcome this challenge. The encounter between technological innovation and agriculture is not new in human history, indeed it has accompanied its moments of greatest growth: from chemical fertilizers and the first gas tractor of the 1800s, until the end of the 1900s, when farmers started to use satellites to plan their work.

Smart farming or precision agriculture is a powerful strategy to reduce the ecological footprint of farming. Minimized or site-specific application of inputs, such as water inputs, fertilizers and pesticides, in precision agriculture systems will reduce the water use in agriculture as well as the emission of greenhouse gases[44]. The overall idea of smart farming is to have a continuous monitoring to farm activity by creating a sensor network.

Today thanks to the Internet of Things (IoT), farmers can use a smartphone to monitor remotely their equipment and crops as well as get statistics on livestock feed or crop. Farmers have already started to exploit IoT in agricultural techniques and technologies to improve the efficiency of their daily work. For example, the sensors positioned in the fields allow farmers to obtain detailed maps of both topography, soil humidity and temperature. Drones have also become a tool for farmers to monitor their land and generate crop data. Pioneering companies such as the John Deere Manufacturing Company have started to connect their tractors to the Internet and have created a method to view data on farmers' harvests. All these techniques contribute to precision agriculture as an interface between agriculture and science. They will permit to observe and record data with the aim of improving production while minimizing costs and safeguarding resources.

All devices and technologies mentioned so far include proximal sensors and remote sensors. None of them can simultaneously provide *in-vivo*, continuously and in real-time information on physiological changes in plants due to abiotic stress or environmental changes. For the reasons discussed in paragraph 1.3, the OECT is the ideal technology to develop a sensor to overcome the limitations of all the other devices mentioned, also combining their potential. In paragraph 1.6 a new sensor called Bioristor will be described. It has been developed in the laboratories of the CNR-IMEM and it is able

to collect biophysical and biochemical information from the inside of the plant *in-vivo*, in real-time and continuously.

1.6 The Bioristor's state of the art

Bioristor is an Organic Electrochemical Transistor (OECT) based sensor whose channel (a functionalized textile fiber) and gate electrodes are directly integrated into the plant stem (Figure 9).

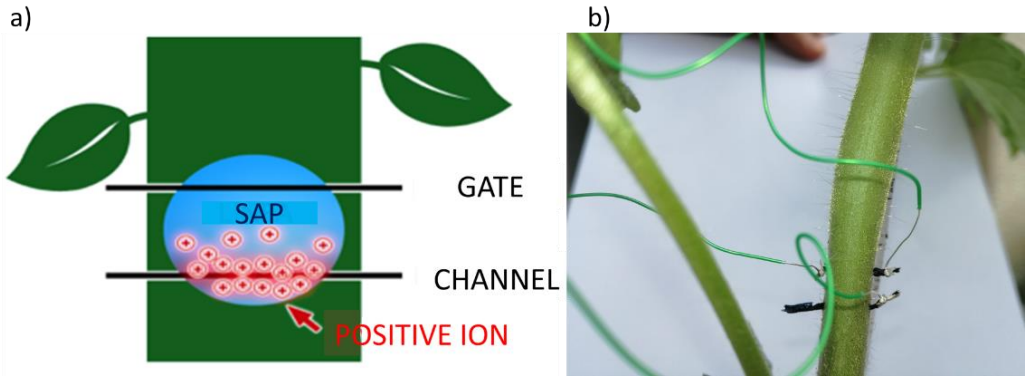

Figure 9: a) Sketch of the Bioristor showing it working principle in the plant system. b) Example of a Bioristor inserted in a stem of a *Vicia faba* plant

When Bioristor was introduced, for the first time in a crop plant as tomato[39], its behavior was consistent with a transistor placed inside a conductive fluid (sap in this case). Following the increase in V_g, the I_{ds} decreased due to the de-doping of the conductive polymer; the lymph of the plant interacted with the Bioristor and therefore the response of the sensor was modulated by the concentration of cations in the lymph. The variation in R for each test plant is shown in Figure 10 and indicates a periodicity ascribable to the circadian cycle: R increased during the period of darkness and fell during the period of light. This observation supported the effectiveness of Bioristor in measuring physiological changes within the plant sap. In fact, the increase of the sensor's response at night followed by a decrease during the day is consistent with the transpiration oscillation and circadian regulation of the photosynthesis[39,45].

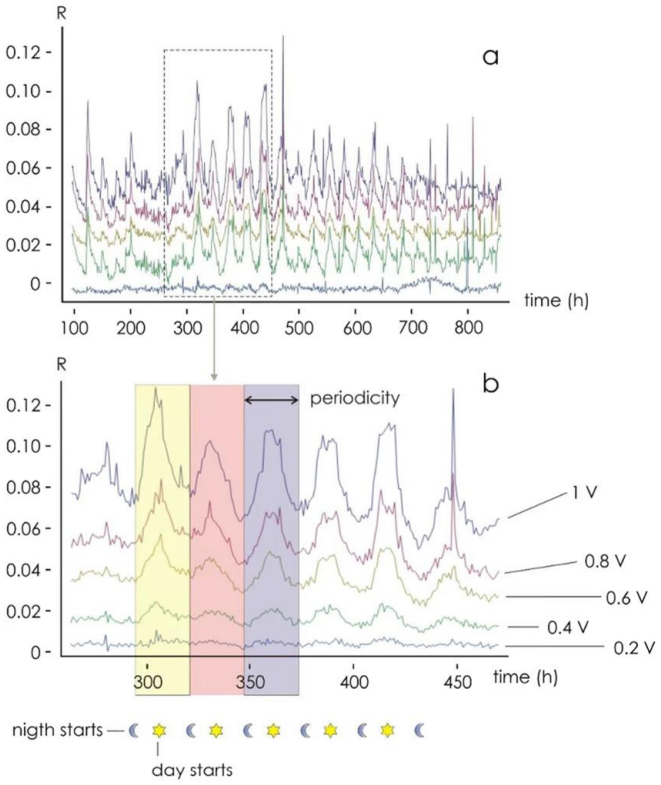

Figure 10: Sensor response (R) over 22 days (a) response at different V_{gs} bias; (b) detail of the sensor response for different gate voltages. Colored overlay highlights three day/night cycles[39]. Reported from Coppedè et al., 2017[39]

After the use in a biological environment, it was mandatory to evaluate the biocompatibility of this new sensor. Analysis of the stem sections of the plants near the functionalized fiber indicated that the introduction of Bioristor did not alter the general morphology of the stem, while the absence of adventitious buds indicated that the vascular connections had not been interrupted. In addition, Bioristor had no impact on plant growth as sensor plants were indistinguishable from controls[39].

Bioristor technology is patent pending (published as BR112019012631A2; EP3559647A1; IT201600130803A1; MX2019007526A; WO2018116149A1) in Europe, USA, Brazil and Mexico and it is owned by Consiglio Nazionale delle Ricerche (CNR).

1.7 Plant response to abiotic stress

Here a brief introduction of the mechanisms triggered by the plant to overcome the principal abiotic stresses are reported. Mainly, abiotic stresses are induced by water scarcity, high salinity of the irrigation water and/or the soil, sub-optimal or over-optimal temperature levels and nutritional

deficiency. From a strictly agronomic point of view, stress related to hypoxia conditions caused by the prolonged flooding and the excessive salinity of the soil are also relevant.

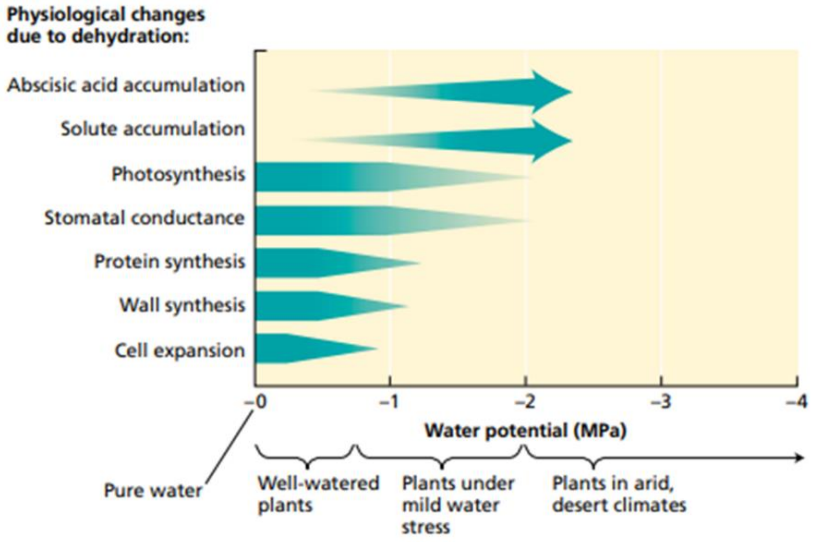

Figure 11: Water potential of plants under various growing conditions and sensitivity of various physiological processes to water potential. The intensity of the bar color corresponds to the magnitude of the process.[46]

Plant responses to environmental stimuli and stresses vary according to stress conditions, although different types of stress often lead to identical or similar responses (Figure 11). At the cellular level, abiotic stress, especially water deficiency (drought and salinity), cause a decrease in the pressure potential. Solutes, concentrated in the cell, are linked to water loss, and are actively accumulated to keep the cytoplasm osmotically balanced. Osmotic adaptation is one of the major components of abiotic stress tolerance and contributes to maintaining pressure potential. The main solutes used in osmotic adaptation include various quaternary amines, amino acids or alcoholic sugars. The accumulation of these osmolytes facilitates water retention in the cytoplasm, the protection of membranes, protein complexes and cellular structures [47].

Plants can continuously absorb water thanks to the difference in water potential between the atmosphere and the plant compartments (Figure 12)[48].

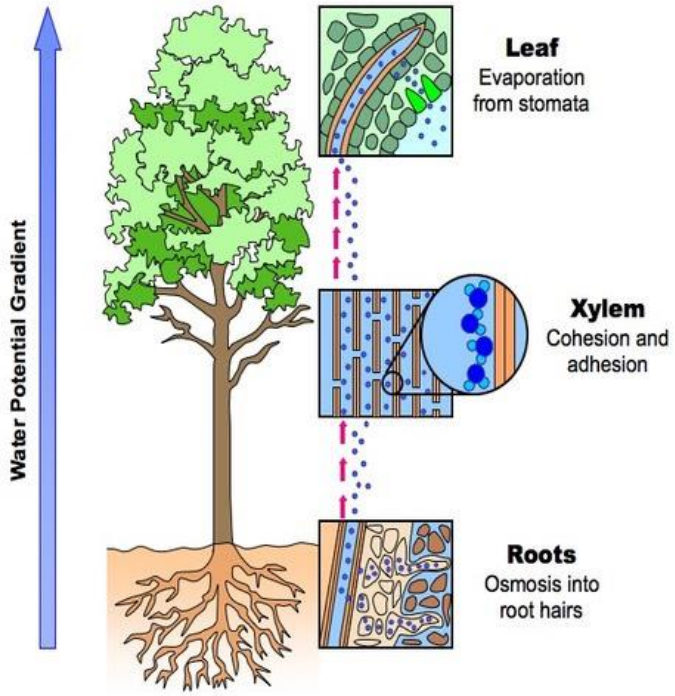

Figure 12. Scheme on how plants absorb water and how the transpiration flux is regulated[48].

As a response of the water loss, the plants trigger a series of defence response mechanisms aimed at preserving the water in the cells. An example are the osmotic osmotic adjustments can depend on concentration increases of a certain number of common solutes such as sugars, amino acids, and ions. Enzymes extracted from the cytosol of plant cells are shown to be very inhibited by high concentrations of ions. Due to the subdivision of the ions, solutes can be accumulated in the cytosol so as to maintain the balance of the water potential within the cell and thus named as compatible solutes. Glycine betaine, proline, polyamines, and certain molecules that are part of sugar metabolism such as mannitol, fructans, trealose, and D-inositol are well known compatible solutes. The synthesis of compatible solutes is important in the regulation that the plants implement in response to the increase of salinity in the root zones. The osmotic regulation that occurs in radical meristems, increasing turgor and maintaining root accretion, is an important component in changes in root growth patterns during drought periods. Yet it is not clear whether osmotic regulation is a response to water stress or whether it is the result of some other factors such as the decrease in growth capacity. The osmotic regulation also takes place at a radical level, even if the process has not been studied in such details as for the leaves. Attempts to increase osmotic regulation in leaves, both genetic and physiological, have resulted in slow-growing plants.

The process of adaptation to stress involves most of the metabolic processes of plants, but generally the most important role is played by plant hormones and, especially by abscisic acid (ABA). The levels of this hormone increase considerably under conditions of stress and the variations in endogenous levels of ABA stimulate a series of metabolic and physiological events (Figure 13) that lead to the acquisition of tolerance [49]. When the onset of stress is quicker, responses intervene that allow the plant to protect itself from immediate dehydration such as the closure of the stomata. Their closure can be considered the first line of defense against drought, because it reduces evaporation from the foliar surface. In fact, during water stress the pH of the xylem sap becomes slightly alkaline (pH 7-8), and this favors the dissociation of ABA → ABA^- + H_3O^+. Since ABA^- does not easily cross the membranes, during water stress more ABA will reach the on-call cells causing the activation of the output channels of K^+ (potassium) and a loss of turgor of the guard cells with the consequent closure of the stomata.

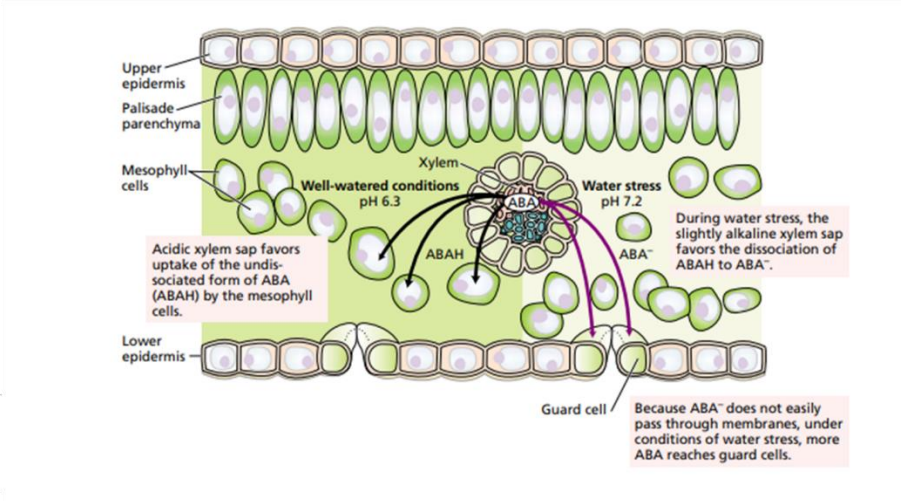

Figure 13: Redistribution of ABA in the leaf resulting from alkalinization of the xylem sap during water stress.[46]

Chapter 2

Material and methods

2.1 The Bioristor preparation

The functionalization process of Bioristor was performed as indicated in Tarabella et al.[50] with slight modifications. Two textile fibers were treated by soaking them for 5 min in aqueous poly(3,4-ethylenedioxythiophene) doped with polystyrene sulfonate (Clevios PH1000, Starck GmbH, Munich, Germany), after which ethylene glycol (10% v/v) and dodecyl benzene sulfonic acid (2% v/v) were added. Fibers were then baked at 130 °C for 90 minutes. Finally, the whole process, from deposition to heat treatment, must be repeated 3 times to complete the preparation. Before functionalization, each thread was cleaned by plasma oxygen cleaner treatment (Femto, Diener electronic, Ebhausen/Germany) to increase its wettability and facilitate the adhesion of the aqueous conductive polymer solution.

Since a degree of degradation and instability was seen in the continuous use of Bioristor in plants, some arrangements were performed in the sensor preparation to increase the duration and the feasibility of Bioristor.

In sections 3.3, 3.4, 5.1 (2019 open field trial) and 5.2, the addition of ethylene glycol was replaced by a treatment with concentrated sulfuric acid (95%) for 20 minutes to increase the crystallinity of the polymer, and therefore its electrical properties, as well as its duration over time[51–54] (Table 1).

In its first version the gate was represented by a silver wire (section 3.1). Since a degree of necrotic tissue was observed following the measurements in tomato for 30 days, the silver wire was replaced by a second functionalized textile thread (Table 1) (Figure 2).

Table 1: Evolution of the Bioristor preparation during the experiments. Different PEDOT:PSS treatment, gate used and gate voltage used in the experiments described in the different chapters (Note thet the experiments are not in chronological order)

Chapter	Treatment	Plant species	PEDOT:PSS Treatment	Gate	Gate voltage
3.1	Drought stress	Tomato	Ethylene glycol	Silver wire	0.6-1 V
3.2	Drought stress and mutants	Tomato	Ethylene glycol	PEDOT:PSS fiber	0.6-1 V
3.3	Drought stress and biostimulants	Tomato	H_2SO_4	PEDOT:PSS fiber	0.5 V
3.4	Drought stress	Kiwi	H_2SO_4	PEDOT:PSS fiber	0.5 V
4	VPD	Tomato	Ethylene glycol	PEDOT:PSS fiber	0.6-1 V
5.1	Drought stress in open field (summer 2018)	Tomato	Ethylene glycol	PEDOT:PSS fiber	0.6-1 V
5.1	Drought stress in open field (summer 2019)	Tomato	H_2SO_4	PEDOT:PSS fiber	0.5 V
5.2	Drought stress in open field (summer 2020)	Kiwi	H_2SO_4	PEDOT:PSS fiber	0.5 V
6	Salt stress	*A. donax*	Ethylene glycol	PEDOT:PSS fiber	0.6 -1V

2.2 Bioristor biocompatibility

To verify the Bioristor compatibility, three plants with the integrated sensor and one control plant were analyzed at the end of the experiment for biocompatibility following the protocol described in Barrs and Weatherley[55]. Sections of stem tissue were prepared using a fresh razor blade and stained with Toluidine Blue O (TBO, Sigma Aldrich, Milano, Italy), a metachromatic stain that produces different colors depending on the polymer to which it adheres. Primary walls (parenchyma,

collenchyma, and phloem) are purple and lignified secondary walls of xylem tracheids and vessels (a subtype of vascular tissue) and sclerenchyma are blue, while some other cells may take on a greenish color. Pictures were acquired with a digital camera equipped with a macro lens. The introduction of Bioristor did not significantly altered the stem morphology and the plant growth since the plants equipped with the sensors were indistinguishable from other plants not monitored used as control (data not shown)[39,56]. Indeed, the insertion of the sensor did not damage the functionality of the vascular tissues, and even if the vascular tissues were interrupted in the insertion point, the normal stem structure was restored immediately after the insertion point[39,56]. Moreover, the use of a textile thread as gate strongly reduced (Figure 2.3), if compared with the silver one (Figure 2.4), the onset of necrosis in the tissues surrounding the sensor[39,56].

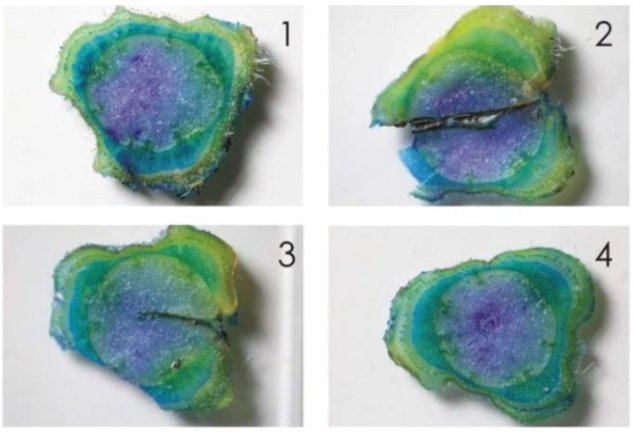

Figure 2: Optical microscope image of stem section after 42 days of continuous sensor measurements: (1) stem area on top, (2) silver gate area, (3) textile fiber area, (4) steam area on bottom.[39]

2.3 Bioristor insertion

Bioristor was inserted in the plant stem by performing a hole in the stem of the plant using a needle. The treated fiber was completely inserted in the stem of plant. The fiber was connected on each end to a metal wire with silver paste to stabilize the connections, forming the “source” and “drain” electrodes (Figure 1b). The transistor device was completed by inserting the gate electrode. In fruit trees such as kiwi (sections 3.4 and 5.2), due to the woody nature of the trunk, a drill was used to perform a 0.8 mm holes in the trunk of the plants for the sensor insertion.

2.4 Bioristor main outputs

In each experiment a constant voltage (V_{ds}=-0.1V) was applied across the main transistor channel, along with a positive voltage at the gate (V_g, see Table 1) which leads to a decrease in channel conductivity due to the cation pushed from the elctrolyte into the channel; the resulting current (I_{ds}) was monitored continuously. The main sensor response parameter (R) used in all experiment, and proportional to the cations present in the electrolyte, was given by the expression $|I_{ds} - I_{ds0}|/I_{ds0}$ where I_{ds0} represented the current across the channel when $V_g = 0$. Upon application of a positive gate bias, gate electrode and the device channel charge capacitively, then a current flowing also through the liquid from the gate to the main channel (I_{gs}) was monitored continuously. The difference $\Delta I_{gs} = I_{gs} - I_{gs0}$ was considered (section 3.3, Chapter 4) to evaluate the sensor wetting status, where I_{gs0} represented the current across the solution when $V_g = 0$[42]. Moreover, two time constants, τ and τ_{gs} of the sensor were evaluated in more complex experiment (section 3.3, Chapter 4) in the context of a multivariate analysis. τ and τ_{gs}, calculated by fitting the non-linear drain and gate current curves (see section 1.3), are related to the time that ions take to enter the polymer, τ, and to the diffusivity of ions in the solution, τ_{gs}[39,56,57], respectively. For R, ΔI_{gs}, τ and τ_{gs} parameters the first derivative as a function of time was also calculated to highlight specific trends and indicated as dR, dτ, dΔI_{gs} and dτ_{gs}[56] (section 3.3, Chapter 4).

To solve PEDOT:PSS degradation problems encountered at gate potentials of 1 V in summer 2018 open field trial (see Chapter 6.1), thanks to an *in-vitro* experiment (data not shown), the gate potential of 0.5 V (Table 1) is identified as optimal value to increase sensor lifetime[58].

2.5 Electronic components for signal readout

Bioristor elements were connected to a NI USB-6343 multifunction I/O device (National Instruments, Austin, TX, USA), which is a multichannel digital analogic converter connected to a PC where current data are processed through an home-made software and then saved in cloud. This requires, especially in field conditions, the presence of several meters of wires connecting the plant with the digital converter. Thus, to facilitate the installation of the sensor, the NI digital converter has been replaced for the most recent experiments (section 5.2). A control unit has been developed in our lab

enabling the reading and transmission of Bioristor signal with an IoT approach (Figure 3). The control unit was developed through Arduino system and connected to a battery powered by a photovoltaic panel, to ensure continuity of measurement. The Bioristor data are saved locally in a micro-SD memory card and transferred to remote server via wireless connection.

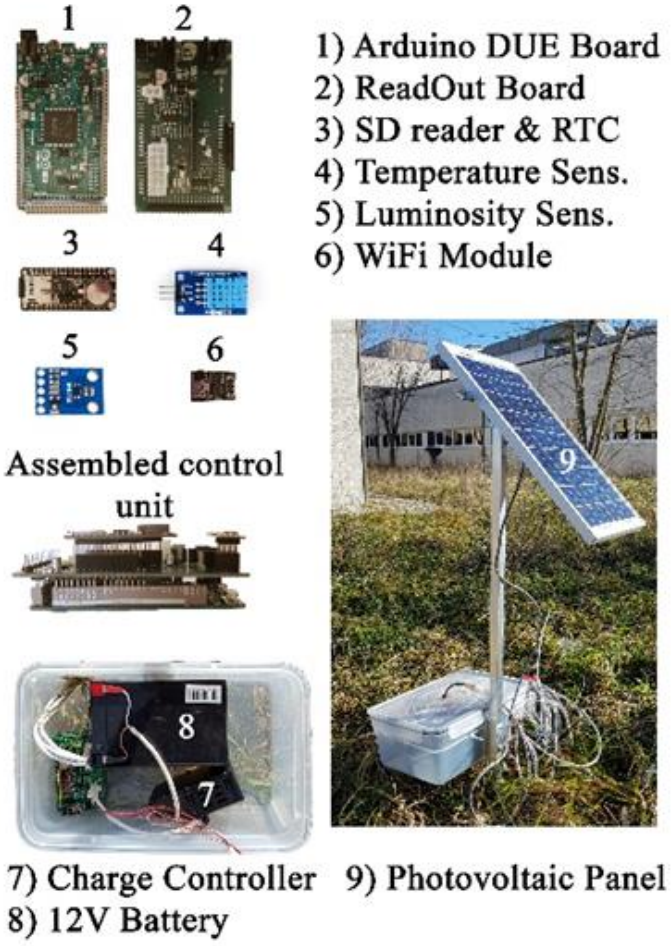

Figure 3: Wireless control unit and its components

Chapter 3

In-vivo early detection of drought stress in plants grown in controlled conditions

This chapter reports the ability of Bioristor to efficiently monitor the effects of water stress in tomato and kiwi physiology and growth in controlled environment. In the first paragraph two experiments were performed on tomato plants, one at IMEM CNR in Parma (pilot experiment) and the main experiment at the Italian phenotyping platform of ALSIA Agrobios – Metaponto. In addition, to support the ability of Bioristor to monitor the physiological variations that the water stress induces, tomato mutant lines identified as potentially tolerant to drought stress thanks to a mutation induced in a gene responsible for abscisic acid production were monitored. In the last paragraph, due to the importance of the Italian fruit production, the effectiveness of the Bioristor in monitoring also tree species as kiwi fruit will be demonstrated.

3.1 Tomato plants

Two experiments in controlled conditions were performed[49]. A pilot experiment, carried out in Parma (Italy), was set up to demonstrate the ability of the Bioristor to respond to drought stress. Then, on the basis of the results obtained in the pilot experiment, the main experiment was performed in the ALSIA plant phenomics facility (Metaponto, Italy)[59].

3.1.1 Materials and Methods

Plant Growth and stress application

In the pilot experiment, the seeds were kindly furnished by ALSIA Metapontum Agrobios Research Center. Seven Red Setter plants were grown up to the stage of 5th fully expanded leaves in 1.5 dm^3 soil-filled pots under controlled conditions, namely, a constant temperature of 24° C, a relative humidity of 50%, and a 16 h photoperiod. The plants were kept fully irrigated until their fifth true leaf had fully expanded, after which a Bioristor was inserted in the stem of each plant (Figure 1A). After 3 days, four of the plants were exposed to drought stress by withholding watering for 14 days (DSI); the plants were then irrigated over 2 days (RE), and, finally, a 6 days stress episode was imposed by withholding water (DSII) (Figure 1A). A set of four plants was kept fully watered as the control[59].

On this basis, the main experiment was performed in the ALSIA plant phenomics facility (Metaponto, Italy). The trial was based on eight Ikram plants, available at the ALSIA Metapontum Agrobios Research Center, grown in 3 dm^3 pots exposed to a 12 h photoperiod (light intensity 180 µmol m^{-2} s^{-1}) with a daytime temperature of 24° C and a nighttime one of 18° C; the relative humidity ranged from 50 to 60%. When the plant reached the stage of 5^{th} fully expanded leaves, the sensors were integrated and 1 day after the implantation of the Bioristor, watering was withheld from four of the plants for 16 days (DSI) and then restored for a further 7 days (RE) (Figure 1B). A limited irrigation 50 cm^3 was supplied to the 3 dm^3 pots to maintain the plant turgor and allow for the acquisition of images (day 8). The remaining four plants were kept fully watered as the control[59].

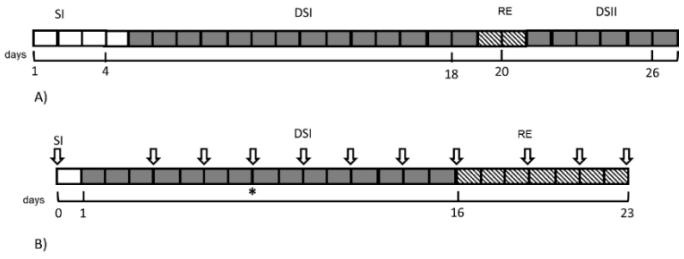

Figure 1: Schematic illustration of the experiments conducted in (A) Parma and (B) Metaponto. White blocks indicate days during which full watering was provided following the Bioristor's implantation (SI), grey blocks indicate days during which watering was withheld (DSI, DSII), and the shaded blocks indicate the recovery phase (RE). Arrows indicate the timing of the Scanalyzer readings and image acquisition, while the black star shows when the emergency irrigation was provided[59].

3.1.2 Bioristor measurement

The Bioristors were prepared, inserted into the plant stems, and connected to a computer, as described in Chapter 2. The calculated R parameter at gate voltage of 0.6V (see Chapter 2) was analyzed with MATLAB (https://uk .mathworks.com/) and Microsoft Excel 2016). The normalized sensor response (NR) was shown as the Bioristor output and calculated as the ratio between the daily mean R of stressed and non-stressed plants[59].

To validate the results obtained with the Bioristor a series of standard physiological analyses were necessary.

3.1.3 Physiological and image analysis

Four controls and four stressed plants have been analyzed for the relative water content (RWC) as reported by Barrs and Weatherley[55], by taking the fully expanded leaf as the sample (two replicates for each plant). Chlorophyll content measurements were performed by using the SPAD 502 meter (Konica Minolta, Ramsey, USA). Measurements from 10 leaves of each plant of varying age and color were selected for measurements made under diffuse lighting. The relative SPAD value was considered. All data were analyzed statistically applying Student's t-test, and the standard error was calculated between replicates[59].

Leaf stomatal conductance was measured from two fully expanded leaves per plant (fourth and fifth leaf) of the Ikram plants, using an SC1 leaf porometer (Decagon Devices, Pullman, WA, USA)[59].

Moreover, images were captured at 2 days intervals from Ikram plants following Petrozza et al.[60], using a Scanalyzer 3D device (LemnaTec GmbH, Aachen, Germany). The imaging, initiated prior to the imposition of drought stress, involved three mutually orthogonal vantage points, using near-infrared (NIR) and white (RGB) illumination. The NIR images were used to evaluate the plants' water content; the RGB ones were for the assessment of both the plants' state of health (green: healthy tissue, yellow: chlorotic tissue, and brown: necrotic tissue) and for morphological measurements; these data were used to calculate the plants' biovolume and height; their biovolume (a parameter proportional to the aerial mass of the plant) was calculated from the expression:

$$\frac{\Sigma pixel\ sideview\ 0° + \Sigma pixel\ sideview\ 90° + Log\ \Sigma pixel\ sideview}{3}$$

following Eberius and Lima-Guerra, and Petrozza et al[60,61].

Plant compactness, which describes how much of the hull area is covered by leaves, was calculated as object area/convex hull area[62]. The NIR index was calculated as weighted mean from the pixel intensities of greyscale NIR images divided into 128 bins, representing a range in leaf water content, while the green index that expresses the fraction of green color detected in the leaves was calculated in accordance with Casadesús et al[59,63].

3.1.4 Results

The monitoring over 26 days of the behavior of four drought-stressed and three well-watered Red Setter plants confirmed the Bioristor's capacity to record day/night changes in the xylem sap's composition[39]. The R parameter fell during the daytime and rose during the nighttime, as was expected (data not shown). When each 24 h cycle of data was averaged to generate a mean NR value, four distinct phases (defined by a slope change) were recognized (Figure 3): the first phase (PI) covered the first 3 days following the sensor's implantation; PII was initiated 24 h after the withholding of water and was characterized by a decrease in NR over a 6 days period, followed by a short 2 days innate recovery (DA). PIII reflected the plants' recovery following rewatering, during which time NR rose back to its pre stress level; finally, during PIV, when the plants were once again deprived of water, NR fell, this time more rapidly than it did during PII.

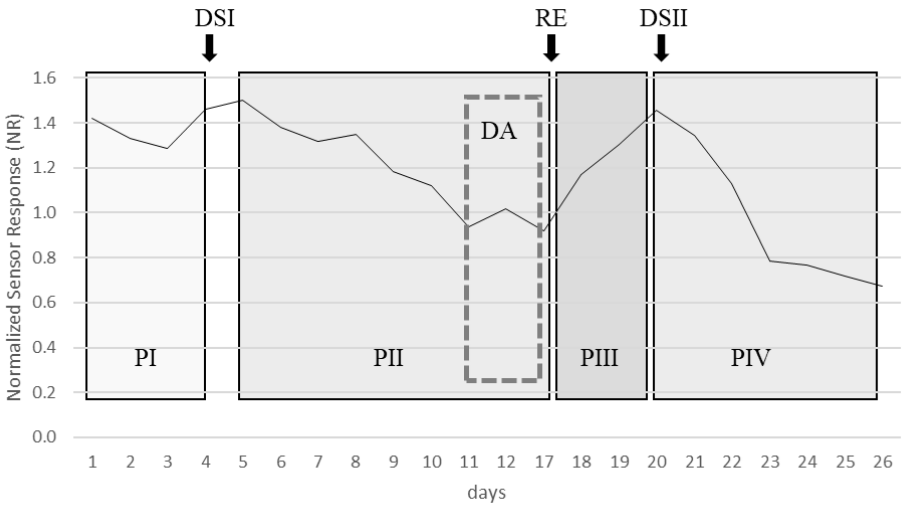

Figure 3: The behavior of the averaged normalized sensor response parameter (NR) used to monitor the drought response of Red Setter plants subjected to two cycles of drought stress (DSI and DSII) interrupted by a rewatering recovery phase (RE). Arrows show the timing of the initiation of each treatment. Data represent the mean of three well-watered (control) and four stressed plants. The various phases have been highlighted by grey boxing: PI—sensor insertion, PII—drought stress, and PIII—post recovery[59]

Measurements of both leaf chlorophyll content (as estimated using a SPAD device, Figure 4A) and relative water content (RWC, Figure 4B) confirmed that the plants were experiencing drought stress (Figure 4B). The SPAD value in the stressed plants significantly increases during the drought stress ($p \leq 0.05$) although only two points have been acquired, and as expected, the RWC consistently decreases by about 23% ($p \leq 0.05$) during the drought stress and is completely restored when the recovery occurred (Figure 4B). The validation of the Bioristor as a tool permitting the early detection of drought stress allowed a more detailed analysis conducted in the main experiment, in which four drought-stressed and four well-watered cv[59].

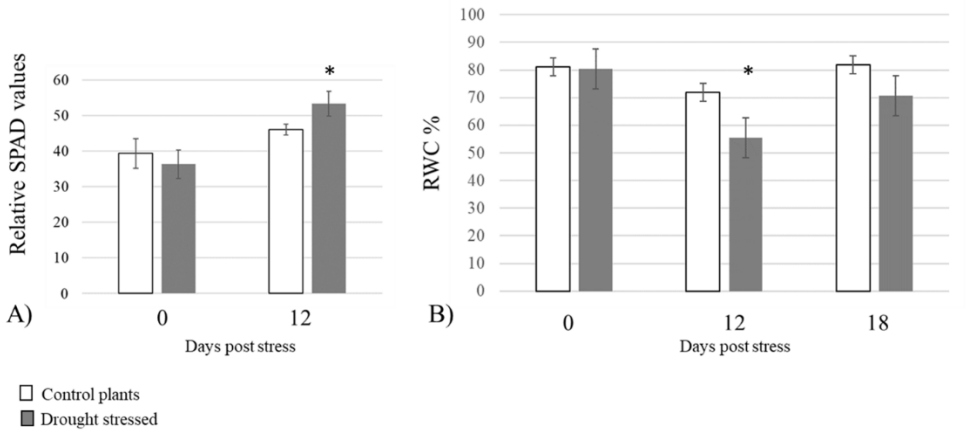

Figure 4: Physiological analyses performed on four drought-stressed plants (dark grey) and the regularly irrigated controls (light grey). (A) SPAD. (B) Relative water content (RWC). Asterisks (∗) indicate significant differences of the drought-stressed plants from the control plants, according to Student's t-test ($p \leq 0.05$)[59].

Ikram plants were continuously monitored over a period of 23 days under controlled conditions (Figure 5). Once again, the slope of the NR parameter was used to define a number of phases. The PI phase followed the implantation of the sensor; during PII, there was an initial (days 2-4) sharp fall in NR as the intensity of the drought stress increased, but over the subsequent 4 days, NR recovered somewhat (DA) but with higher extent as for the Red Setter cultivar[59].

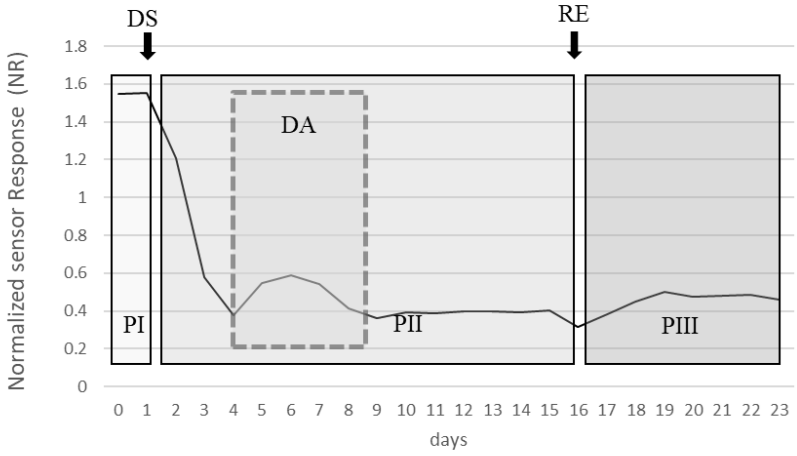

Figure 5: The behavior of the averaged normalized sensor response parameter (NR) used to monitor the drought response of Ikram plants subjected to drought stress. DS: period during which water was withheld; RE: rewatering recovery phase. The data represent the mean of four well-watered (control) and four stressed plants. The various phases have been highlighted by grey boxing: PI—sensor insertion, PII—drought stress, DA—drought avoidance, and PIII—post-rewatering recovery[59].

The stress applied had a strong effect on stomatal conductance, a widely used indicator of drought stress[64], over the period 7-14 days after the withholding of water reducing it by 4-5-fold in comparison to the well-watered plants (Figure 6). Reductions in stomatal conductance not only reduce transpiration water loss from the leaf but also constrain their photosynthetic activity, due to the limitation imposed on gas exchange[65]. An equivalent, although less pronounced, stomatal conductance response was, in retrospect, also recognized in the Red Setter plants monitored in the pilot experiment, suggesting the existence of genotypic variation for the response. However, this defense mechanism failed as the stress period was prolonged, as was shown by the resumed fall in NR over days 7-9, after which the parameter remained at a low but stable level through to 23 day. A slight increase in the NR was observed corresponding to the limited irrigation operated (days 10-16). PIII was initiated upon the plants' rewatering, during which period NR increased to a level which was maintained through to the end of the experiment. This level was, however, much lower than the baseline obtained at the start of the treatment, reflecting a degree of irreversible damage caused by the stress (Figure 7D). Overall, the conclusion was that a stress response was detectable through the negative trend of the NR parameter already within the first 30 h following the withholding of water.

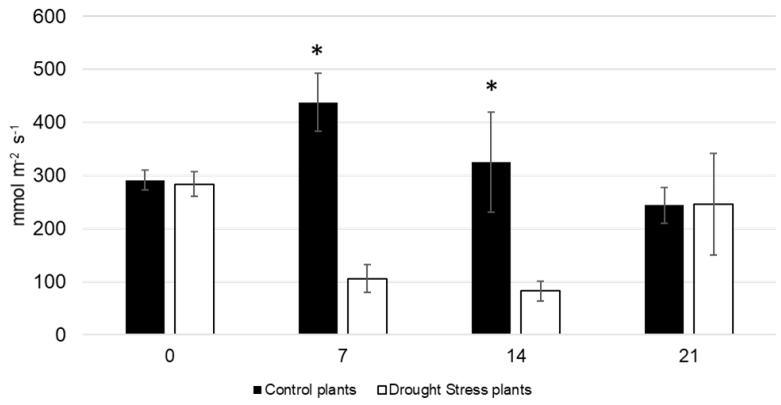

Figure 6: The response of stomatal conductance to moisture deficiency. Control and drought-stressed Ikram plants were assayed after 0, 7, 14, and 21 days of treatment. Asterisks (∗) indicate significant differences of the drought-stressed plants from the control plants, according to Student's t-test ($p \leq 0.05$)[59].

In the main experiment, imaging was used to monitor the phenotypic response to the stress treatment (Figures 7A and 7B).

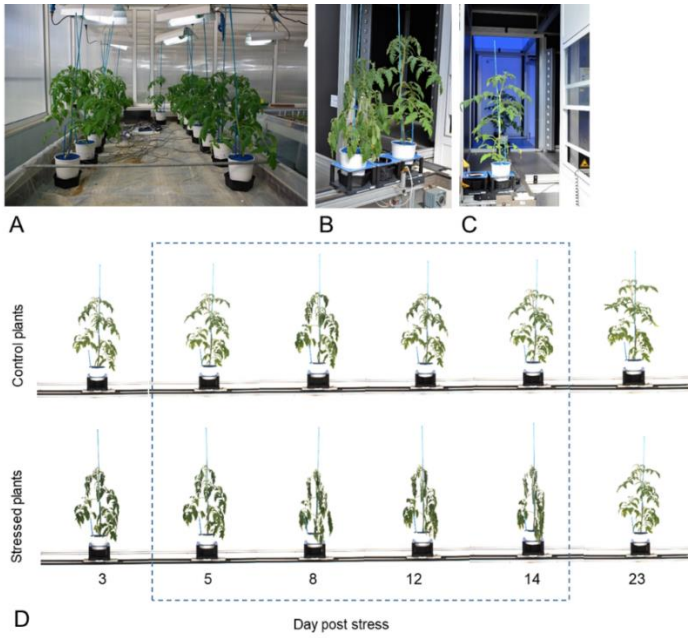

Figure 7: High-throughput phenotyping experiment: (A) plants implanted with a Bioristor; (B, C) drought-stressed and well-watered plants during the process of image acquisition; (D) the plants monitored continuously with a Bioristor and scanned every other day with the Scanalyzer over a period of 23 days[59].

The chosen indices involved four based on RGB images (digital biovolume ,Figure 8A; plant height Figure 8B; plant compactness Figure 8C; and green index, Figure 8D) and one based on NIR images (hydration index, Figure 8e). The growth of the plants, as indicated by their biovolume, height, and compactness, their greenness, and their hydration status were all strongly affected by the drought treatment. Changes in plant compactness and height were clearly visible, while the green and NIR-based indices first became detectable after 6-8 days (Figure 8E). Biovolume fell markedly over the first 8 days of the stress and were not recovered following rewatering (Figure 8A). The stress triggered severe wilting (Figures 8B and 8D); within 6 days of the withholding of water, the height of the stressed plants was 15% lower than that of the well-watered plants (Figure 8B). Plant compactness differed significantly between the treated and control plants within 4 days of the withholding of water; the stressed plants lost turgor, which steadily increased their compactness over the period 4-14 days; a gradual recovery occurred following rewatering and the compactness reached the level shown by the controls at the end of the experiment (Figures 7D and 8C). A similar trend was observed for the NIR intensity. For the control plants, the NIR-based index rose strongly over the first 6 days; this was also the case, although less markedly, for the stressed plants. For the latter, the index fell between days 7 and 10, until emergency irrigation was supplied to prevent plant death; the level was fully restored by rewatering carried out on day 16. The green index of the stressed plants fell slightly over

the initial 12 days following the withholding of water, then remained steady, in contrast to the response of the control plants, which comprised a continuous fall over the whole measurement period (Figure 8D)[59].

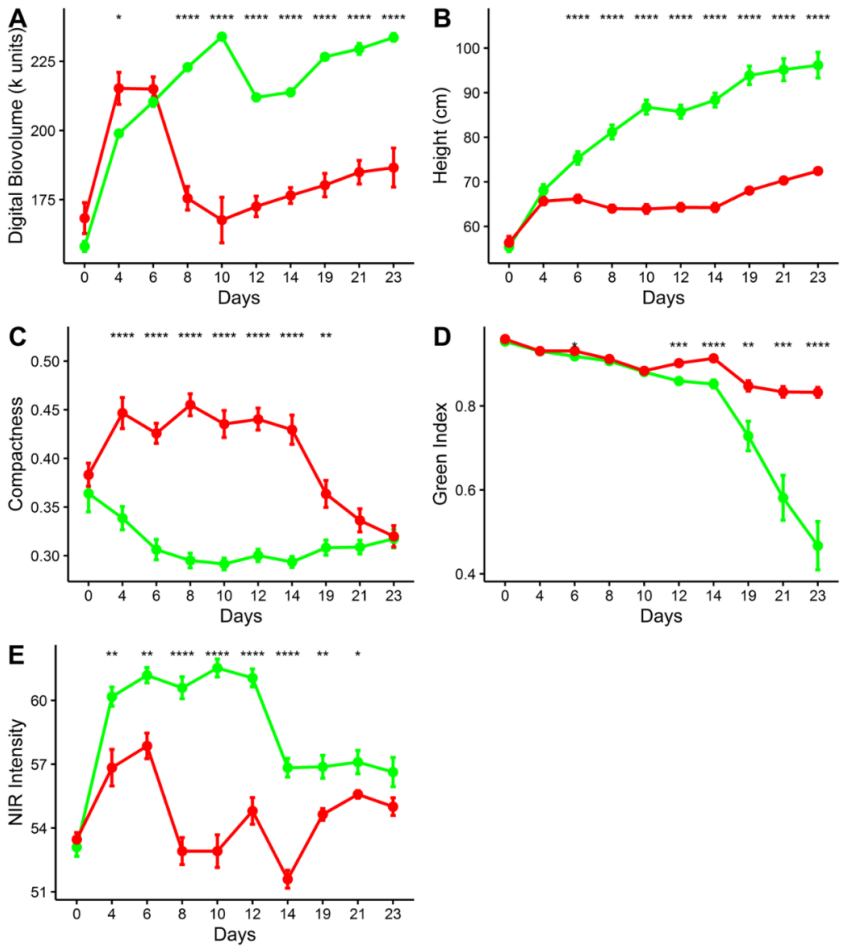

Figure 8: Indices derived from the Scanalyzer experiment imaging data on control plants (green) and drought-stressed plants (red): (A) digital biovolume, (B) plant height, (C) plant compactness, (D) green index, and (E) NIR intensity Asterisks indicate significant differences of the drought-stressed plants from the control plants according to ANOVA (****0 ≤ p ≤ 0.0001, ***p ≤ 0.001, **p ≤ 0.05, and *p ≤ 0.01)[59].

The ability of the Bioristor to monitor physiological mechanisms strictly related to the changes of ion concentration in the plant sap in relation to the transpiration stream is strongly supported by the correlation analysis performed[59]. In fact, a strong and highly significant correlation between the sensor response (R) and the stomatal conductance (SC) ($r = 0.82$, $p \leq 0.001$; Figure 9) was observed, highlighting also a clear separation of the stressed and non-stressed samples indicating a strong influence of DS on the R value[59].

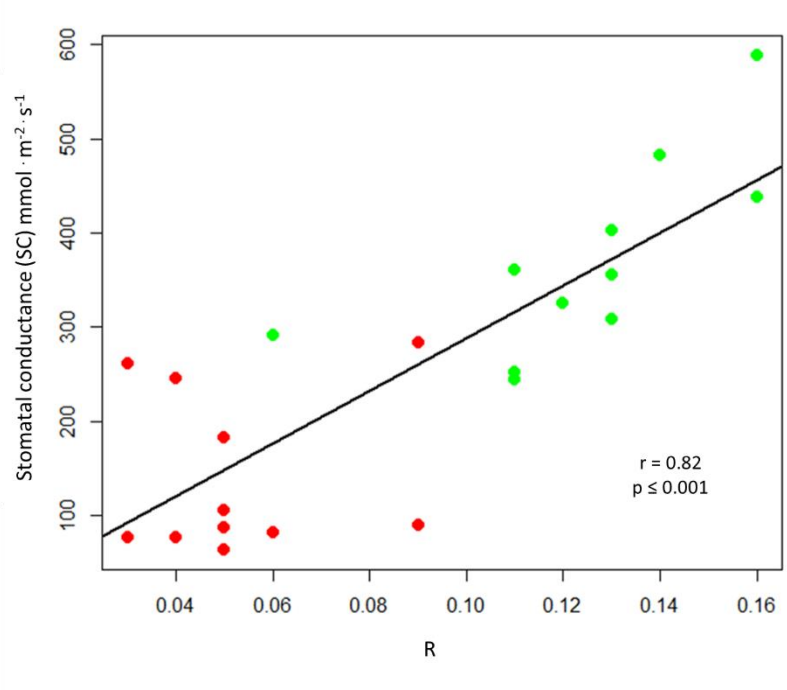

Figure 9: Scatter plots of the sensor response (R) and stomatal conductance (SC) measured on control plants (green) and drought-stressed plants (red). The scatter plot and linear regression displayed indicate a strong correlation between the two variables, with a correlation coefficient of r = 0.82. p ≤ 0.001 indicates the statistical significance level of the observed correlation[59].

To confirm the suitability of the Bioristor to complement the image-based high-throughput phenotyping techniques, we performed a Pearson correlation analysis between the digital biovolume as the index of drought stress[66] and the *in-vivo* Bioristor sensor response. A good and significant correlation (r = 0.66, p ≤ 0.001; Figure 10) was observed between the two variables, firstly confirming the occurrence of the drought stress, and secondly supporting the suitability of the Bioristor to monitor *in-vivo* the drought stress profile in plants. A comprehensive correlation analysis of all image-based index and manual-based measurements allowed us to observe a high correlation between the sensor response and those parameters linked with the transpiration process and the water use efficiency (SC and DB) and to exclude, at least in this experiment conditions, a direct correlation with the NIR intensity (NI), the green index (GI), and compactness (Figure 10)[59].

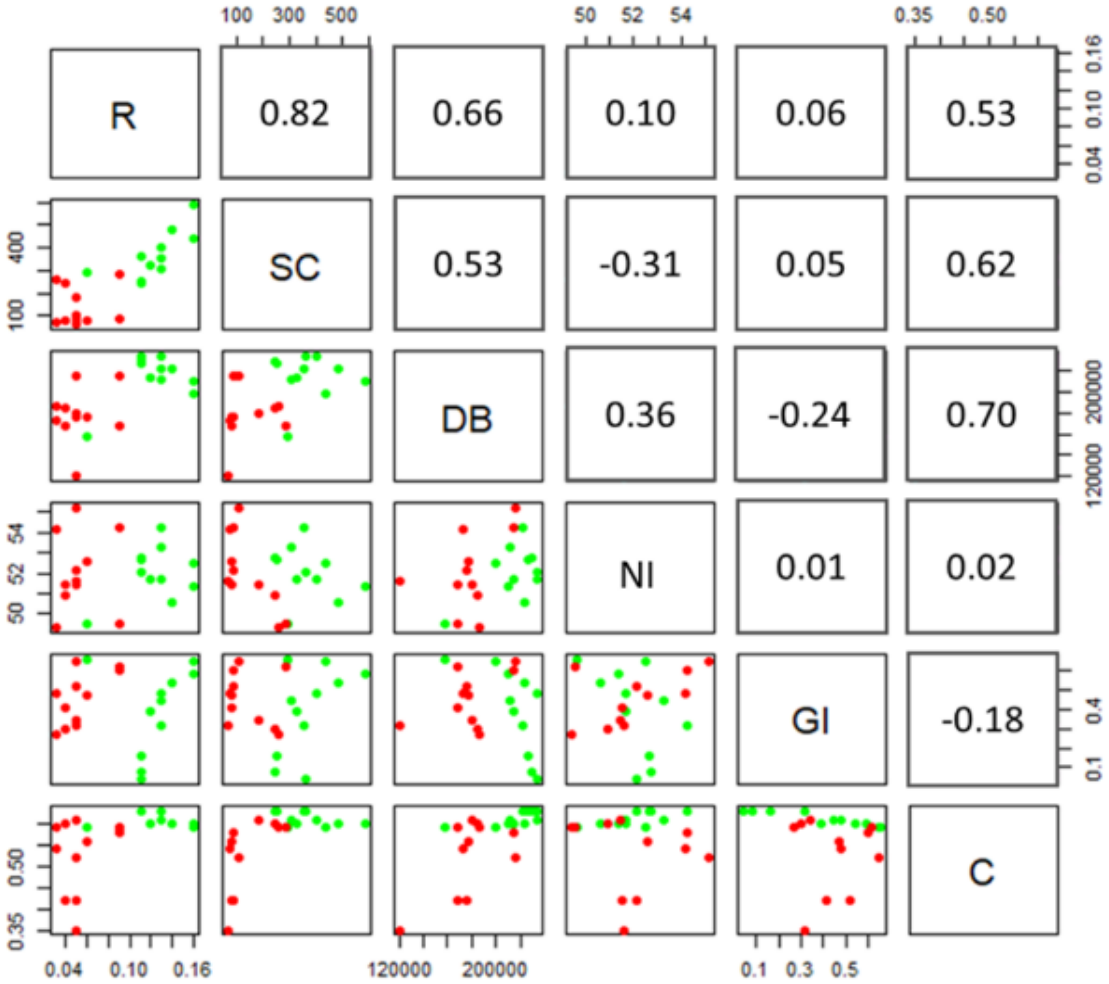

Figure 10: Correlation of the acquired physiological and morphological measurements including the Bioristor response (R), image-derived data (DB: digital biovolume; GI: green index; NI: NIR intensity; C: compactness), and manually determined stomatal conductance (SC). Red dots indicate stressed plants; green dots indicate control plants

In addition, to evaluate the overall phenotypic profile and distinguish plants of different agronomic groups, we performed a principal component analysis (PCA) evaluating the compactness (C), green index (GI), stomatal conductance (SC), sensor response (R), NIR intensity (NI), and digital biovolume (DB) as variables. The first two components explain 71.1% of the variability (Figure 11). The first PC (PC1) explains almost a half (49.1%) of the phenotypic variation, which perfectly separated stressed plants from control plants. Stomatal conductance (SC) and digital biovolume (DB) have large positive loading on the PC1. The regularly irrigated controls and the drought-stressed plants are well separated in the biplot indicating the efficacy of the drought treatment[59].

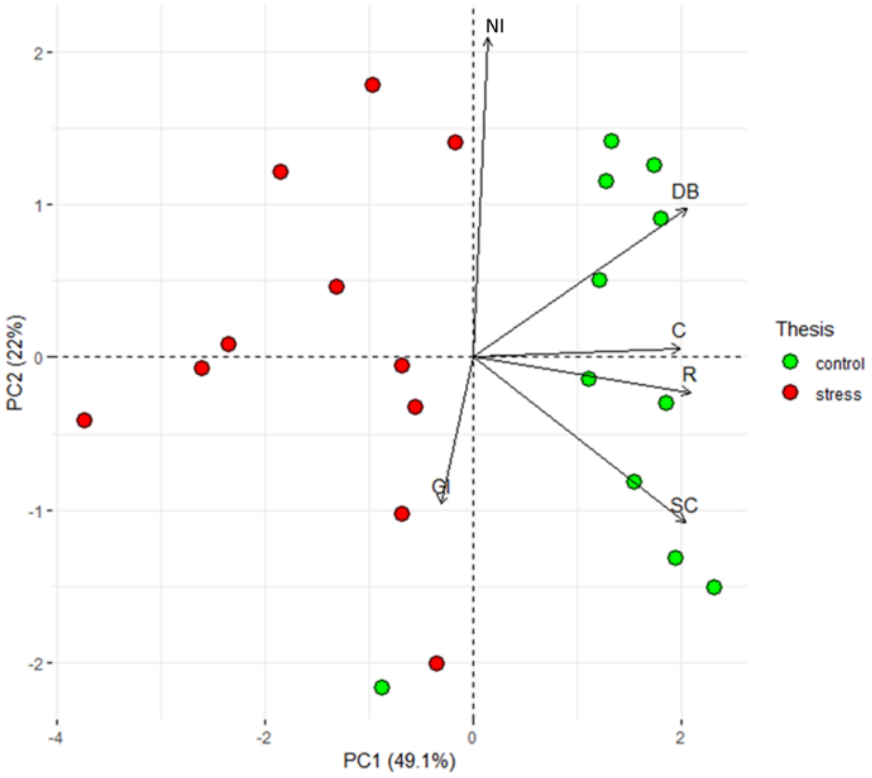

Figure 11: Biplot showing the PCA results. The first two PCs display 71.1% of the total phenotypic variation observed in 11 days of drought stress. The component scores (shown in points) are colored according to the agronomic groups (red, drought stressed plants; green, control plants). The component loading vectors (represented in lines) were superimposed proportionally to their contribution. C: compactness; GI: green index; SC: stomatal conductance; R: sensor response; NI: NIR intensity; DB: digital biovolume[59].

3.2 Understanding the defence response mechanism by monitoring the tomato mutant *Lcy-e1*

Here a small introduction on the strategy used to obtained the novel tomato mutant lines called TILLING and its importance in plant breeding will be given The goal of this experiment is to understand whether Bioristor is able to detect the improvements in the plant defense response operated by the introduced mutation in the *Lcy-e* gene. The *Lcy-e* gene is involved in the metabolic cascade that ends with the biosynthesis of abscisic acid (ABA), that is one of the key players in water stress tolerance. Therefore, the increased biosynthesis of ABA could lead to the generation of plants more resistant to water stress. This experiment was conducted in collaboration with the ALSIA genetics laboratory.

3.2.1 Mutagenesis and TILLING to dissect gene function in plants

Briefly, being among the main factors of phenotypic diversification, hereditary genotypic variation is one of the fundamental drivers of evolution. Thus, natural alleles and induced mutations were used as tools to study the gene function of plants and to develop crops with agronomically important characteristics (http://mvgs.iaea.org/). The Targeting Induced Local Lesions in Genomes (TILLING) method is considered the most robust, transverse, productive, and being non-transgenic allowed to use the obtained lines as material for breeding[67,68]. In TILLING mutagens such as ethylmethanosulfonate (EMS) are typically used to induce random single point mutations throughout the genome. The adult plant resulting from a mutagenized seed is called chimera because different cells that make up the plant are characterized by different mutations (M1). In a second step the chimeras must be dissolved by self-fertilization or *in-vitro* techniques before the mutation screening (M2). In the third and last step the DNA of each M2 is collected for mutation screening, while the seeds of M3 are collected and stored as a reserve of germplasm.

ALSIA Metapontum Agrobios developed and exploit the LikoTILL Tomato TILLING database (http://www.agrobios.it/tilling/) which allows search on-line of images and phenotype data of an EMS tomato (cv Red Setter) mutant collection and allow us to validate the Bioristor efficacy in detecting physiological changes upon drought on this extraordinary material

3.2.2 Materials and Methods

Plant Growth and stress application

ALSIA performed the identification and characterization of induced point mutations in *SlLcy-e* gene (accession number Solyc12g008980) was done on the Red Setter TILLING platform[69] according to the experimental conditions described in Dalmais et al., 2008[70]. The *Lcy-e* gene encodes the lycopene ϵ-cyclase that, by using lycopene as substrate and along with lycopene β-cyclase, makes α-carotene and consequently lutein (Figure 12). The allelic variation *Lcy-e1* was identified and showed modifications in the carotenoid content of leaves and fruits, theorizing a consequent increase of the amount of abscisic acid (ABA) in the plant, and therefore an improvement of the stress tolerance.

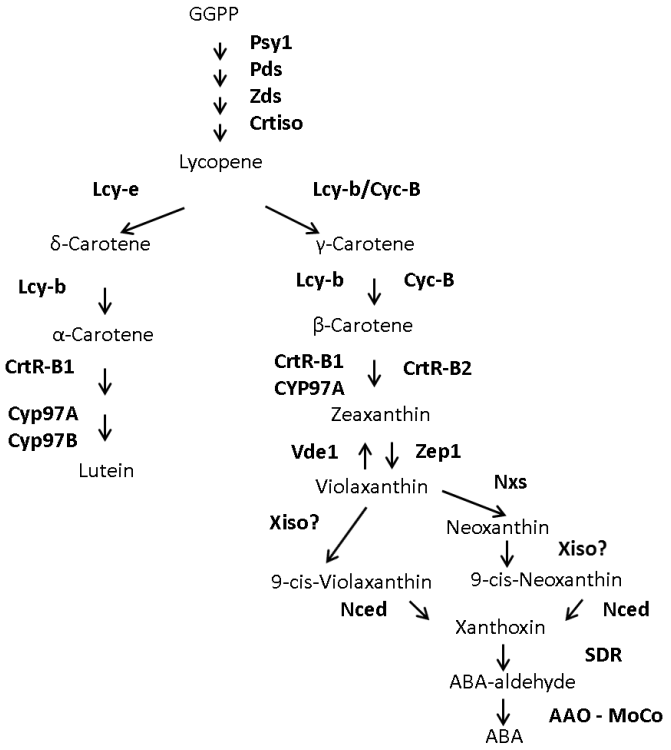

Figure 12: The ABA metabolic pathway. Each word in bold indicates an enzyme.

Mutant plants and Red Setter wild type used as control were grown both in greenhouse at 22 °C day, 16°C night and 12h day length. The experiment took place during the last two weeks of July in the ALSIA greenhouse with an average daily temperature of 30°C, a relative humidity of 45% and solar

radiation of 167 Par, 15 plants of Red Setter control genotype and 15 plants of lcy-e1 were grown in 16 cm diameter soil-filled pots and fully irrigated until the 5th-6th true leaf stage.

At this development stage, for each genotype, 7 plants were irrigated with 250 ml of water twice daily, early the morning and in the evening. 8 plants were exposed to drought stress by withholding watering for 12 days. Before the drought stress imposition, leaf material was collected from mutant and control tomato genotypes (day 1) and from stressed and well-watered plants at 4 and 10 days. At 1-, 4- and 10-days leaf material was harvested at same time in the morning (9:00 AM) and for each genotype and for each experimental condition (stress and no stress application) leaf tissue was harvested from 3 independent plants (3 biological replicates). The sampled green material was soon stored at -80 °C then lyophilized and used in the carotenoid analysis measurements.

Bioristor monitoring

The Bioristors have been prepared, inserted into the stems of plants, and connected to a computer using a multichannel digital analogic converter (National Instruments Corporation), following the method described in Chapter 2. The calculated R parameter at gate voltage of 0.6V (see Chapter 2) was analyzed with MATLAB (https://uk .mathworks.com/) and Microsoft Excel 2016). Then it was mediated over the day to smooth out day/night oscillations for each of four theses. The normalized sensor response (NR) was shown as the Bioristor output and it was calculated as the ratio between R of stressed and non-stressed plants.

Finally, an analysis of the principal components (PCA) using the "prcomp" function of R (https://cran.r-project.org/doc/ FAQ/R-FAQ.html#Citing-R) has been performed to distinguish the different phenotypic profiles of the two theses. The relationship between variables provided by the different image indices, Bioristor and stomatal conductance have been analysed represented as biplot (R package factoextra)[71].

Biochemical, Physiological and Imaging analysis

To validate the results obtained with Bioristor, ALSIA performed the analyses of the carotenoid content as previousely described in D'Ambrosio et al 2011[72]. The two-leaf stomatal conductance was also measured for each plant, using a porometer SC1 (Decagon Devices, Pullman, WA, USA).

Non-destructive plant phenotyping, the image analysis was carried out through the use of phenotyping Scanalyzer 3D LemnaTec GmbH by taking three images: one from top view of the plant and two

from side view (0 ° and 90 °). The imaging, initiated prior to the imposition of drought stress (day 1), using near-infrared (NIR) and white (RGB) illumination. The NIR images were used to evaluate the plants' water content; the RGB ones were for the assessment of both the plants' state of health (green: healthy tissue, yellow: chlorotic tissue, and brown: necrotic tissue) and for morphological measurements; these data were used to calculate the plants' biovolume and height; their biovolume (a parameter proportional to the aerial mass of the plant) was calculated from the expression:

$$\frac{\Sigma pixel\ sideview\ 0° + \Sigma pixel\ sideview\ 90° + Log\ \Sigma pixel\ sideview}{3}$$

following Eberius and Lima-Guerra, and Petrozza et al[60,61].

Plant compactness, which describes how much of the hull area is covered by leaves, was calculated as object area/convex hull area[62]. The NIR index was calculated as weighted mean from the pixel intensities of greyscale NIR images divided into 128 bins, representing a range in leaf water content.

Those measurements were coupled and statistically analyze to validate the Bioristor measurements.

3.2.3 Results

Seven stressed and three well-irrigated tomato plants for each genotype (Red Setter wild type and mutant) were *in-vivo* monitored for a total of 14 days. The trend of the two curves starts to differ from the beginning of the water stress (day 1). In particular, NR of wild type plants showed, as expected and previously reported, a drastic and continuous decrease with two drought avoidance picks at day 3 and 4 as previously reported for the same cultivar[59]. Then, the sensor response reached a steady level at day 4 that continue till the end of the drought stage (Figure 13).

On the contrary, the NR of the mutant plants showed a slight decrease after 12h from the beginning of the stress and then the slope showed a rapid and continuous increase up to day 4 reaching maximum values leading to hypothesize the accumulation of osmolytes and compounds triggered by a defense response. From day 4 to day 10, the NR slope rapidly decrease indicating a stress condition, reaching

at day 10 an NR value comparable with the pre-stress. A second increases was observed from half of day 10 till the end of the experiments.

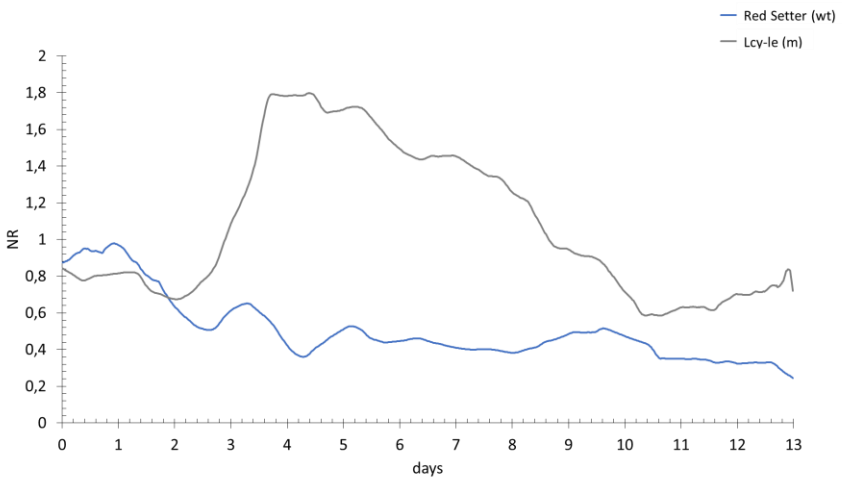

Figure 13: Plot of the daily smooth average of the NR measured on all *Lcy-e1* mutant plants (gray line) and wild type Red Setter plants for all days (blue line).

The chosen indices involved three based on RGB images (digital biovolume, plant, plant compactness, and green index) and one based on NIR images (hydration index). The growth of the plants, as indicated by their digital biovolume, height, compactness and their hydration status were not strongly affected by the drought treatment.

By performing the Analysis of Variance (ANOVA) on R values of controlled and stressed plants for both treatments to consider all possible variables, showed a high significance difference between all four theses ($p \leq 0.001$) throughout the stress period of the experiment.

The correlation analysis carried out between the data collected by Bioristor and both imaging and physiological surveys confirms that Bioristor can monitor the physiological mechanisms related to changes in ionic concentration in the lymph of the plant, in relation to the transpiration flow of the latter. A strong, highly significant correlation has been observed between sensor response (R) and stomatal conductance (SC) ($r = 0.74$, $p \leq 0.001$; Figure 14).

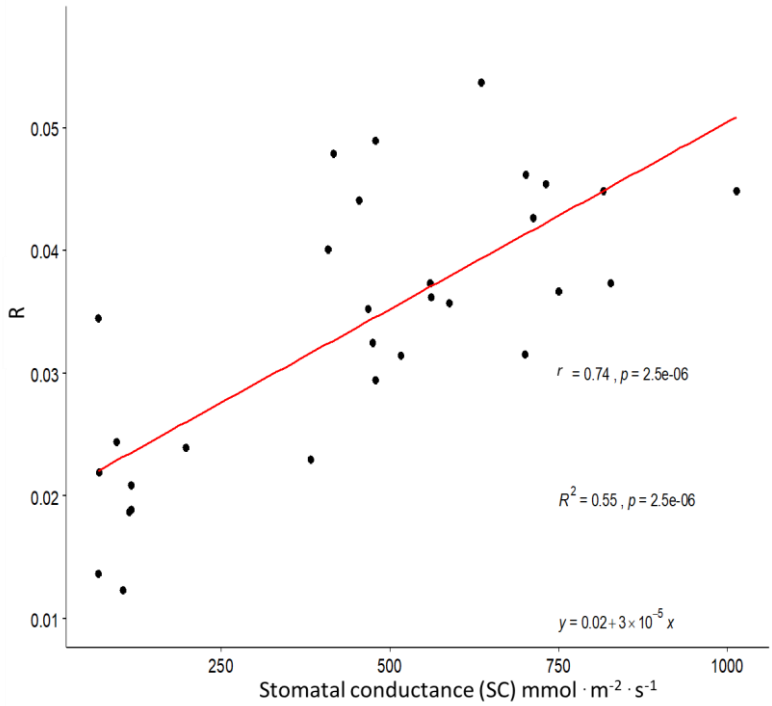

Figure 14: Scatter plots of the sensor response (R) and stomatal conductance (SC) measured on control and drought-stressed plants for each genotype. The scatter plot and linear regression displayed indicate a strong correlation between the two variables, with a correlation coefficient of r = 0.74. $p \leq 0.001$ indicates the statistical significance level of the observed correlation.

The trend R values, and trend have been compared with those recorded thanks to high throughput imaging techniques. For this purpose, the R value was correlated with the digital biovolume as a clear stress indicator[66]. A strong and significant correlation ($r=0.7$, $p \leq 0.05$; Figure 15) was observed, demonstrating the validity of the sensor response the effectiveness of Bioristor to monitor *in-vivo* physiological effects of water stress on plants.

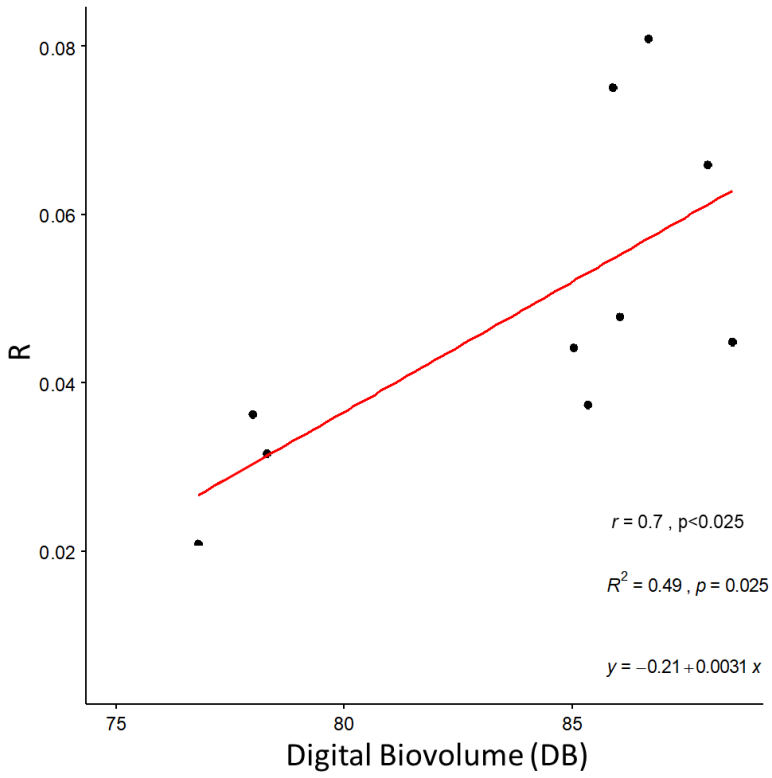

Figure 15: Scatter plots of the sensor response (R) and stomatal conductance (SC, mmol) measured on control and drought-stressed plants for each genotype. The scatter plot and linear regression displayed indicate a strong correlation between the two variables, with a correlation coefficient of r = 0.7; $p \leq 0.05$ indicates the statistical significance level of the observed correlation.

The first two components (PC1 and PC2) explain 83.6% of the variability of the described phenomenon (Figure 16). The first PC (PC1) explains 62.31% of the phenotypic variation, and perfectly separates the genotypes and the different treatment. The wild type stressed plants are separated in the biplot from all other genotypes, indicating that drought stress strongly impacted on all traits analyzed. The presence of the mutant genotypes with the control wild type not stressed, suggest the importance of the mutation in relieving the effects of drought stress.

The PCA confirms that R and stomatal conductance are positively correlated (R^2=0.55, $p \leq 0.01$) as previously demonstrated[59,73,74].

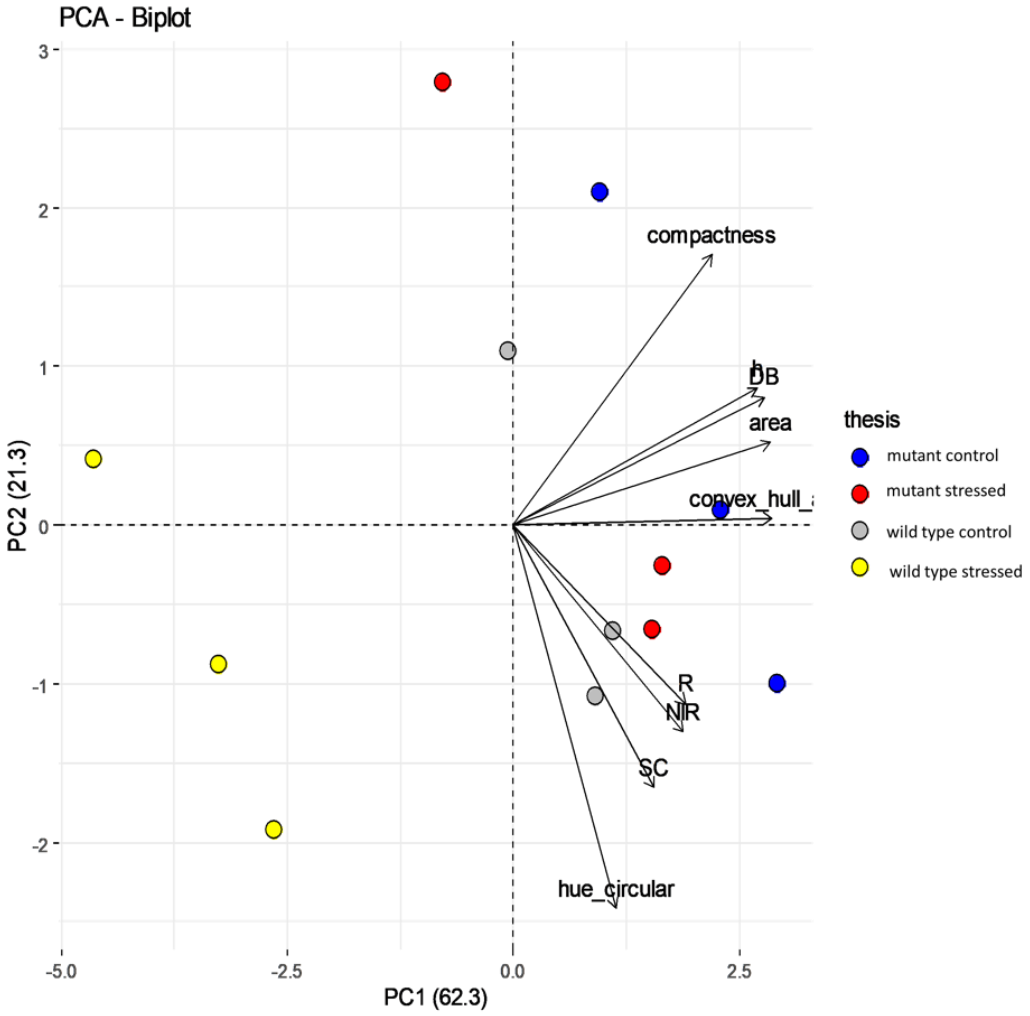

Figure 16: Biplot showing the PCA results. The first two PCs display 83.6% of the total phenotypic variation observed. The component scores (shown in points) are colored according to the combination of agronomic and genomic groups blue, control mutant plants; red, mutant water stressed plants; grey, wild type control plants; yellow, wild type water stressed plants). The component loading vectors (represented in lines) were superimposed proportionally to their contribution. C: compactness; SC: stomatal conductance; R: sensor response; NIR: NIR intensity; DB: digital biovolume; h: height; area; convex_hull_area; hue_circular.

A further step of analyses was conducted to direct link the R values with different drought tolerance of the genotypes analyzed because of the specific mutation carried in the *Lcy-e1* mutant.

With this purpose a correlation analyses was performed between R and the violaxantina content showing a high and significant correlation (R^2=0.67, $p \leq 0.001$) between these traits (r=0.82, $p \leq 0.001$; Figure 17), suggesting a link between the increase in NR in stressed mutants and the increase in violaxanthin produced in the *Lcy-e1* mutant.

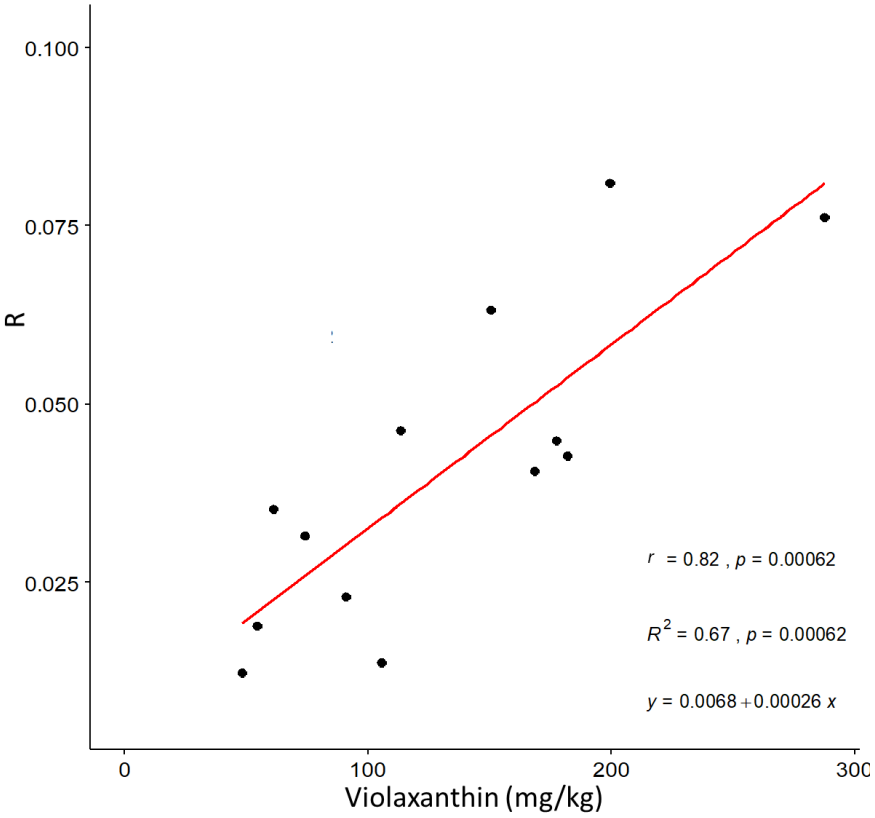

Figure 17: Scatter plots of the sensor response (R) and violaxanthin measured on control and drought-stressed plants for each genotype. The scatter plot and linear regression displayed indicate a strong correlation between the two variables, with a correlation coefficient of r = 0,82; p ≤ 0,001 indicates the statistical significance level of the observed correlation.

3.3 The use of biostimulants to reduce drought stress effects in agriculture. Can Bioristor detects biostimulants effects?

The use of biostimulants on water-stressed plants is a promising new approach to limit the effects of water scarcity on plants[75–77]. This section will describe the monitoring of biochemical and physiological effects of glycine betaine on stressed plants. Exogenous glycine betaine applications have been proven to induce the expression of genes involved in oxidative stress responses, with a restriction of ROS accumulation and lipid peroxidation in cultured tobacco cells under drought[78] and salinity stress, and even stabilizing photosynthetic structures under stress[79].

3.3.1 Material and methods

Plant Growth and stress application

The experiment was performed at the Catholic University's laboratories (Piacenza, Italy). The trial was based on 12 plants. Here a commercial biostimulant composed by glycine betaine > 30% w/v was used, as a source of glycine betaine, in doses of 100 mL per each treated plant. When the plant reached the stage of the first flower, the sensors were integrated and after 4 days, six of the plants were treated with glycine betaine. Later, 6 drought-stressed and 6 well-watered plants have been monitored from day 7 for 4 days; within each thesis there are 3 plants treated with glycine betaine and three untreated plants (Table 1). The stressed plants were then irrigated over 36 hours from day, and, finally, a 2 days stress episode was imposed to all plants by withholding water (Table 1).

Table 1: Schematic illustration of the experiments conducted by Catholic University's laboratories (Piacenza, Italy).

Days	*Operation*
4	glycine betaine treatment
7-11	1st drought stress
11-12	Recovery
12-14	2nd drought stress (all plants)

Bioristor measurement

The R index (analyzed with MATLAB (https://uk .mathworks.com/) and Microsoft Excel 2016) was smoothed on days to eliminate variations related to the circadian cycle.

Data were statistically analysed using R software v3.4.1 package 9 (https://www.r-project.org/). Principal components analysis (PCA) and k-means cluster analysis were performed using the "prcomp" function in the R package factoextra[71] (https://cran.stat.unipd.it/bin/windows/ contrib/3.5/) and showed as a biplot. PCA and k-means cluster analyses were performed to better dissect the single components of the defence response. The first two principal components (PC1 and PC2) and the corresponding component loading vectors were visualized and summarized in a biplot, in which component scores (indicated in dots) were colored according to thesis classification.

3.3.2 Results

Tomato plants were monitored over 14 days.

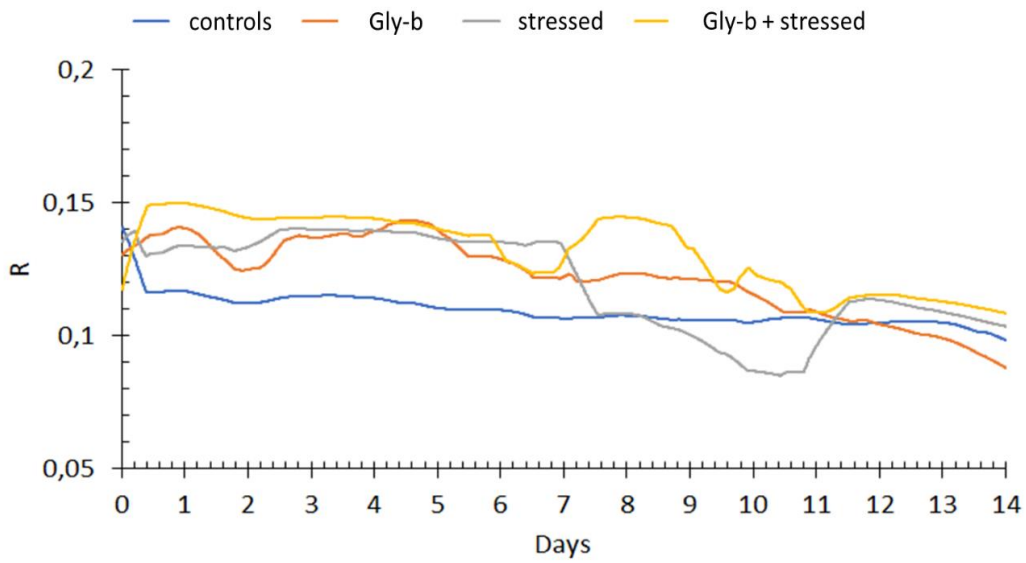

Figure 18: Plot of the daily smooth average of the R measured on all well-watered plants (blue line), biostimulant treated plants (orange line), drought stressed plants (grey line) and drought stressed plants treated with biostimulant (yellow line) for 14 days.

All the plants have been irrigated regularly irrigated at 90% of field capacity for 7 days. This was evident also when R was analysed and a same trend in the sensor response for all thesis was observed. From day 7 irrigation was suspended for 4 days to three plants control and three biostimulant treated plants. The slope of the R in the stressed plants decreases of about 35% in this time window while, the R of the stressed plants treated with glycine betaine, showed a rapid increased of the R signal that remains stable for 48 h, reasonably as a consequence of the establishment of the onset of defence responses. After a small decrease, the R slightly increased again as a second round of defence response. Then the R slowly decreases until the end of the stress period.

From day 11 to day 12, the irrigation was restored for all theses, which involved a reset of the R signal more consistent for the stressed plants, and the stressed treated plants. From day 12 until till the end of the experiment a drought stress was re-imposed and a slight decrease in the R response observed in all thesis with the exception of the control (Figure 18, blue line).

The ability of Bioristor to fine detect the onset of the drought stress, is clearly evident at day 5 where the regular irrigation was suspended as immediately detected by Bioristor that showed a drop of the sensor response.

In Figure 19a, we reported all Bioristor measure (see Chapter 2) expressed as a function of the first two principal components, PC1 and PC2. Each point in the diagram describes the state of the system measured at specific times for each plant.

PCA was performed for all plants and then validated by cluster analyses. The first two principal components (PC1 and PC2) explain 57.7% of the total variance and allowed for a clear separation of variables in two different groups (Figure 19b) confirming the hypothesis that effects of drought stress on plants physiology are correctly tracked by the sensor. The first PC (PC1) explains 39.1% of the phenotypic variation and shown a clear separation of two super groups, in fact controls and the stressed plants are well separated in the biplot. The sensor response (R) and its first derivative (dR) are negatively correlated with ΔI_{gs} and $d\Delta I_{gs}$ (sensor wettability status indices, see sections 1.3 and 2.4), respectively. From the PCA plot analyses, the control super-group seems to be more influenced by R and dR, thus on the cation dissolved in the plant sap. Moreover, drought stressed treated plants belong to the super group of control plants, supporting the effectiveness of glycine betaine in enhancing stress tolerance in plants. Controls and the stressed plants are well separated in the biplot indicating. Moreover, drought stressed treated plants belong to the super group of control plants, proving the effectiveness of glycine betaine in increasing stress tolerance of plants. The two super groups well irrigated and stressed plants were also confirmed by the cluster analyses. In addition, this separation showed that also pre-treated stressed plants belong to the first group, confirming the ability of glycine betaine in increasing plant resistance to water stress. After PCA, sample points are clearly separated in two clusters: thus, the technique correctly operates sample classification on the basis of their originating time of measurement.

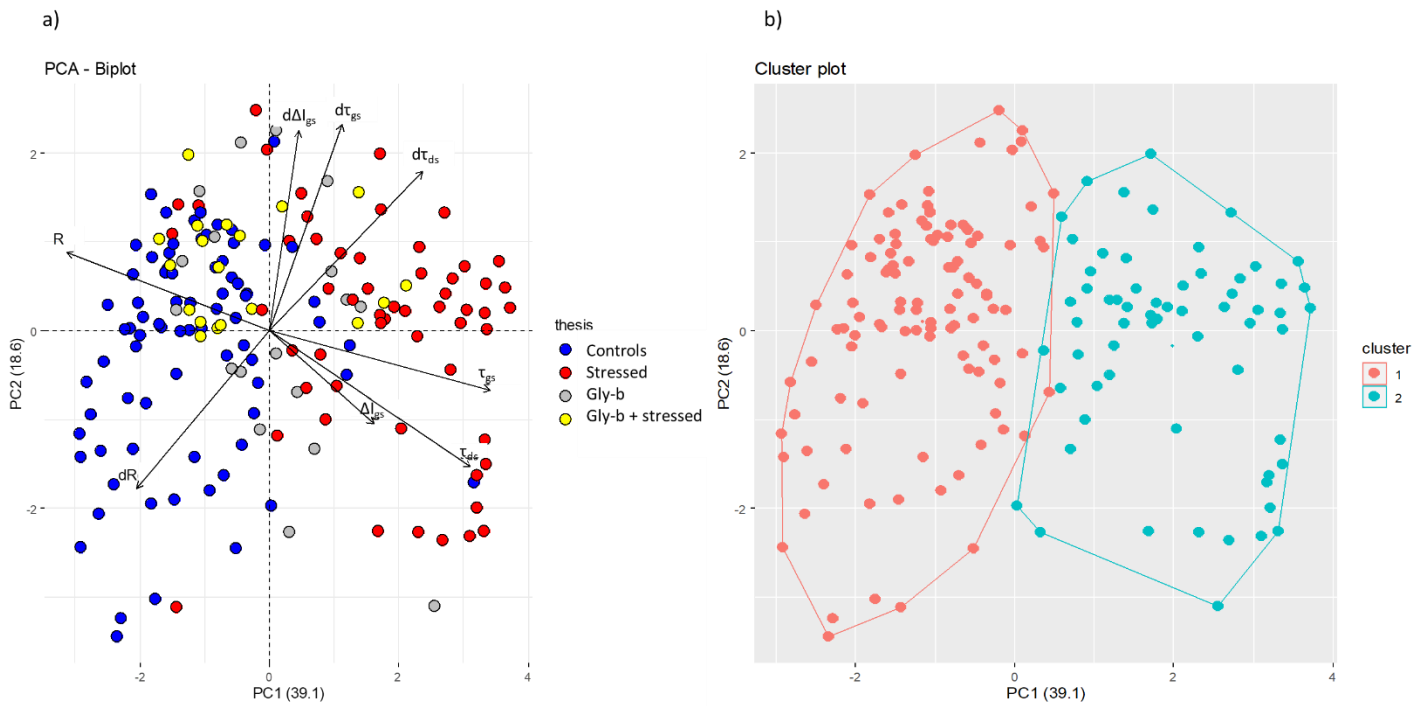

Figure 19: a) Principal component analysis (PCA). The component scores (shown in points) are coloured according to the agronomic groups: blue, control untreated plants; red, stressed untreated plants; grey, wild type control treated plants; yellow, treated stressed plants, ΔI_{gs}; difference between minimum and maximum current gate values, τ and τ_{gs}; time constant. From the acquired data, the first derivative of R, ΔI_{gs}, τ and τ_{gs} (dR, $d\Delta I_{gs}$, $d\tau$ and $d\tau_{gs}$) were calculated. The first two components PC1 and PC2 explain the 57.7% of the variability observed. Each dot represents a plant each day. b) The clustering was performed using k-means distance calculation

3.4 Bioristor monitoring of fruit trees (*Actinidia chinensis*, kiwi fruit) under drought stress

The effectiveness of the Bioristor in detecting the physiological response to drought stress in a horticulture species such as tomato, this chapter aim at demonstrating the effectiveness of Bioristor in monitoring fruit tree species as *Actinidia chinensis* (kiwi fruit).

3.4.1 Materials and Method

Plant growth and stress conditions

The experiment was conducted at the laboratories of CNR-IMEM in Parma on five kiwi plants kindly supplied by Apofruit Italia - Coop. Agricola and grown outdoor in 7 dm^3 pots in May 2020. Pots were irrigated at field capacity and weighed to monitor the soil RSWC (Relative Soil Water Content). Pots weight was monitored throughout the experiment and compared with the weight of the pot at field capacity to obtain on the percentage of the irrigation volume and, indirectly, on the amount of the water losses form plant and soil transpiration. Plants were randomly divided into 2 control plants and 3 stressed plants. All plants were watered daily to field capacity until day 2, to allow the sensor to settle. From day 2 controlled plants were regularly irrigated up to 80% of the field capacity, while drought stress was imposed by irrigating up to 60% of the field capacity. Being outside plants were subjected to climate conditions, thus a storm occurred between day 5 and day 6 complete restored the field capacity in all thesis, thus a second round of drought stress was imposed by keeping the plants at 60% of the field capacity (Table 2).

Table 2: Schematic illustration of the experiments conducted kiwi plants in controlled environment.

Days	*Irrigation*
0-2	Field capacity (100%)
2-5	I differential irrigation (control: 80%, stress: 60%)
5-7	Rain (recovery)
7-12	II differential irrigation (control: 80%, stress: 60%)

Bioristor monitoring

Bioristors were prepared and inserted in the plants trunk and connected to a computer using a multichannel digital analogic converter (National Instruments Corporation), following the method described in Chapter 2. The R index (analyzed with MATLAB (https://uk .mathworks.com/) and Microsoft Excel 2016) was smoothed on days to eliminate variations related to the circadian cycle.

Physiological measurments

Being the first time that a fruit tree was measured with Bioristor a series of physiological measurements were performed to ground validating the Bioristor output. In detail the relative water content (RWC)[55] was recorded in two fully expanded leaves for each plant and calculated as reported by Barrs and Weatherley, 1962[55].

3.4.2 Results

The R values mediated over the day to smooth out day/night oscillations (Figure 20) were collected and analysed for a total of 12 days.

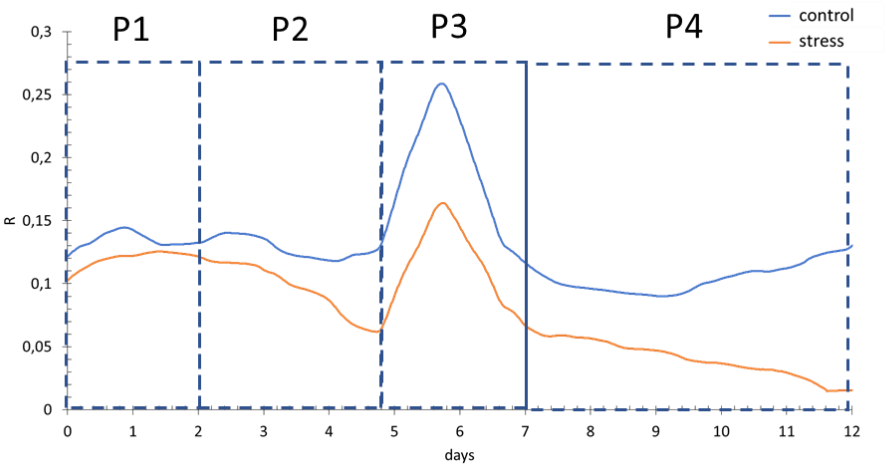

Figure 20: Plot of the daily smooth average of the R measured on all well-watered plants (blue line) and drought stressed plants (red line) for 12 days of measurements.

Four distinct phases have been recognized in the kiwi measurements with Bioristor according to the R variations. The first phase (P1, day 0-2) identifies the first two days after the implantation of the sensor; the second phase (P2, day 2-5) is evidenced by a constant and continuous decrease of stressed plants' R that corresponds to the beginning of the decrease of the irrigation. On the contrary, control plants showed a steady level of the R signal being regularly irrigated. The third phase (P3, day 5-7) is characterized by an increase of R for both theses related to a storm registered in those two days that completely restored the plant hydration level. The registered increased of R values ranging between 116 and 175 % can be due to the strongly increases of the air relative humidity surrounding the plant

leaves causing in turn a reduction in transpiration and of the water flux in the xylem causing the consequent concentration of solutes in the sap (see Chapter 3).

During the fourth phase (P4, day 7-12) a second and prolonged drought events occurred in correspondence of which the Bioristor measured a greater and more sudden decrease of R value of the stressed thesis. In addition, if we compare the percentages of irrigation with the daily trend of R of both theses, the irrigation of the stressed thesis goes below 80% during the fourth phase and reaches 60% only from day 8. This data is consistent with the greater decrease of the signal of R that distinguishes phase four.

3.5 Discussion

Plants commonly experience periods of drought in the course of their life cycle[80]. Drought stress therefore represents a critical constraint for crop productivity[81]. The ability to detect drought stress before it causes irreversible physiological and morphological damage is important for crop management, to increase the water use efficiency in agriculture and to accelerate the selection of more adaptable crop varieties to drought. Conventional phenotypic assays for drought tolerance are often labor intensive and rely on the operator experience, so the development of automated phenotyping platforms represents a promising advance[82] in plant breeding and precision agriculture. Current platforms combine the robotic handling of plants with sensors and high-end computing to capture high-resolution, highly precise data in a high-throughput mode[82]. Their ability to collect data in real time in a nondestructive manner allows for potential insights to be gained into the temporal response of large numbers of plants to a particular treatment. Moreover, an image-based index (RGB, NIR, and FLUO) is increasingly used to study the plant defense response mechanisms upon drought stress both in controlled conditions[81] and in the open field[83]. The development of both proximal and remote sensors has been accelerating in the last decade, however, the availability of simple-to operate and affordable sensors which can be implanted within the plant is still missing. In this scenario, Bioristor represents a model technology for generating *in-vivo* high-resolution data able to monitor the plants' physiological status in real time and continuously. The Bioristor was able to detect for the first time *in-vivo* the onset of drought stress within 30 h from the water withholding, and this is extremely relevant in terms of water use sustainability in the open field. In addition, its capacity to monitor the plants' physiological status on a continuous basis, rather than relying on sampling at a series of

discrete time points, should greatly enhance the data's value in the context of understanding how plants respond to drought stress. Plant breeding in order to release variety more adaptable to the predicted changes in climate demands detailed knowledge of the mechanisms underlying the tolerance of plants to water deficiency and their ability to escape the stress. Changes in the composition of the xylem sap can represent a major component of the drought defense machinery. Moisture deficiency inevitably reduces a plant's water content, thereby altering both the concentration of solutes in its transpiration stream and the mass of solutes exported from its roots at a given time[84]. Several reports described the changes in nutrient and ion uptake and transport in plants during the occurrence of drought stress. In particular, a reduction in nutrient uptake by the roots partially due to the reduction in soil moisture was observed, which causes a decreased rate of nutrient diffusion from the soil matrix to the absorbing root surface[85] and translocation to the leaves[86,87]. During stress, a reduction in the general mineral accumulation[87] in the plant tissues together with a general low nutrient availability in the soil and lower nutrient transport in plants was also reported[85,88]. Stomatal closure is also a known mechanism of drought resilience that reduces transpiration, the nutrient transport from the roots to the shoot, and causes an imbalance in active transport and membrane permeability, resulting in a reduced absorption power in the roots[85,89–91]. A direct measurement of the plant sap content during the drought stress also demonstrated that the amount of K^+ ions gradually decreased in the xylem sap of maize plants[88]. The Bioristor has been designed to detect the movement and concentration of electrolytes through the vascular tissues. Its application in the context of tomato and kiwi plants exposed to drought stress has shown that changes in both the composition and the concentration of key solutes occurred within 30h of the withholding of water. Xylem flux, transpiration rate, solubilization, and translocation of solutes are all negatively affected by drought stress in a range of plant species[88,92–95], including tomato[92,96] and kiwi[97]. In addition, the development of more drought-resistant crop plants needs and an in-depth understanding of the adaptive mechanism and responses to water stress. Since bioristor was proposed as tool for *in-vivo* phenotyping, was used to monitor new tomato lines carrying a mutation in the *Lcy-e* gene that should promote an higher accumulation of ABA in drought stressed plants, conferring higher tolerance to this stress. Several papers have described the importance of ABA as hormones of the abiotic stress response; in these conditions the slight pH alkalinization (from pH 6.3 to pH 7.2) leads to the dissociation of ABA[46] in ABA^- and H_3O^+. Chemically, the hydronium ion (H_3O^+) behaves as a cation, whose growth leads to a net increase of the Bioristor response. To confirm the ability of the Bioristor to monitor the high concentrations of ABA contained in the xylem of mutant plants, a high correlation between violaxanthin and the response of the Bioristor has been observed. A similar trend has also been identified in tomato plants that before being stressed had been treated with glycine betaine. Indeed

the increase in R of treated plants increases for 48 hours from the onset of stress as a consequence of the detection of the ABA accumulated, translocated and compartmentalized in xylem sap due to the combined effect of glycine betaine and drought stimulate the production of ABA[98], as well as its translocation and compartmentalisation[77]. Moreover, the ABA accumulation involves the release of potassium from the guard cells causing the loss of turgor of the guard cells and the consequent stomatal closure[46].

Here our data support the hypothesis that, as a result of the reduction in the transpiration rate in the early phases of the plant defense response, a reduction in the concentration of ions in the xylem sap[88], and a significant increase of ABA in mutant plants. The integration of the Bioristor data with image-based analyses has provided insights into the timing of the tomato phenotypic and physiological response. It suggests that at the start of the drought stress response, a change in the transport, allocation, and production of metabolites and ions occurs within the plant, which acts as a signal for stomatal closure and the subsequent decrease in transpiration. The high correlation coefficient between the sensor response (R), stomatal conductance (SC), and digital biovolume (DB) confirms the hypothesis that the Bioristor can detect ions and molecules related to the drought stress and, in particular, those dissolved and transported through the transpiration stream, thus efficiently detecting the occurrence of drought stress immediately after the priming of the defense responses. A difference in the extent and timing of a possible drought avoidance (Figures 3 and 5) was observed between the two cultivars tested, together with the different responses to water stress monitored between red setter wild type plants and mutants (Figure 13). These findings open new perspectives for the use of a Bioristor as a tool to study and select drought tolerant genotypes and varieties. Finally, the combination of the image based of the phenotyping platform, and of the Bioristor values in a PCA, allowed for the clear separation of stressed and unstressed plants and the clear identification in the plot of the mutant genotypes. Similar results were obtained when plants were treated with biostimulants, where a clear signal was observed in the mutant lines and correlated to the *Lcy-e1* mutation.

These results here described paves the way to deepen the knowledge in the onset of the defence mechanism triggered during the drought stress with a focus on the ionomics.

Chapter 4

In-vivo monitoring of the effects of Vapour Pressure Deficit (VPD) on plant physiology

Vapour pressure deficit is widely consider as the driving force of the water uptake from the soils since has a strong impact of plant transpiration[99] and is one of the main environmental features impacting on protected cultivations[56] that so far produced about 50% of the fresh vegetables due to the reduction of land and water availability.

The greenhouse environment, if properly managed, can significantly increase yield and quality; in fact, more than 1560 world producers choose controlled environment for vegetables cultivation, with 405,000 hectares of greenhouse space dedicated to vegetable production worldwide[100]. In the upcoming years, the application of greenhouse automation, sensors, and distributed and pervasive computing will allow provision of the optimal growth and cultivation conditions for vegetables[101].

Technology should be improved to better controlled and set greenhouses to reduce the carbon and water footprint. Among the parameters that can be controlled, VPD plays a major role in estimating the real loss of water by the plant and for increasing plant water use efficiency notwithstanding its indirect evaluation through the measure of air temperature and relative humidity[102]. From a physics perspective, water transport along the soil-plant-atmosphere continuum is a passive process driven by gradients of free energy. As mentioned before, the driving force for water movement is the transpiration rate that is determined by changes in VPD along the gas phase (from internal leaf to the atmosphere) and is expressed as a combined function of air temperature and relative humidity[103–106]. Previous papers investigated the effects of VPD on the transpiration rate[107] and on plant growth (mainly on decreased leaf area)[108] and highlighted that VPD regulation can improve water use efficiency, with concomitant improvements in biomass and fruit production[109]. The possibility to monitor the effects of VPD changes is becoming of great interest in greenhouses with technology developers aiming to provide fine regulation of atmospheric moisture to positively affect the reduction of water consumption and improve water use efficiency under cultivation. However, so far, few remote and proximal devices have been tested and are available to monitor the environmental conditions as humidity, temperature, lux, and CO2 content (Table 1) and in turn to assess the VPD.

The implementation of tools to correlate the effects of VPD environmental on the plant physiology is mandatory to increase the efficiency of indoor growth and production.

Table 1. Climate remote sensors for environment measuring of VPD[56]

Sensors	**Type of sensor**	**References or web link**	**Technical notes**
Smart Bee system	Remote	https://hightimes.com/grow/understanding-vapor-pressure-deficit/	Measure of air temperature and humidity
Microcontroller run in Arduino	Remote	Ramos-Fernandez et al., 2016[110]	Fuzzy modelling
Pointed Microclimate sensor	Proximal	https://www.30mhz.com/industry/agriculture/	infrared temperature sensor+vented temp/ humidity sensor
Digital infrared thermometer (Model GM320)	Proximal	Zhang et al., 2017[111]	
smart sensor	Remote	Millan-Almaraz et al., 2010[112]	air temperature, leaf temperature, air relative humidity, plant out relative humidity and ambient light
Pulse One	Remote	https://getpulse.co/	Remote monitoring of temperature, RH, light, and VPD
Micro Grow's Water Pro	Remote and proximal	https://microgrow.com/	Irrigation controller through environmental monitoring with 11 sensors. VPD is included and estimated by temperature and relative humidity
Digital infrared thermometer (Model GM320)	Proximal	Zhang et al., 2017[111]	Measure of the leaf temperature
ATMOS 14	Climate remote sensors	www. growlink.com	temperature, relative humidity, barometric pressure, and vapour pressure

The focus of this chapter is to gain additional information on how VPD can affect the ion status in the plant sap and to establish a correspondence between the R (the response of the OECT) and a physical characteristic of the system, paving the way for the use of Bioristors as an innovative tool to achieve a sustainable use of natural resources.[56]

4.1 Material and methods

Plant growth and environment conditions

Five tomato plants (*S. lycopersicum L.*) cultivar Ikram were grown in 2.6 L pots up to the initial phase of flowering development[109] 0.4 m^3 h cabinet, under a 16 h photoperiod; the Relative Humidity (RH) ranged from 55–70%. The growth chamber was equipped with a EasyLog data-logger (Lascar Electronics Ltd., Salisbury, UK) to monitor and register constantly the temperature (T) and RH (Table 2, Vurro et al., 2019)[56].

Table 2: Daily average of Temperature (T, °C), Relative Humidity (RH, %) and Vapor Pressure Deficit (VPD, kPa) for the 15 days of the experiment.[56]

Days	T (°C)	RH (%)	VPD (Kpa)
0	23,093	63,376	0,864
1	22,292	55,813	0,993
2	22,875	63,712	0,838
3	24,386	100,566	-0,014
4	23,757	102,733	-0,066
5	23,743	103,451	-0,084
6	23,462	103,816	-0,091
7	22,566	103,972	-0,090
8	21,917	85,128	0,320
9	21,077	62,786	0,784
10	21,449	75,313	0,530
11	22,382	101,208	-0,027
12	22,715	102,917	-0,067
13	23,331	103,503	-0,083
14	23,007	86,625	0,307
15	22,644	71,000	0,664

Plants were kept fully irrigated until their last phase of vegetative development, after which a Bioristor was inserted in the stem of each plant between the third and fourth leaves (Figure 1A,C)[56].

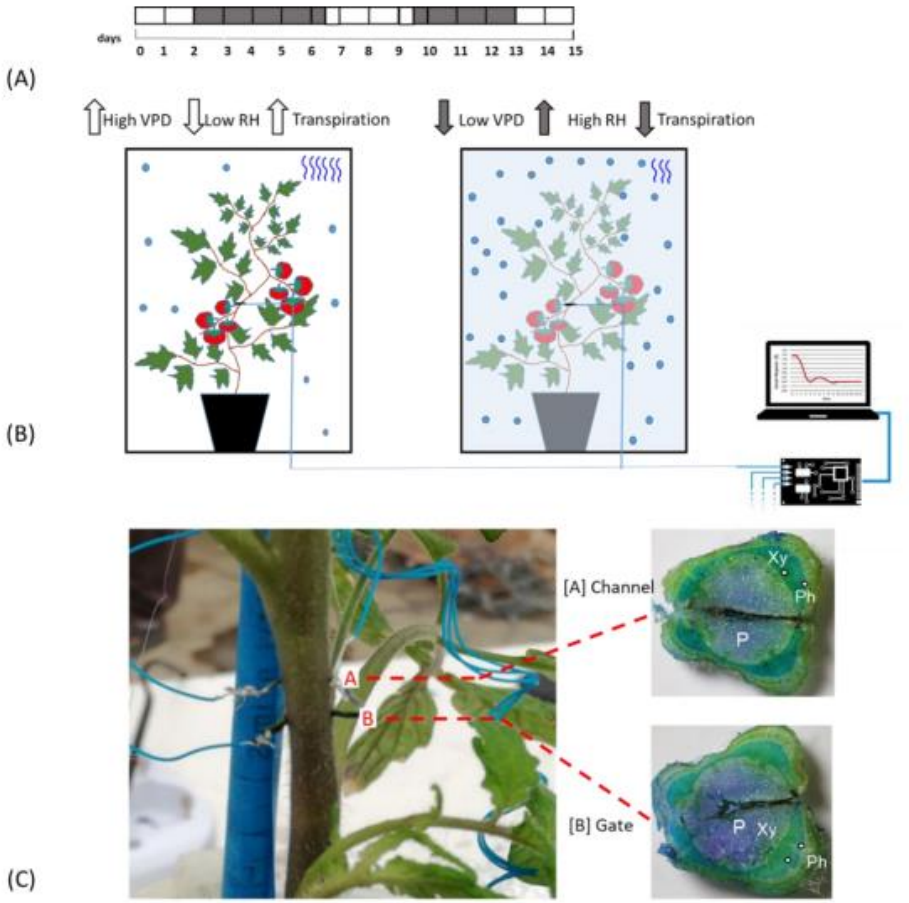

Figure 1: Experimental Outline. (A) Time line of the experiment. White blocks indicate the days in which plants are under normal VPD (0.1 and 0.8 kPa); grey blocks indicate the days of low VPD value (between 0.0 and −0.1.; (B) Scheme of the Bioristor measurements in high (left) and low (right) VPD conditions, the increases or decreases in the expected transpiration rate is also indicated as blue wave in the box; (C) Bioristor insertion in a tomato plant: A, channel and, B, Gate. The sections of the stem indicating the tissues crossed by the Bioristor are reported and the vascular tissue interested by the Bioristor are indicated P, pith; Xy, xylem; Ph, phloem[56].

All plants were irrigated over 2 days post insertion, and then exposed to low VPD by nebulization of 100 mL of water in the cabinet previously sealed with PVC film (2–7 days, Figure 1A). 200 mL of water was supplied to the plants when the growth chamber was opened and plants exposed to an increased VPD (7–10 days). From day 10–13 the VPD was again altered to confirm the previously observed mechanisms from 13 to 15 day, Figure 1A). On the basis of the parameters recorded with the data-logger, the VPD value was calculated as follows[56,113,114]:

$$VPD = \left(1 - \frac{RH}{100}\right) SVP$$

where RH is relative humidity and SVP is Saturated Vapour Pressure. The Saturated Vapour Pressure (SVP) was calculated applying the following equation[113]:

$$SVP = 610.7 \times 10^{\frac{7.5T}{237.3+T}}$$

where T is the temperature measured in the growth chamber[56].

Bioristor measurement

The Bioristors was prepared and inserted in the stems of plants and connected to a computer using a multichannel digital analogic converter (National Instruments Corporation), following the method described in Chapter 2. The calculated R parameter at gate voltage of 1V (see Chapter 2) was analyzed with MATLAB (https://uk .mathworks.com/) and Microsoft Excel 2016) to smooth out variations related to the circadian cycle.

Statistical analysis

Data were statistically analysed using R software v3.4.1 package 9 (https://www.r-project.org/). Principal components analysis (PCA) was performed using the "prcomp" function in the R package factoextra (https://cran.stat.unipd.it/bin/windows/contrib/3.5/)[71] and showed as a biplot. The first two principal components (PC1 and PC2) and the corresponding component loading vectors were visualized and summarized in a biplot, in which component scores (indicated in dots) were coloured according to time classification. PCA was performed for all plants and validated by cluster analyses.

4.2 Results

Analyses of the Bioristor Response in Relation to the VPD

The Bioristor response (R) continuously monitored for 15 days in 5 plants in altered Vapour Pressure Deficit (VPD) conditions (Figure 1A, B) and showed a specific trend in sensor response (R) following small changes in the VPD values[56].

Although inserted in the plant stem, the high biocompatibility of the sensor, has been confirmed (Figure 1C). The introduction of Bioristor did not alter the overall morphology of the stem and of the plant growth since the plants equipped with the sensors were indistinguishable from other plants not monitored used as control (data not shown). Indeed, the insertion of the sensor did not damage the functionality of the vascular tissues, and even if the vascular tissues were interrupted in the insertion point (Figure 1C), the normal stem structure was restored immediately after the insertion point as also previously reported in Coppedè et al[39]. Moreover, the use of a textile thread as gate strongly reduced, if compared with the silver one, the onset of necrosis in the tissues surrounding the sensor (Figure 1C). The day and night trend of R was verified and showed a decrease during the day and an increase during the night tracing the circadian rhythm under normal growth conditions (data not shown) as previously shown in Coppedè et al[39]. When VPD and R were plotted together an opposite trend was observed (Figure 2). After the expected adaptation period due to sensor integration (days 0–2), when VPD was decreased from 1 to 0.7 Kpa a rapid positive slope of the R was observed for two days (days 2–4, 48 h) followed by a smooth decrease of R in constant VPD conditions (Figure 2A).

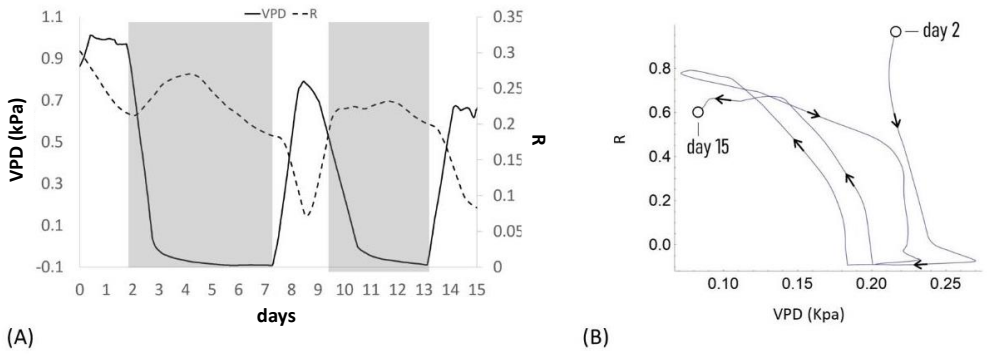

Figure 2: A) Plot of the average of the R measured on all plants for all days at Vg = 1 (dashed line) and the calculated VPD trend (solid line); (B) Diagram of the sensor response of the system (R) and the VPD reporting the trajectories described, the arrows indicate the direction of the curve from the beginning to the end of the experiment[56].

When VPD was rapidly increased (0–0.7 kPa; day 7.5) R rapidly dropped, showing a complete opposite trend with respect to VPD. When the VPD was decreased (9 day) R returned to higher values and remained almost constant, to decrease again when VPD was increased (13 day, Figure 2A). When R and the VPD are plotted one as a function of each other and the resulting trajectories are parameterized by time, over approximately 13 days, the curve folds upon itself completing several loops, further indicating that the R and VPD variables are anti-correlated (Figure 2B)[56].

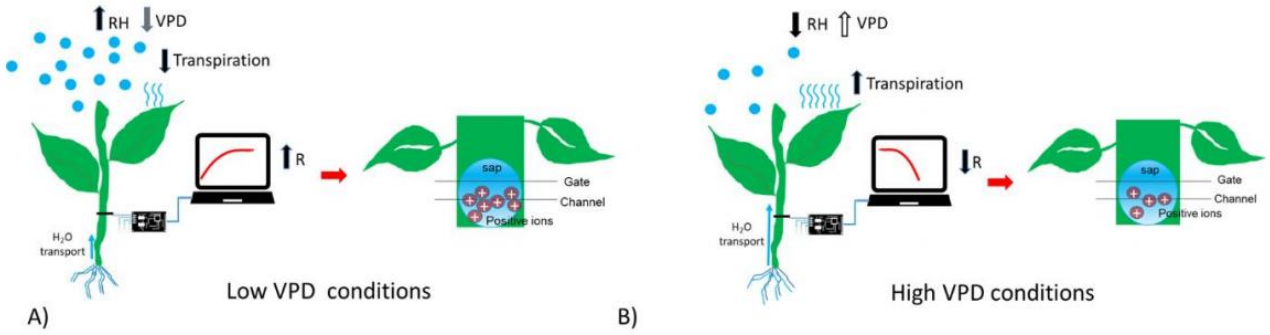

Figure 3: Scheme reporting the sensor response (R) in (A) low VPD conditions; (B) high VPD[56]

To summarize, in presence of high humidity and low VPD, thus low transpiration conditions, the Bioristor showed a positive increasing trend (high R, Figure 3A); while in low humidity, and high VPD thus high transpiration the Bioristor response showed a minimum (Figure 3B).

The electrolyte (in this case the plant sap) is an integral part of the OECT device; variations in its ionic concentration affect the device properties[32,50]. Another parameter that can be affected by changes in the plant sap ion composition and concentration is τ that gives the time of how fast the channel of the OECT will be de-doped and is directly linked to the diffusion properties of charged species in electrolyte solution (atomic mass, net charge, diffusion coefficient). τ was also acquired to give further information on the ionic composition of the plant sap[37,39,56,57].

When τ in comparison to R was studied, we noted (Figure 4) that in some portions of the diagram they are correlated, being in an inverse relationship, while in other portions there is a poor correlation between variables.

Recalling that R is related to the quantity of ions in solution, while τ is related to the inverse of both ion quantity and mass[16], we can observe an increasing R value is indicative of solutions becoming enriched with more ions of the same type. Moreover, we reported an increasing value of τ, without a

correlation with a decrease of R that is indicative of solutions becoming enriched with ions with larger mass. The slope of R and τ determined as a function of time, indicates whether the transformation of the system is of the first (1) or second (2) type, or a combination of the two τ and the VPD trends were comparable (Figure 5)[56].

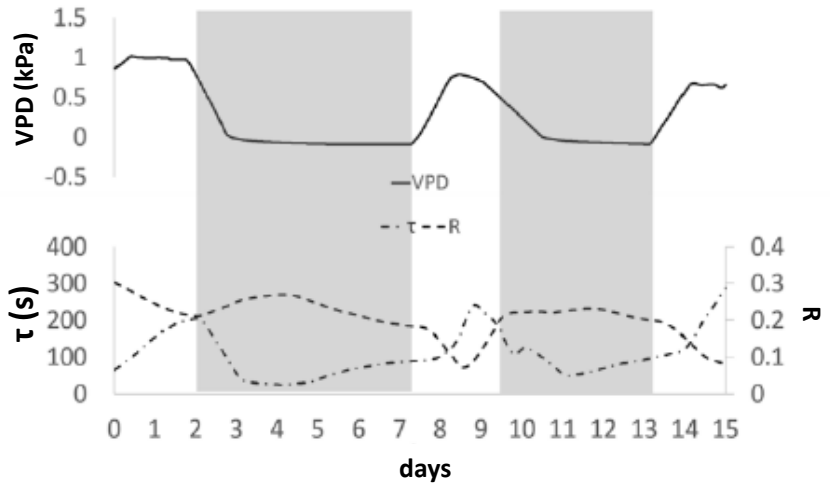

Figure 4: Average of R measured during the day on all plants at Vg = 1 (dashed line), τ signal (dashed and pointed line) and the calculated VPD trend (solid line). Grey block indicates when the Low VPD conditions were applied[56].

A close analysis of the time dependence of τ and VPD, allows the shift of τ and, with the VPD phase in advance by ~12 h (Figure 5). This may be attributed to the different diffusivity of the ions dissolved in the solution, suggesting that Bioristor reveals the changes occurring in the ion uptake, storage and distribution triggered by the plant in altered environmental conditions[56].

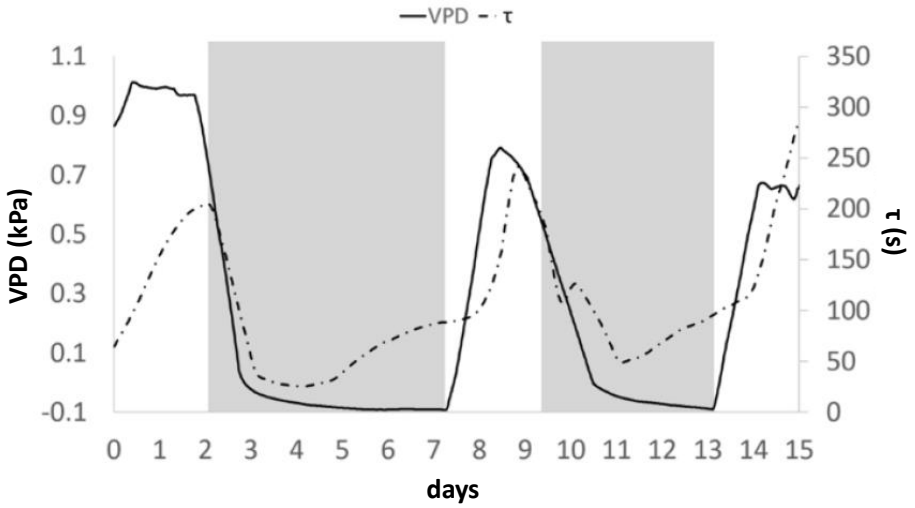

Figure 5: Average trend of τ (dashed pointed line) and VPD (solid line). Grey block indicates when the Low VPD conditions were applied[56]

A biplot was produced and including all variables[56]. The first two principal components (PC1 and PC2) and the corresponding component loading vectors were visualized and summarized in a biplot, in which component scores (indicated in dots) were colored according to time classification. PCA was performed for all plants and validated by cluster analyses. PCA is a statistical technique of analysis that reduces the dimensionality of a data-set still retaining much of its informative content. After PCA, a signal is decomposed into a few variables (termed principal components), that are representative of the state of the system.

In Figure 6, we report the system's response expressed as a function of the first two principal components, i.e., PC1 and PC2. Each point in the diagram describes the state of the system measured at specific times. Samples measured at the same time have the same color. For the analysis, we have considered 5 different time groups (i.e., days 2, 3, 6, 8 and 8.5), and 5 samples (plants) for time group[56].

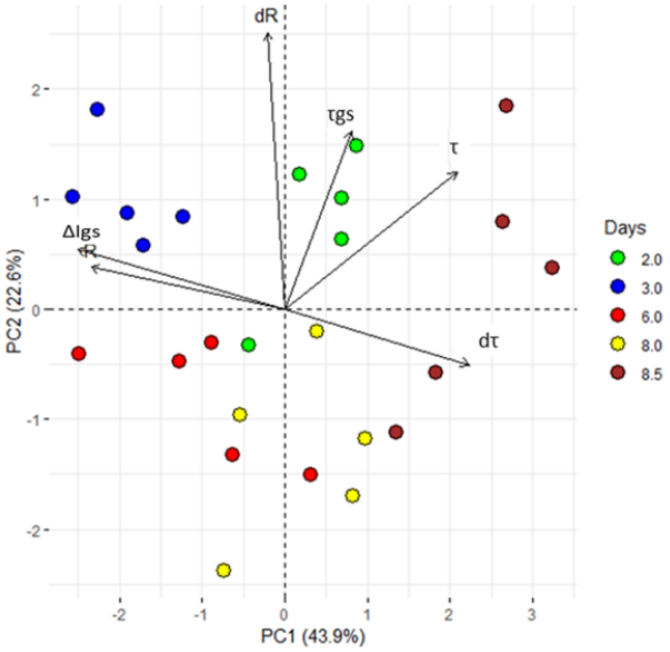

Figure 6: Principal component analysis (PCA). ΔIgs; difference between minimum and maximum current gate values, τ and τ_{gs}; time constant. From the acquired data, the first derivative of R and τ (dR and dτ) was calculated. Values, exhibited clear separation between the groups with different periods of exposure to VPD variations (2, 3, 6, 8 and 8.5 days). The first two components PC1 and PC2 explain the 66.5% of the variability observed. Each dot represents a plant[56].

PCA shows that the first two principal components explain the 66.5% of the total variance. Moreover, a clear separation of PC variables for all considered times (Figure 6) confirms the hypothesis that alterations in the VPD are correctly tracked by the sensor and encoded in the system's response, R. After PCA, sample points are clearly separated in clusters: thus, the technique correctly operates sample classification on the basis of their originating time of measurement. Since the time at which a sample is measured encodes information about the VPD history of a plant, the fact that the PCA (that is a mathematical transformation of the signal R) discriminates between different time steps automatically implies that the response R is indicative of VPD changes, confirming the initial hypothesis. The groups including 8 and 8.5 days can be considered as an individual super-group, where the plants responded to a VPD increase. The analyses of the correlation between R and VPD at 15 days ($r = -0.80$; $p \leq 0.05$) further supports the anti-correlation between the two variables and the ability of Bioristors to sense changes in VPD. In addition, the plant-to-plant variability in terms of VPD-R-correlation was verified and the single plant R and VPD trends were measured for the entire length of the experiment (Figure 7). No significant difference was observed between all plants considered or in the average of the sensor response over 15 days (about 60 measurements per day)[56].

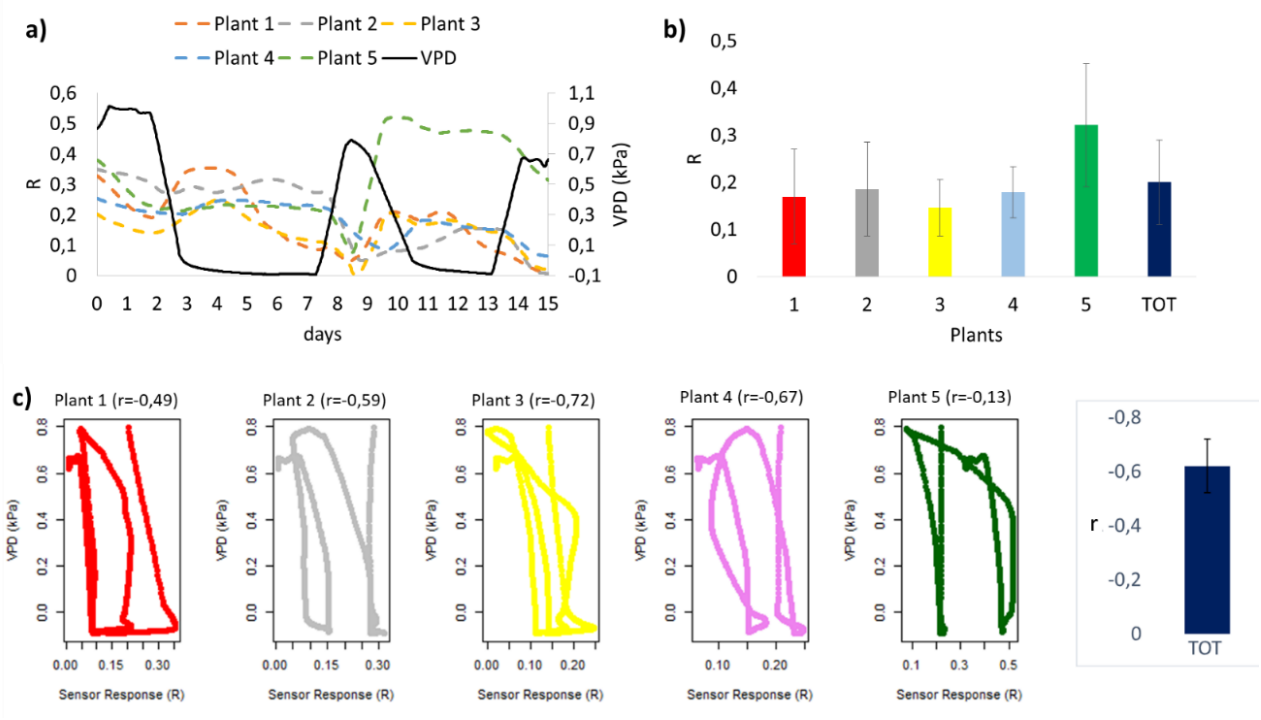

Figure 7: (a) Plot showing the average of the individual plant R measured at V_g=1V (Plant 1-5, dashed colored lines) and the calculated VPD trend (black line); (b) Average and standard deviation of R values for each plant (colored bars) and considering all plants (dark blu bar) performed over 15 days; (c) Scatter plots of the individual plant R and VPD. The scatter plot indicated a high negative correlation between the two variables for plant 1 and 2, and a strong negative correlation for plant 3 and 4 ($p \leq 0.05$), the total correlation coefficient ρ is also indicated (dark blue bar)[56]

Time constant (τ) analysis

A consistent positive correlation between τ and the VPD values was observed ($r = 0.88$; $p \leq 0.05$). To support the observed 12 h time lag, we measured the degree of similarity of the VPD and τ functions using cross correlation. We applied a varying displacement ϕ between the VPD and τ functions, then we calculated the cross correlation between functions as their inner product. The resulting cross correlation is displayed in figure 8 as a function of ϕ. The value of ϕ in correspondence of which the cross correlation is peaked, indicated the lag between the VPD and τ. For this configuration, the lag is of nearly 12 h[56].

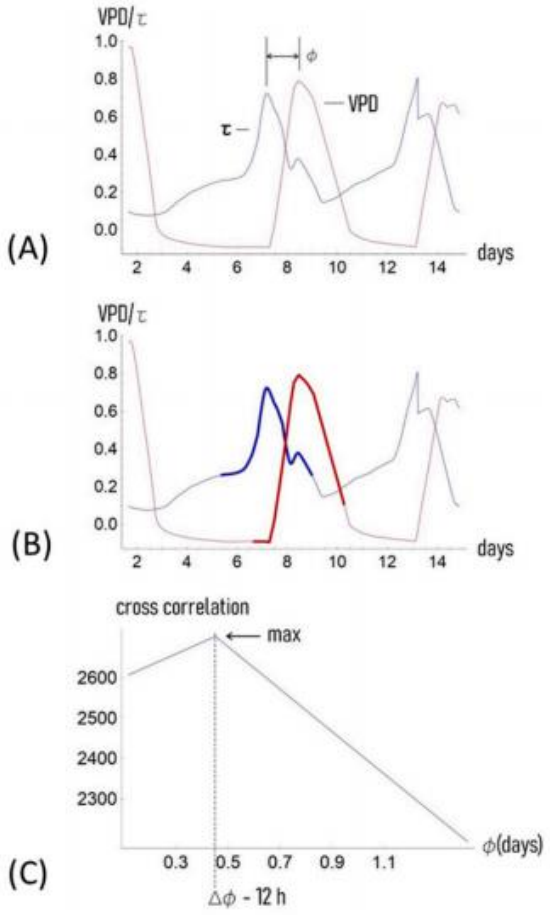

Figure 8: The VPD and time constant (τ) functions measured as a function of time (A). Of the originating functions, we isolated the portion of the functions curves around the maximum (B). We then performed the cross correlation between functions, as a function of the arbitrary time lag ϕ: the peak of the cross correlation indicates the lag between functions that, for this configuration, is approximately of 12 h (C)[56].

In view of the reported sensor features (R and τ), a closer analysis of the first 84 h (3.5 days), characterized by a VPD decrease was done performing a PCA analyses. The first two PCs explain the 69% of the total variance and the PCA scores are separated into four groups. In particular, the loading directions indicated that the first two groups were more influenced by τ (thus on the type of ion dissolved in the sap) than the others (Figure 9).

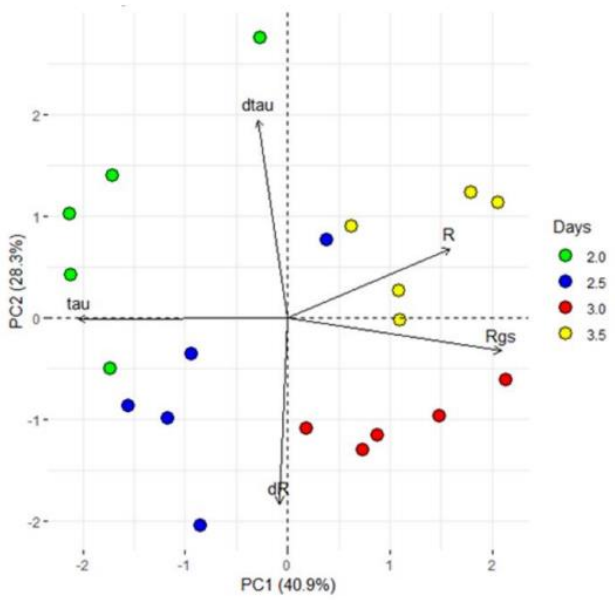

Figure 9: PCA used the processed data, which consist of the sensor response (R), the difference between minimum and maximum current gate values (ΔI_{gs}), the sensor constants time (τ and τ_{gs}) and the first derivative as function of time of R and τ (dR and dτ) and exhibited clear separation between the groups with different periods of exposure to VPD variations (2, 2.5, 3 and 3.5 days). The first two components PC1 and PC2 explain the 69.2% of the variability observed[56].

4.3 Discussion

The analyses of the changes in the R value and trend following changes in the environmental VPD, support by *in-vivo* measurements the recently reported data on the effects of an alteration of VPD conditions on plant water use efficiency and growth summarized in a strong reduction in the transpiration rate, plant hydraulic conductance, and water flow in general[111]. The novelty resides in the acquisition of this information directly at xylem level, continuously and in real time. It is well documented that R increases as a consequence of the increased ionic content of the tested solution, in this case the plant sap[37,39,50]. In low VPD conditions and low transpiration rate, the Bioristor always responded with a rapid increase of the R value (2–4 days and 9–12 days; Figure 2), presumably because of the accumulation of electrolyte (mainly as Na^+ and K^+)[115,116] in the xylem sap as consequence of stomatal closure and the subsequent reduction of the transpiration stream[117]. On the contrary, by increasing VPD from 0.1 to 0.8 kPa the transpiration stream seems to be restored with a reduction of the concentration of ions in the xylem that is evidenced by the Bioristor response (rapid increase of R)[59].

The possibility to monitor the changes in the plant xylem sap composition, during low VPD and high relative humidity condition, is of great interest towards the plant health field.

Firstly, a fine tune of greenhouse environmental conditions guided based on the real plant health conditions can concretely reduce the CO_2 footprint and the environmental sustainability of greenhouse production.

Water and leaves wetness can also play a key role in the establishment of pathogen diseases.

Several factor impacts on the ability of pathogen to reach and colonized plant tissues and among these, the degree of leaves wetness, and in particular the water droplets on the leaf surface, plays an important role in pathogen infection[118,119]. Thus, the capability to detect and measure directly from the plants the increased amount and exposure time of water can foster the identification of the right time to perform treatment, reducing the number of treatments and increasing the sustainability of the agriculture production.

Chapter 5

Optimization of water management in open field through OECT-based *in-vivo* sensing

Based on the results obtained in controlled environment and already described in the Chapter 3, the natural evolution of the Bioristor application, being a good indicator of the drought stress occurring in plants, was its application in open field to optimize the water use efficiency in ensuring crops yield and quality. In this chapter, the application of Bioristor in real field systems will be described.

Three seasons (2018, 2019 and 2020) and two different crop species as tomato and kiwi were monitored. The summer ’18 trial was carried out thanks to the collaboration with Mutti S.p.A., one of the biggest italian companies in the production and processing of tomatoes. Most of the trials were conducted during the PORFESR project POSITIVE in collaboration with CIDEA (Centro Interdipartimentale per l'Energia e l'Ambiente), universities (Catholic University of Sacred Heart and University of Bologna) and companies (Mutti S.p.A. and Apofruit) to develop scalable protocols for precision agriculture with the aim of improving water management in agriculture.

5.1 *In-vivo* monitoring of tomato plants in open field

This section follows the description of tomato plants monitoring through the Bioristor during the 2018 and 2019 trial.

5.1.1 Material and methods

Field trials description

Summer 2018 and 2019 field trials were carried out at the experimental farm of Podere Stuard, in Parma (60 m a.s.l., 44° 48' 29.888" N 10° 16' 29.074" E) in two different experimental fields, respectively. Heinz 340 variety was tested both years. In the Table 1 are collected all the operations carried out during both trials.

Table 1: Field operations conducted during the 2018 and 2019 trial

Open field trial	*Day*	*Operations*
2018	0	Bioristor insertion Soil probe placement
	6	Actara 25 WG
	8	Differential irrigation
	16	Quantum R-OK Dimetomorf plus copper
	63	Harvest
2019	0	Bioristor insertion
	13	Differential irrigation
	23	Soil probe placement
	33	Ridomil Gold R WG Quantum R-OK
	41	Treatment for noctuids
	60	Harvest

The field was organized in three plots, each divided into three rows for each treatment. The middle row of each plot was considered for Bioristor measurements by measuring 10 plants for each water regime. Each plot was irrigated with different irrigation volumes established based on the water council defined by Irriframe (https://www.irriframe.it/Irriframe) and conventionally follow in the farm. Thus, the thesis hereafter identified as 100%, 80% and 60% were selected.

In 2019 trial, a fine diversification of the water regime was performed based on 2018 results. Thus 80%, 60% and 20% were identified and monitored.

A randomize block design was applied, and 5 plants each block of irrigation were monitored by the Bioristor.

Irrigation and phytosanitary treatments

Differential irrigation started on day 8 and day 13 respectively for the summer 2018 trial and the summer 2019 trial, after a period of sensor settling in the plant and a subsequent signal stabilization. Before those days, for both trials, the same amount of water was provided to all thesis, in line with the daily advices by the Emilia Romagna's system Irriframe for an optimal irrigation (100%). The irrigation rate is based on the time of use of the drip watering system.

In addition, phytosanitary treatments were necessary during both seasons. In the 2018 trial, due to the occurrence of aphids infestation in the field, plants were treated at day 6 with Actara 25 wg, and with two different fungicide (Quantum r-ok and Dimetomorf with copper) at day 16.

Throughout the 2019 trial, fungicide treatment with Ridomil Gold R WG and Quantum R-OK was necessary on day 33; an additional treatment for noctuids was required on day 41.

Agronomic measurements: Soil probe and meteorological data

Agricultural Support soil humidity probes (Figure 1) were installed at 9, 18 and 27 cm depth in both seasons in correspondence of the plot monitored with Bioristor. According to the manufacturer instructions, probes need for 10 days to settle.

In our experiments (2018, 2019) data from the soil sensors were available from day 0 and day 23, respectively (Figure 2).

Figure 1: Soil humidity support during summer 2018 and summer 2019

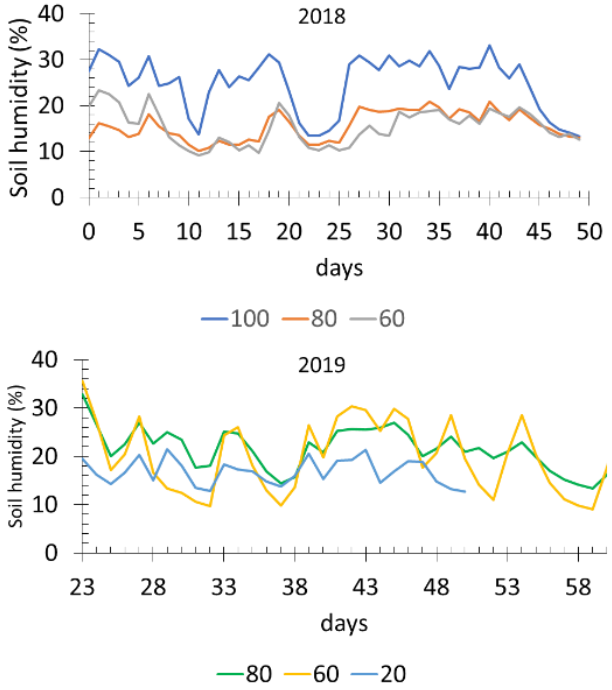

Figure 2: Soil humidity daily mean of probe at 9-18-27 cm depth for summer 2018 trial (a; blue: 100%, red: 80%, gray: 60%) and summer 2019 trial (b, green: 80%, yellow: 60%, light blue: 20%)

Moreover, rainfall volume (Figure 3) as well as relative humidity (Figure 4) at 2 m above the ground were collected with the agrometeorological station of the ARPAE located in each field.

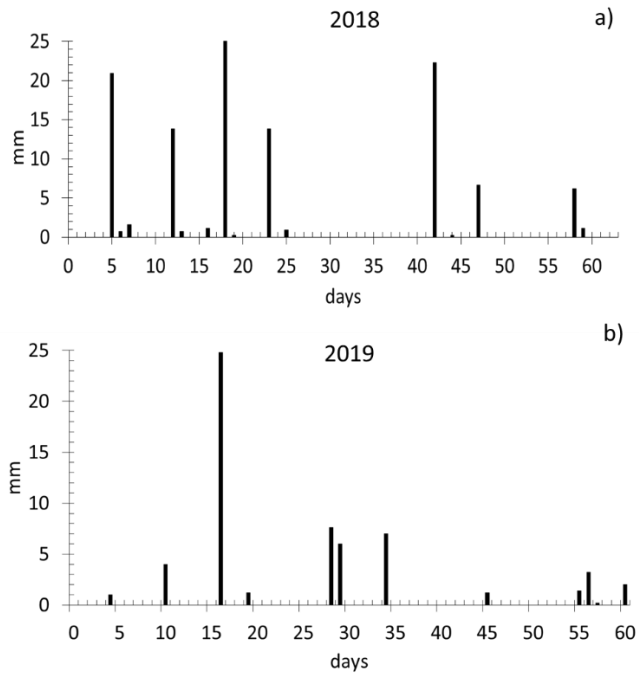

Figure 3: Cumulative daily rainfall measured during summer 2018 (a) and summer 2019 (b)

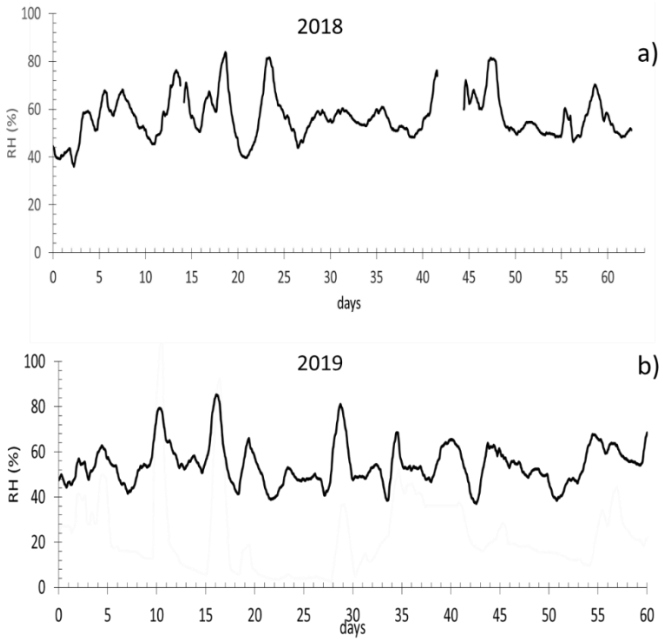

Figure 4: Relative humidity (RH) measured during summer 2018 (a) and summer 2019 (b)

Bioristor measurements

The Bioristors were prepared, inserted into the plant stems, and connected to a computer as described in Chapter 2 (Figure 5). Then, the calculated R value at gate voltage of 0.6 V (see Chapter 2) was analyzed with MATLAB (https://uk .mathworks.com/) and Microsoft Excel 2016) to smooth out day/night oscillations.

Figure 5: Bioristor implantation in field. A) plot and wires connecting the NI converter and the plants, B) Bioristor in site, C) Bioristor holder and connectors

Physiological analysis

To validate the results obtained with the Bioristor a series of standard physiological analyses were necessary. Five plants and two plants for each thesis in 2018 and 2019 trial, respectively, have been analyzed for the relative water content (RWC) as reported by Barrs and Weatherley[55], by taking the fully expanded leaf as the sample (two replicates for each plant). Chlorophyll content measurements were performed by using the SPAD 502 meter (Konica Minolta, Ramsey, USA). Measurements from 3 leaves of the same plant used for RWC analysis of varying age and color were selected for measurements made under diffuse lighting. The relative SPAD value was considered.

During 2018 trial leaf stomatal conductance was measured from one fully expanded leaf of seven plant per thesis, using an SC1 leaf porometer (Decagon Devices, Pullman, WA, USA). All data were analyzed statistically applying Analysis of Variance, and the standard error was calculated between replicates.

5.1.2 UAV image analysis

In 2019 trial thanks to the collaboration with Stefano Amaducci Labs of Catholic University of Sacred Heart in Piacenza, multispectral images were captured at days 26, 32, 46 and 52 (three flights per day: 9:00, 12:00, 15:00) to ground validate the results obtained with Bioristor. Multispectral images were acquired using the Micasense RedEdge-Mx multispectral sensor. Among the vegetation indices obtained from the multispectral images, the NDVI (Normalized Difference Vegetation Index)[120] was chosen to validate the Bioristor measurements being NDVI, a well-established vegetation index, used to estimate the health and vigor of plant vegetation. NDVI is calculated as[121]:

$$NDVI = \frac{(R_{800} - R_{680})}{(R_{800} + R_{680})}$$

where R_{800} is the reflectance at 800 nm and R_{680} at 680 nm. Due to the high NIR reflectance of chlorophyll, this index is used to detect plants greenness[122].

5.1.3 Results

Pilot tomato field trial (2018 season)

In summer 2018 the Bioristor was able to monitor, for the first time, the tomato plants growth in field conditions for 63 days covering the entire development season from the end of flowering to the harvest (Figure 6).

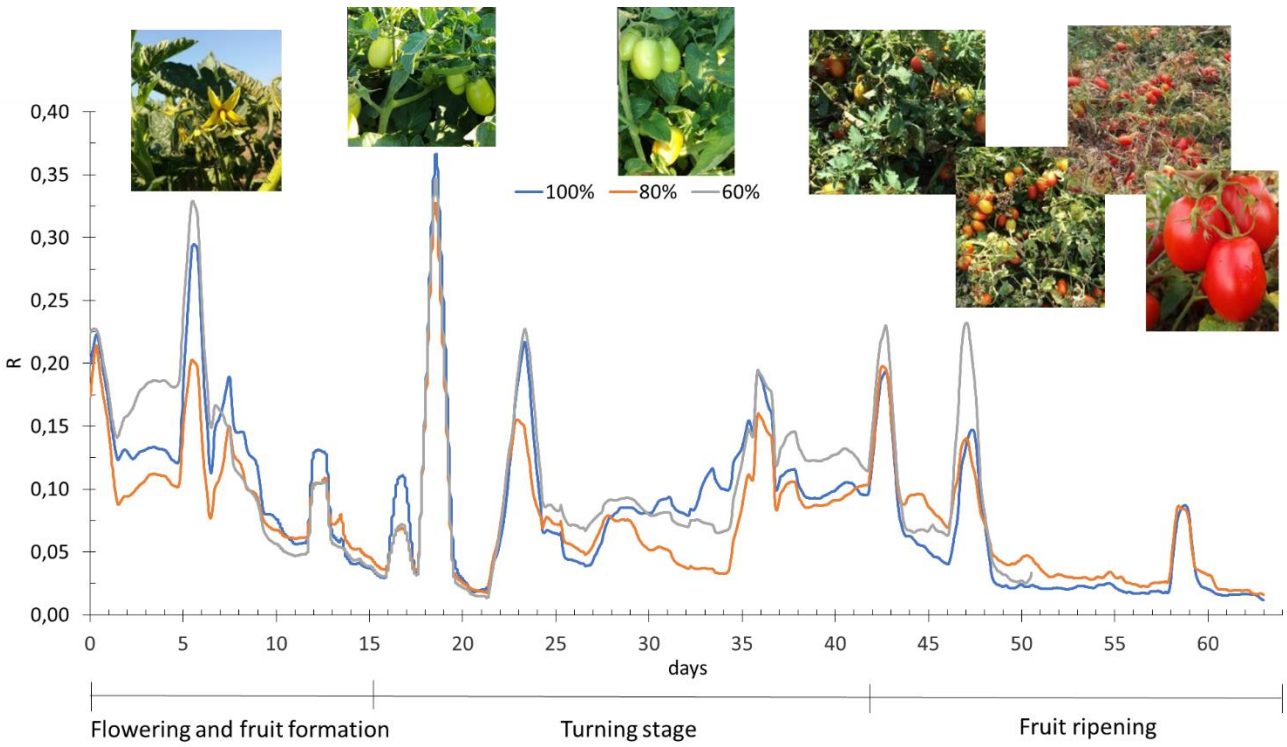

Figure 6: Bioristor measurements in 2018 season (63 days).

The sensor response gives us a clear picture of the plant status during the entire course of the experiments. An increase in R between 200% and 400%, was observed at each rainfall event, although not proportional to the mm of precipitation.

This finding suggests that wet leaves cause VPD to decrease, leading to a significant decrease in transpiration with associated blockage of ion and solute transport in the xylem[111], resulting in an increase in R that lasts until the leaves are completely dry[56].

The association of the R trend with the relative humidity of the air confirms this finding (Figure 7).

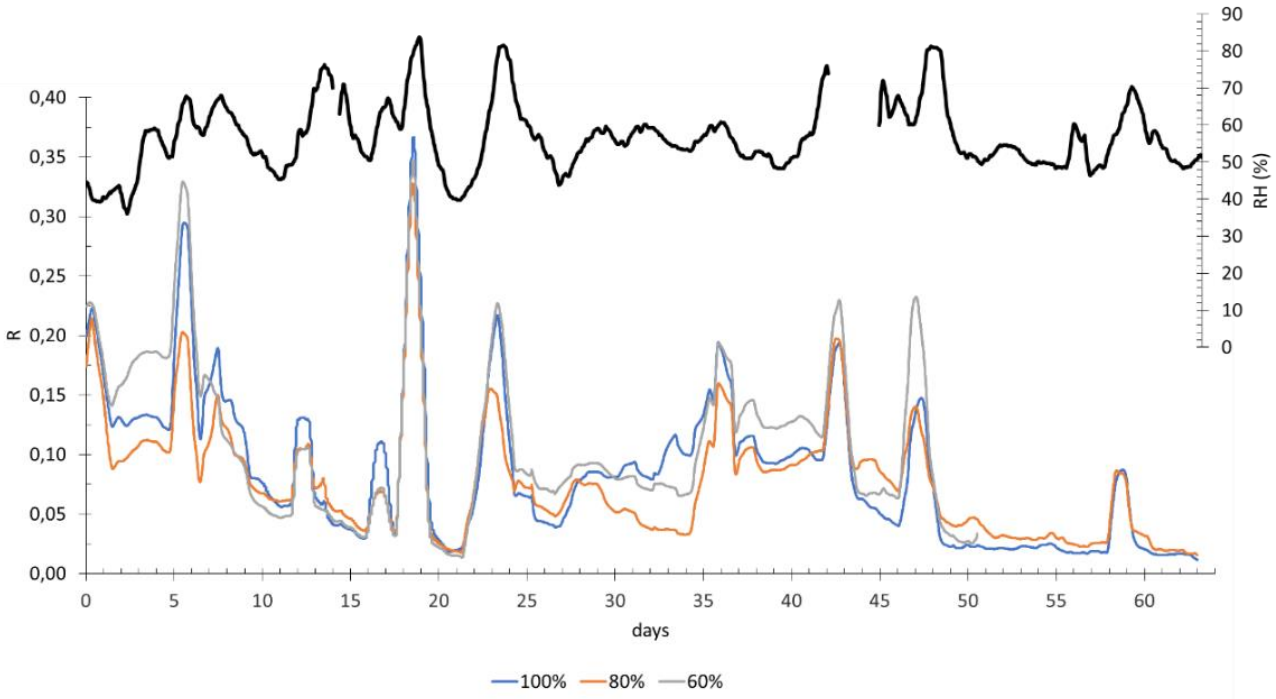

Figure 7: Plot of R trend (100% thesis: blue line, 80% thesis: red line, 60% thesis: gray line) with relative humidity of the air (black line)

This last result further supports the previous reporter relationship between R and VPD variation in the environment (See Chapter 4).

By analyzing the R trend in the time, it is clear that because of the extremely rainfall season, the thesis showed a similar behavior in the sensor response for the entire monitoring season and according to the R response trend, the entire analyses time-course revealed four phases (Figure 8) worth to be commented. The first phase (P1, 0-5 days) is the result of the sensor integration in the plant and a settling phase for the sensor the second phase (P2, 5-22 days) is characterized by a constant and continuous decrease in the R signal of all theses. This decrease in the R response, usually attributed to the occurrence of drought stress, was deeply analyzed since the irrigation plan showed enough water was given. By looking the management plan, the beginning of P2 coincides with the use of an anti-aphid (ACTARA 25WG) whose active ingredient is thiomethoxan, a neonicotinoid that promotes the plants growth and triggered a defense response like those used under drought stress. This leads to an R trend like the one encountered in drought stress conditions. Indeed, the third phase (P3, 22-44 days) was the most interested once of the entire season. The reduction of rain events and the increases of the environmental temperatures allowed to observe a separation between thesis in the R response. Days from 28 to 34 are the core measures of the entire season were all thesis showed a significantly different ($p \leq 0.05$) R response.

While the 100% thesis does not show a significant difference till day 33 with the 60% thesis. a significant increase, as expected, was recorded between 80 and 60% theses. From days 31 and 35 the R of the 60% thesis decreases between 10% and 40% compared to the control, and a larger decrease (from 40% and 60%) was observed in the 80 % thesis. Our data suggest the occurrence of a stronger severe stress in the 80% thesis. These data are in accordance with those recorded with the soil sensors, (Figure 2a). Finally, the fourth phase (P4, 40-63 days) is characterized by a progressive decrease in R due probably to the beginning of fruit ripening. Indeed, in this period, the dry substance progressively increases in the fruit, with consequent leaves senescence and reduction of transpiration[123].

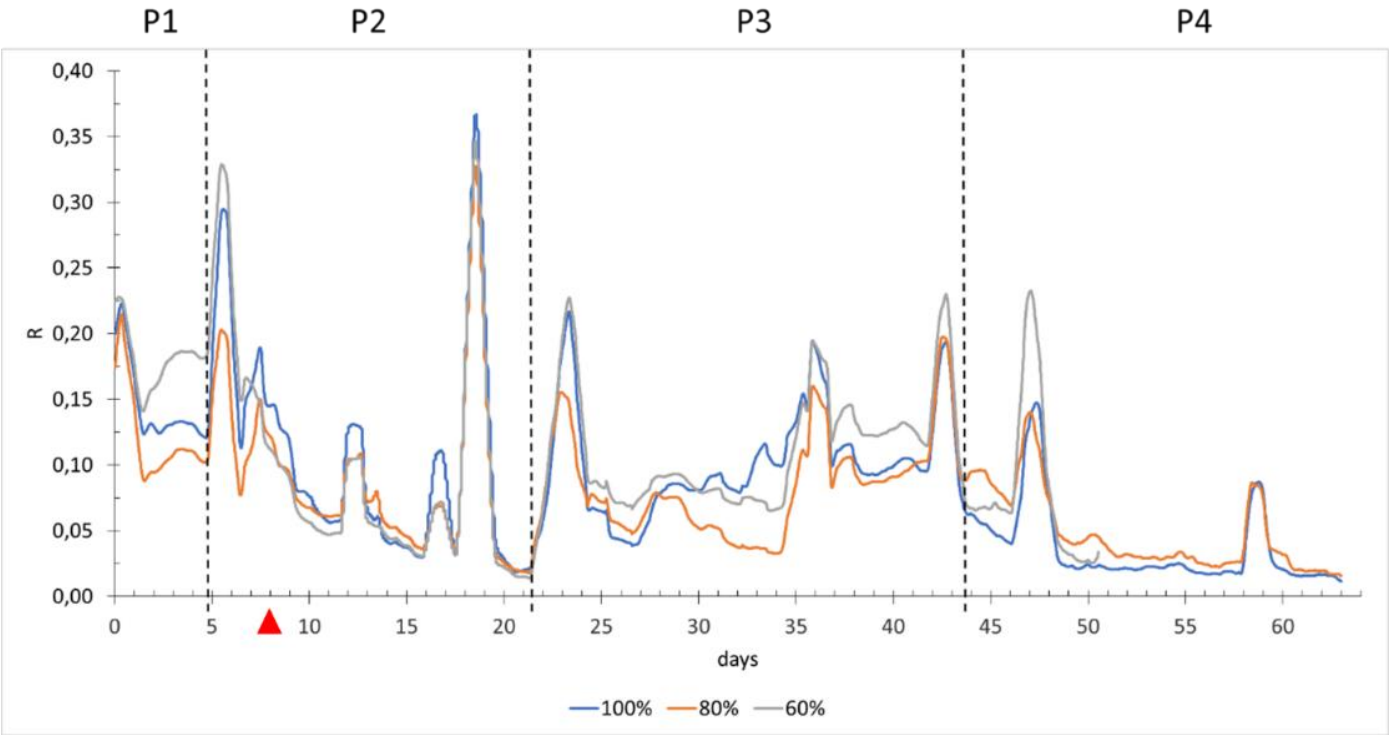

Figure 8: Plot of the daily smooth average of the R measured on 100% thesis (blue line), 80% thesis (red line), 60% thesis (gray line) for 63 days of measurements. Differential irrigation starts at 8 day (red triangle).

Regarding the operational life of the sensors, 75% of the installed Bioristors functioned correctly during the whole experiment. However, from day 22 eight sensors (not included in the analysis) were replaced to evaluate a possible drift effect.

Figure 9 shows the increase in the response of R resulting from the replacement of the sensors. The nature of this function was found in the treatment of the conductive polymer used, as well as in the gate potential used, and thus resolved as described in Chapter 2 in subsequent experiments.

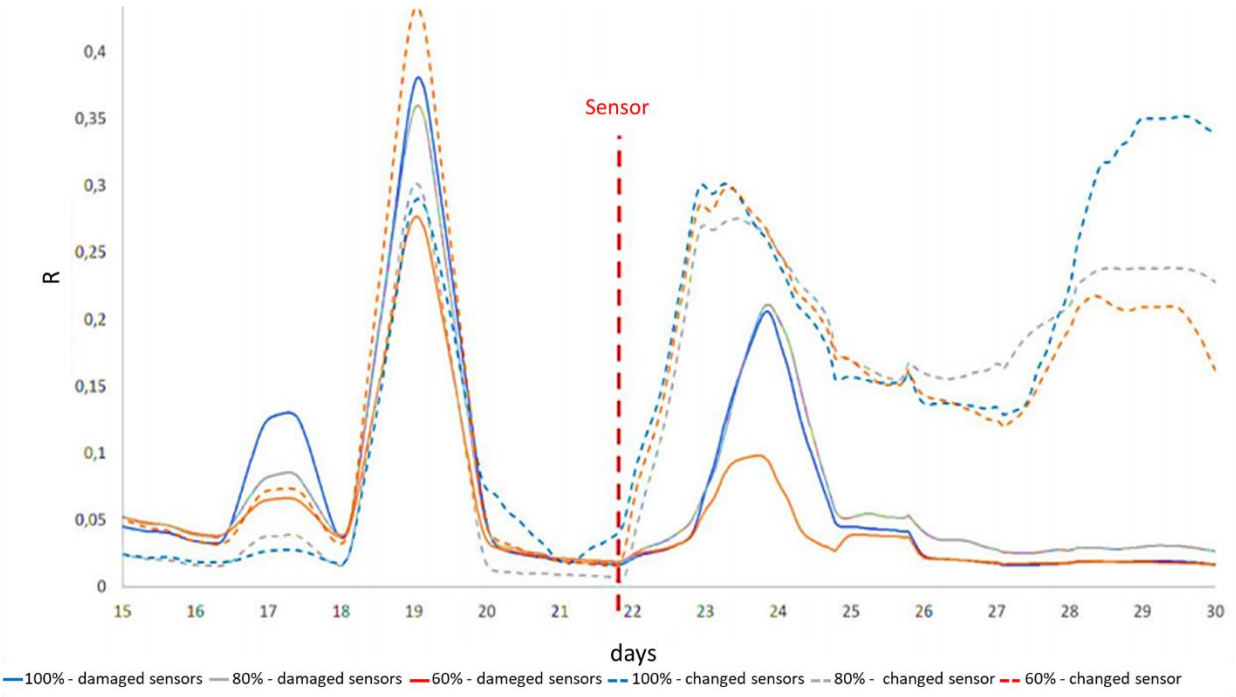

Figure 9: Sensor drift. Solid lines: damaged sensor; dashed lines: changed sensor. The colors indicate the smooth mean of R for each thesis (blue: 100%; gray: 80%; red: 60%)

The physiological measurements are in accordance with the Bioristor data. The stomatal conductance and the RWC data, collected through the experiment, do not showed any significant difference between the thesis for all time points. As expected, although not significant between thesis, both the SPAD and the stomatal conductance values showed an expected reduction at day 50 due to the senescence process at maturity. (Figure 10)

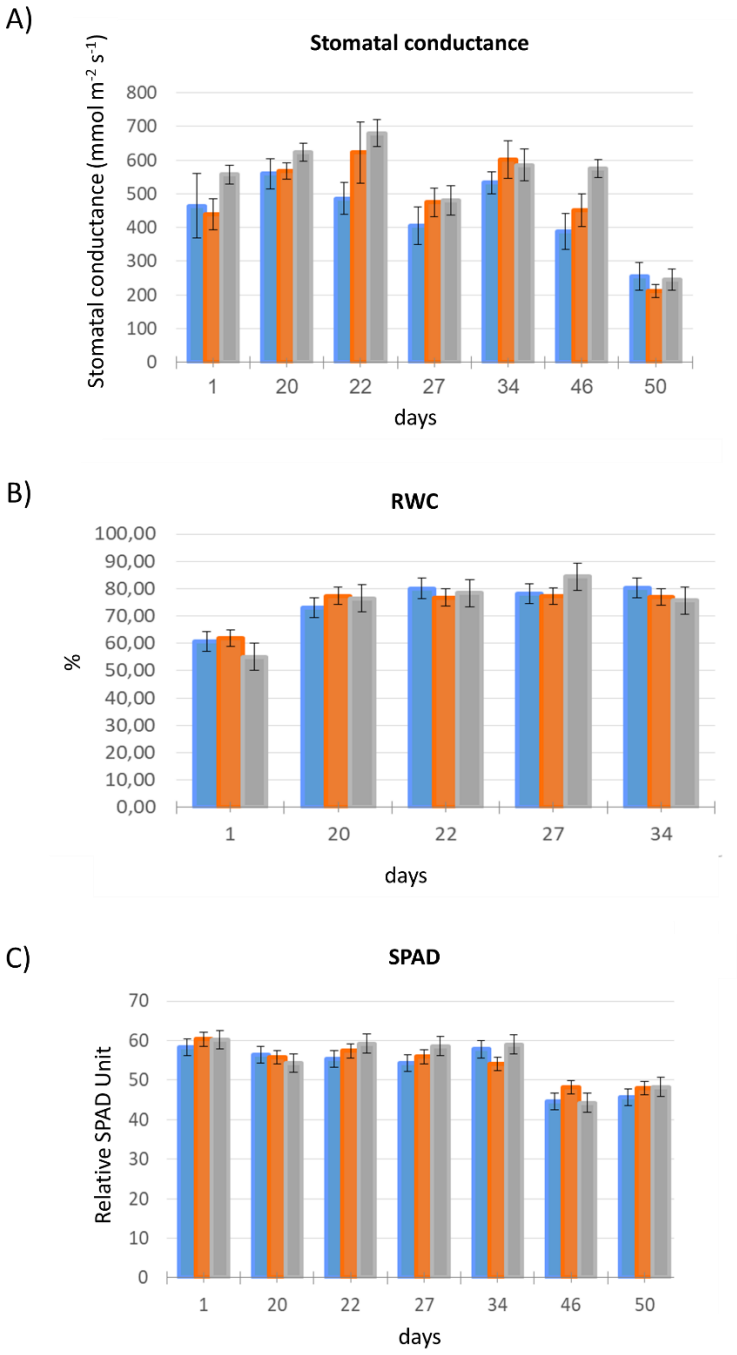

Figure 10: Physiological measurements collected at 1, 20, 22, 27, 34, 46, 50 days. (A) Stomatal conductance using SC-1 Decagon Porometer; (B) Relative Water Content (RWC); (C) SPAD relative unit to measure chlorophyll content. Color bars indicate 100% thesis (blue), 80% thesis (red) and 60% thesis (gray). Error bars represent standard error

To make some statement regarding the suitability of Bioristor, to efficiently monitor the changes in plant sap ion composition correlated with the drought stress, and to hypothesis its use as tool to fine tune the irrigation, the evaluation of yield was performed by Stuard and Mutti. In particular, the analyses of the commercial yield % was considered and revealed no significant difference between

the theses. Through 2018 trial, according to the Bioristor it would have been appropriate to irrigate the entire field at 60% of field capacity, except for a 7-day period (29-35 days) when only the 100% thesis has not signaled any decrease. This allowed us to calculate the potential % of water saving operable by using the Bioristor to guide the irrigation system and established as the 36%.

Second tomato field trial (2019 season)

In 2019 Bioristor allowed to monitor continuously and in real time 60 days the growth of tomato plants in open fields confirming 2018 findings (Figure 11).

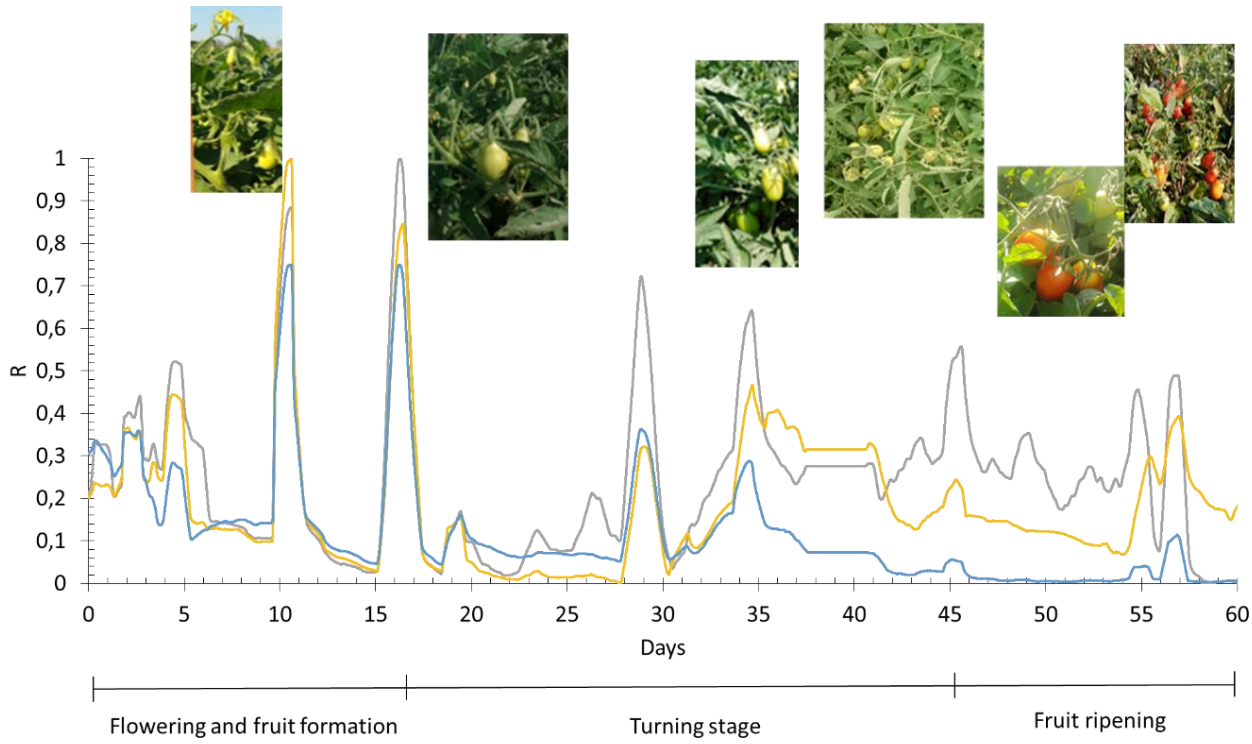

Figure 11: Bioristor measurements in 2019 season (60 days).

An increase in R was observed during rain showers with picks proportional to the gravity of the precipitation. (Figures 3b) showing larger range of variations in comparison with 2018 (100-600%), confirming that an increase in the relative humidity leads to a decrease in VPD and in turn to a decrease in transpiration resulting in an increase in R (Figure 12). The greater increase in R during the 2019 trial rains suggests that leaf area was greater, resulting in a greater number of wet leaves

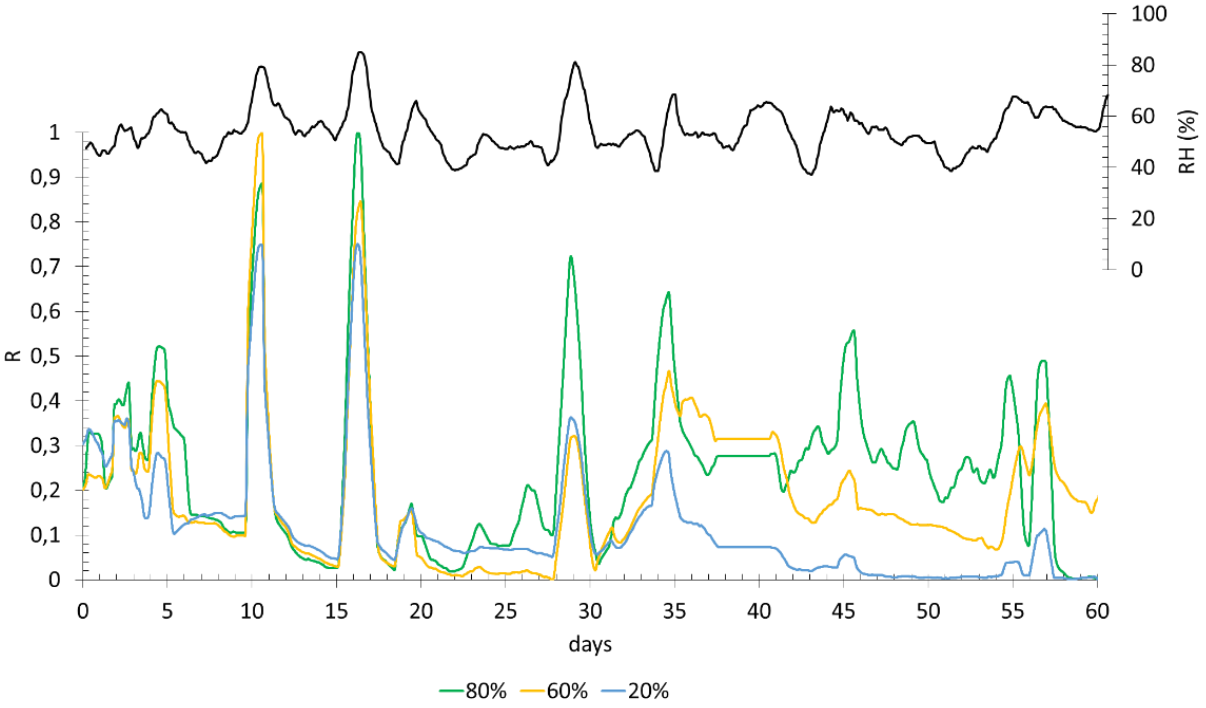

Figure 12: Plot of R trend (100% thesis: green line, 80% thesis: yellow line, 60% thesis: light blue line) with relative humidity of the air (black line).

Four phases can be identified in the total R tend for the trial. The first phase (P1, 0-5 days), as for 2018 correspond to the installation phase of the sensor. In the second phase (P2, 5-23 days), no significant difference was observed between thesis and this is due to frequent and abundant rain events occurred (Figure 3b) that mask the effect of the differential irrigation started on day 13 (Figure 13). During the third phase (P3, 23-35 days) the 80% and 20% theses showed a similar trend, and significantly differently from the response of the 60% thesis ($p \leq 0.05$) but not within them. Although not consistent with irrigation volumes, this trend is confirmed by soil moisture volumes, especially since day 28 (Figure 2b). Only in the last phases, an appreciable and significant difference occurs in the R trend of the thesis (P4, 35-60, $p \leq 0.001$). Here the R of the 20% rapidly drop till the end of the experiment, while 80 and 60% are well separated according to the given amount of water only from day 42 (Figure 2b).

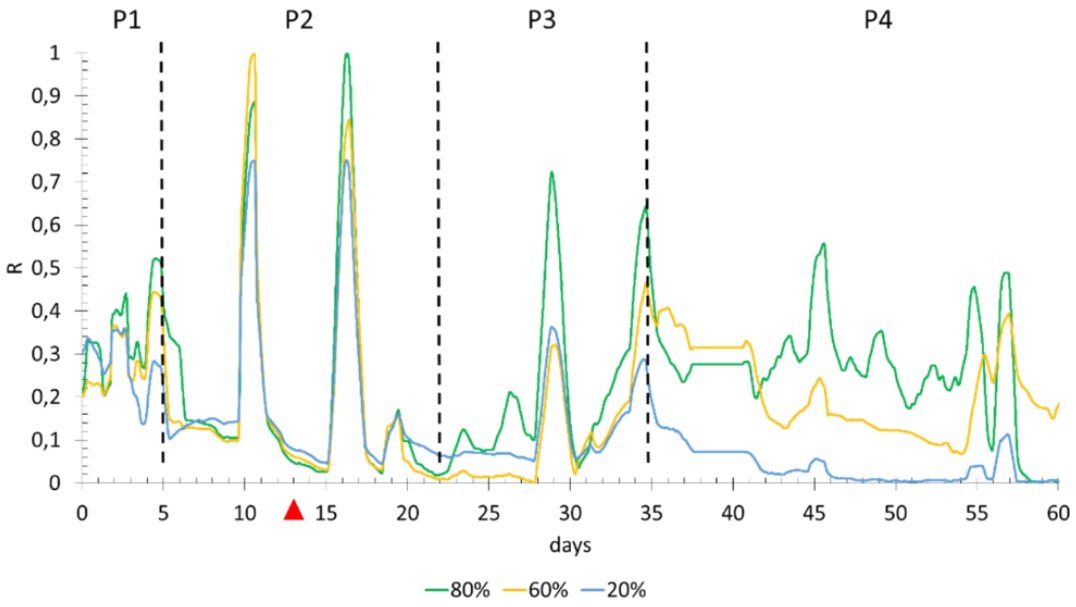

Figure 13: Plot of the daily smooth average of the R measured on 80% thesis (green line), 60% thesis (yellow line), 20% thesis (light blue line) for the 2019 season (60 days of measurements). Differential irrigation began at 13 day (red triangle)

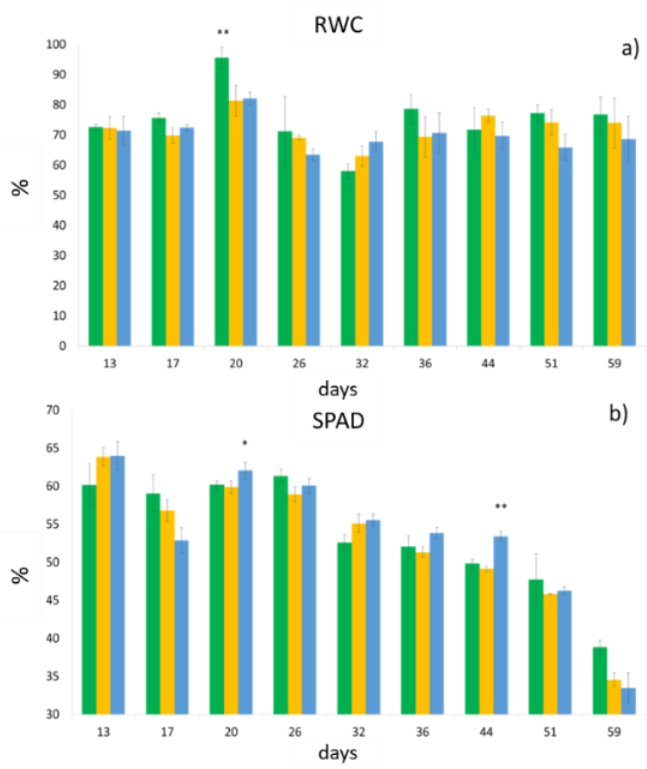

Figure 14: Physiological measurements. Plants were tested at 13, 17, 20, 26, 32, 36, 44, 51 and 59 days. (A) Relative Water Content (RWC); (B) SPAD relative unit to measure chlorophyll content. Different colors indicate 80% thesis (green), 60% thesis (yellow) and 20% thesis (light blue). Error bars represent standard error. Asterisks indicate significant differences of the drought-stressed plants from the control plants according to ANOVA ($p \leq 0.01$, $**$; $p \leq 0.05$, $*$).

The evaluation of the physiological tests performed was not completely consistent with the Bioristor data. A significant difference mainly between 80 and 20% thesis at day 20 was observed for RWC and SPAD (Figure 14). Interestingly, the RWC data and the Bioristor data do not agree specifically in the initial days of phase 3, reinforcing the concept that Bioristor can look at microscale level in the plant physiology revealing hidden aspects of the plant defence response during drought.

The physiological data confirm however the similarity of the health status occurring in the 80 and 60% thesis and highlighting that the thesis at 20% irrigation is the most affected by the drought stress.

Sensor validation with multispectral indices

A ground validation of Bioristor with known, used, and accepted indices is needed to foster its use as tool for precision agriculture in open field.

Thus, the NDVI index was chosen as effective index of the health status and obtained from the multispectral images captured by the drone flights. The research group of Prof. Amaducci flew over the field during the season in frame of the POSITIVE project.

Here we present the NDVI data only as indicator of the exploitability of the R as alternative and *in-vivo* index of the plant health status.

The NDVI values were over 0.8 for the entire season indicating plant in good health status, well hydrated and not affected and reflect the physiological data. NDVI data agree with the Bioristor data clearly separating the 20% thesis form the 80% and 60% once.

However, when plotted together, R and NDVI (Figure 15) showed a good level of correlation highlighting that if present an appreciable difference is visible between the 60 and 80 % thesis with the 20% thesis.

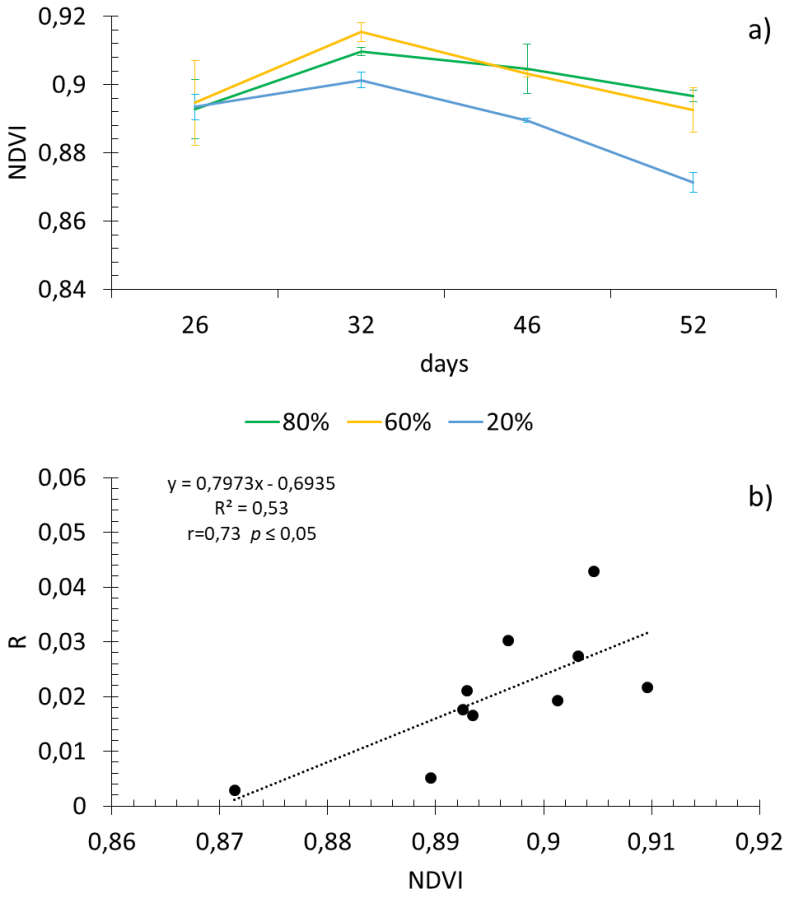

Figure 15: a) NDVI index derived from the drone flights on sensor parcel and adjacent parcel. Imaging data on 80% thesis (green), 60% thesis (yellow) and 20% thesis (light blue). b) correlation analysis between NDVI index and sensor R.

Fruit harvesting was carried out at the end of the trial and, as expected the 20% thesis was the most affected in terms of yield considering the percentage of commercial yield (80: 71.8%; 60: 70.8%; 20: 64.4%).

This experiment supports the hypothesis that Bioristor can significantly help in defining the right amount of water in the right time when needed perfectly in line with the precision agriculture dogma.

During the 2019 trial, the Bioristor suggested irrigating the field for the entire season at 60% of regular irrigation except for two periods between days 23 and 28, and between days 42 and 54, when 80% irrigation was required. Here, the calculated percentage of water that could have been saved without preventing yield and quality was estimated in 34% totally in agreement with the pilot experiment in 2018.

5.2 *In-vivo* monitoring of kiwi plants in open field

Aim of this work is the application of Bioristor as novel technology to cope with water scarcity for agriculture and food security (www.fao.org/docrep/) and achieve the UN sustainable development goals[124]. Widen the type of crops and production is mandatory to concretely impact of the water management in agricolture. Thus, during the project, the Bioristor was tested to monitor a woody fruit plants (G3 - yellow kiwi) irrigated with two different irrigation councils, in season 2020. In Cesena cultivation conditions, kiwifruit seasonal irrigation volumes can reach about 10–12,000 m^3/ha (Holzapfel et al., 2000)[125]. In view of the foreseen climate change and reduced water availability for agricultural sector (Doll, 2002)[126], it is important to develop new and more efficient irrigation strategies for this crop (Torres-Ruiz et al., 2016)[127].

5.2.1 Material and methods

Field trial description

The kiwi trial was conducted at the Severi farm in Cesena (41m a.s.l. N 44° 8' 20.76" E 12° 14' 35.339"), in collaboration with the food cooperative Apofruit, a leader in the production and commercialization of fresh vegetables and fruit (http://www.apofruit.it/en). In the commercial vines two differently irrigated blocks were identified and equipped with 8 Bioristors each block on four plants (2 sensors per plant, Figure 16).

The sensors were mounted on two-year-old branches (Figure 17) one oriented at east and one at west of the yard. In this experimental setup, a wireless controller was developed and employed. Each controller serves 4 sensors, and it is powered by a battery connected to an 80W photovoltaic panel placed on top of the field (see Chapter 2).

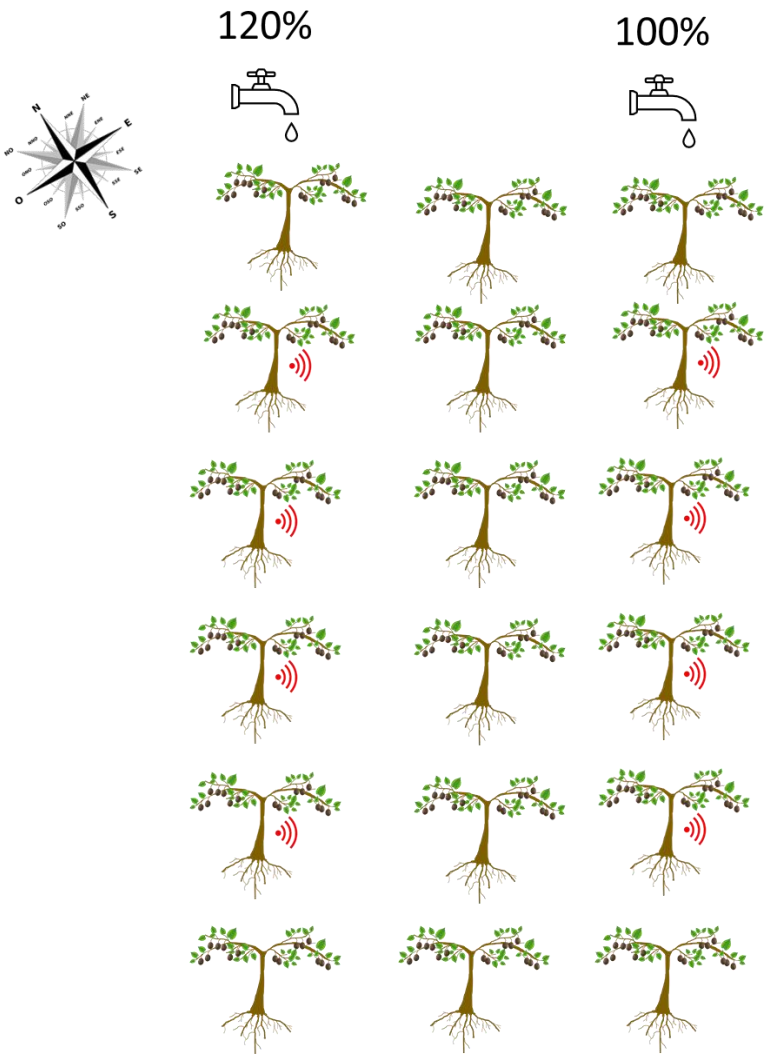

Figure 16: Kiwi vines and Bioristor installation map. Blue circle and red circle indicate plants irrigated at 100% and 120% of regular irrigation, respectively

Figure 17: a) Bioristor installed in kiwi fruit in vines; b) example of the wireless controller connected to an 80W photovoltaic panel placed on top of the field; c) control unit detail formed by Arduino DUE board, charge controller and 12V battery

Irrigation

Two systems were used in combination in this experiment: the microjet and drip system. The two plots monitored with Bioristor were differentiated in a 100% thesis, and one 100%+ extra 20% given with drip irrigation.

Agronomic measurements: Soil probe and meteorological data

Here, the rainfall events (Figure 18) volume, soil humidity (Figure 19b) and temperature (Figure 19a) at 9, 18 and 27 cm depth are reported as indicated the Bluleaf service (http://www.bluleaf.it/) from SYSMAN Progetti & Servizi S.r.l, furnishing the DSS (Decisional Support System) to the Severy farm.

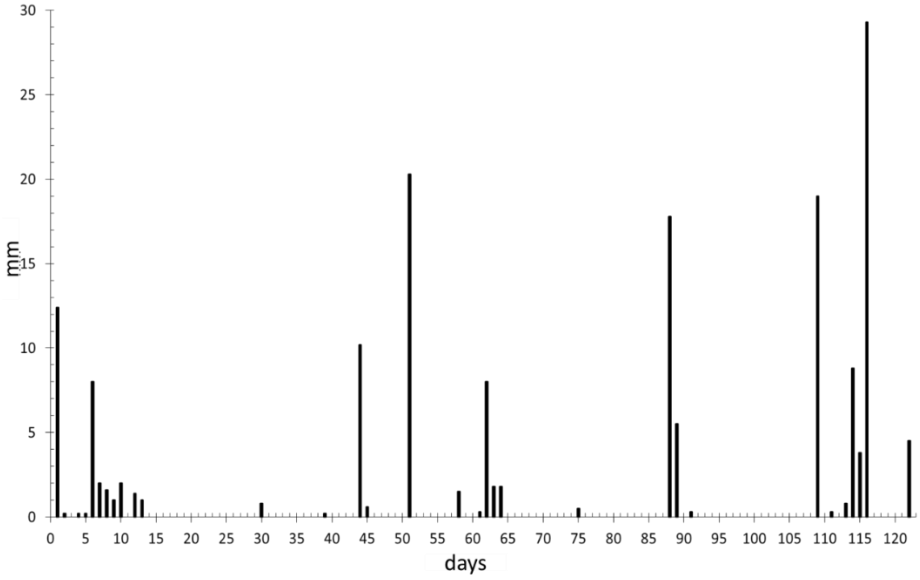

Figure 18: Cumulative daily rainfall measured during summer 2020 trial

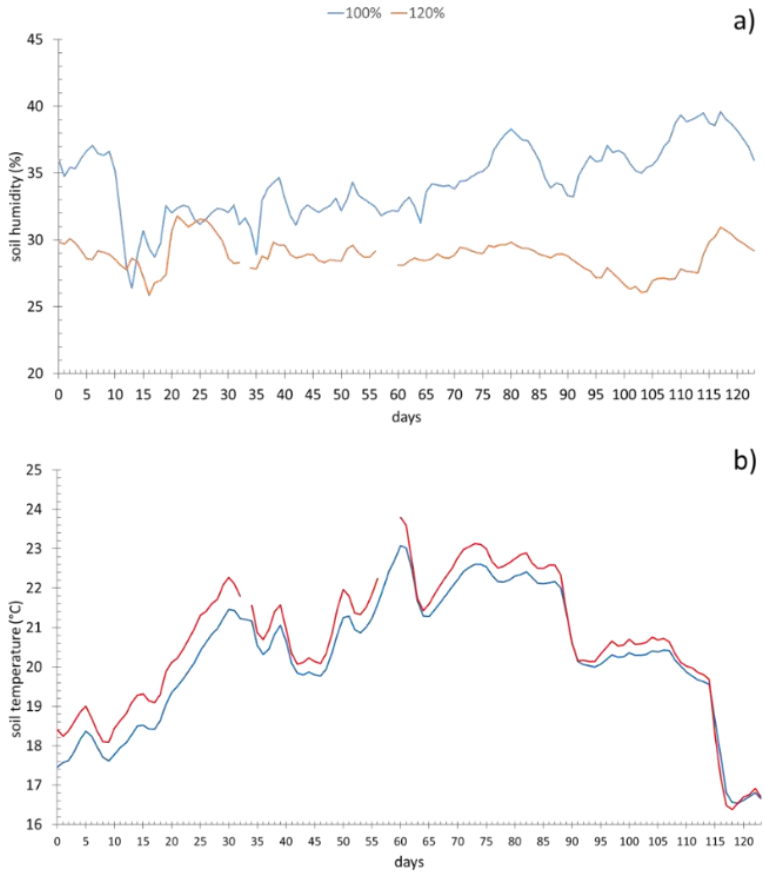

Figure 19: Soil humidity (a) and temperature (b) daily mean of probe at 9-18-27 cm depth for summer 2020 trial (blue: 100%, red: 120%)

Bioristor measurements

Bioristors were prepared and inserted into the plant stems through the use af a drill, and connected to a wireless station, as described in Chapter 2. Then, The R parameter (analyzed with MATLAB (https://uk.mathworks.com/) and Microsoft Excel 2016) was mediated over the day.

Physiological analyses

A set of physiological measurements was performed during the experiment in collaboration with Prof. Luigi Manfrini (University of Bologna) but are not here presented.

5.2.2 Results

The first result is the demonstration of the operability of Bioristor also in kiwi fruit in open field continuously for 123 day (4 months). As reported for tomato, also in kiwi, the Bioristor was able to detect the rainy events by an increase of the sensor response R as a result of a decrease in transpiration although with smaller values with respect with tomato (18-25%). This can be due to the type of training adapted for kiwi cultivation, usually at pergola that prevents the canopy to be completely reached by rain, leading thus to a smaller increase in the sensor response (Figure 20).

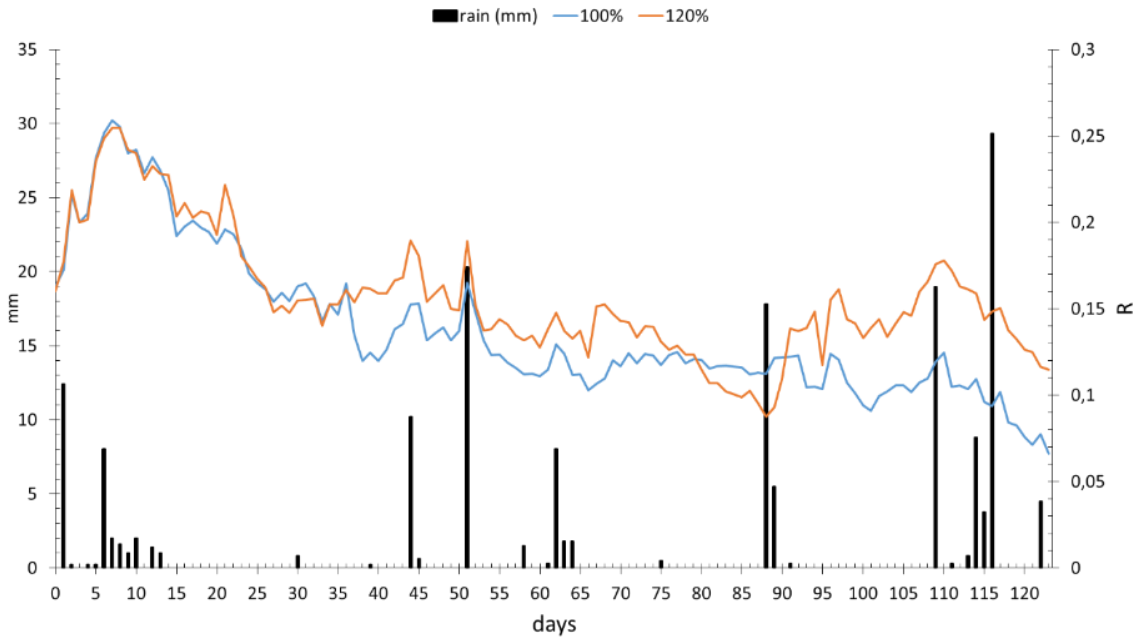

Figura 20: Rainfall events (black histogram) and Bioristor response (blu: 100% thesis; red: 120% thesis).

The sensor response has been analysed and divided in four phases (Figure 22). Although differently irrigated, during the first phase (P1, 0-36 days), the two theses had a superimposable trend. Upon an exchange with the runner of the field, the differentiation was not imposed resulting in a 100% of water given for both theses. However, the volume of water used in this 36 days was not sufficient to prevent the occurrence of a severe drought stress as highlighted by the rapid and continuous decrease of R until day 27 that remains steady till day 36.

Here an interesting information is gained by the application of Bioristor. Although the irrigation was considered sufficient and, as reported in Figure 21, the soil humidity indicates similar and normal values (30-35%), the Bioristor enabled the detection of a severe drought stress occurring in both thesis (Figure 20).

These data are supported also by the Bluleaf DSS that recorded an intense drought stress in the indicated dates (data not shown).

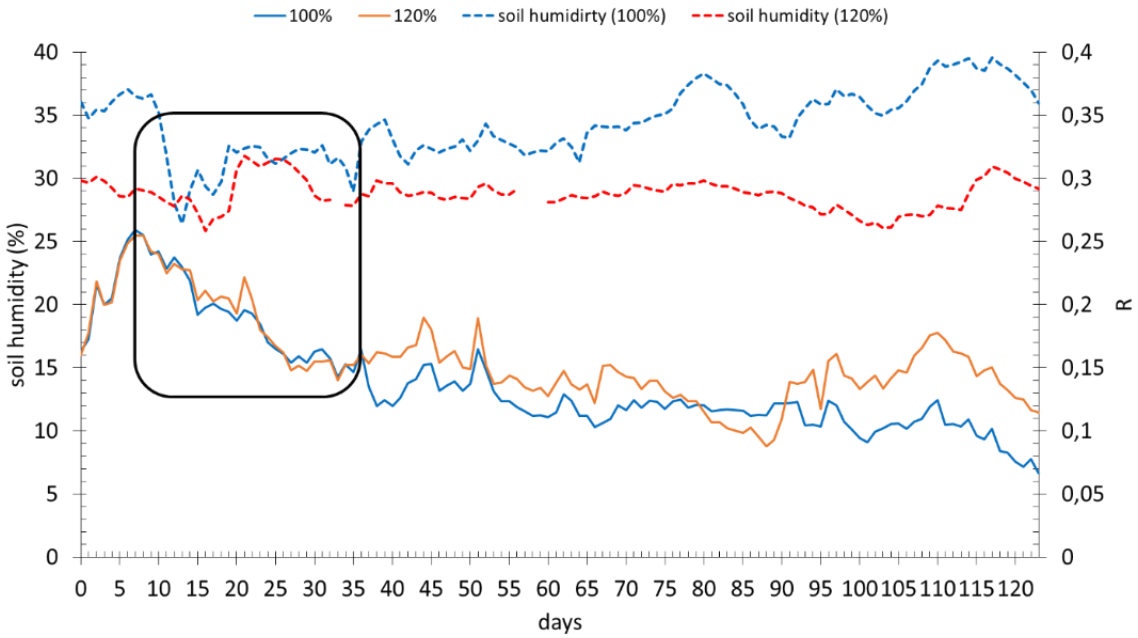

Figure 21: Kiwifruit agronomic measurements: soil humidity (blue dashed line: 100% thesis; red dashed line: 120% thesis) and Bioristor response (blue: 100% thesis; red: 120% thesis).

The second phase (P2, 36-67) starts with the significant and evident differentiation for the R value of the two theses ($p \leq 0.001$), in accordance with the water volumes used for each thesis. The third phase (P3, 67-110 days) is characterized by the completely different trend observed in the two theses. The 120% thesis revealed a severe stress in 67-89 days, as also confirmed by physiological tests (data not shown), followed by a recovery period that brings the R of the 120% thesis back to pre-stress values by the end of the phase. In contrast, as expected, the 100% thesis remains stable throughout the duration of the third phase. Finally, the signals of both theses decline following the onset of fruit ripening (P4, 110-123 days). As in tomato, also in yellow kiwifruit the dry substance progressively increases in the fruit, with consequent leaves senescence and reduction of leaves transpiration[123].

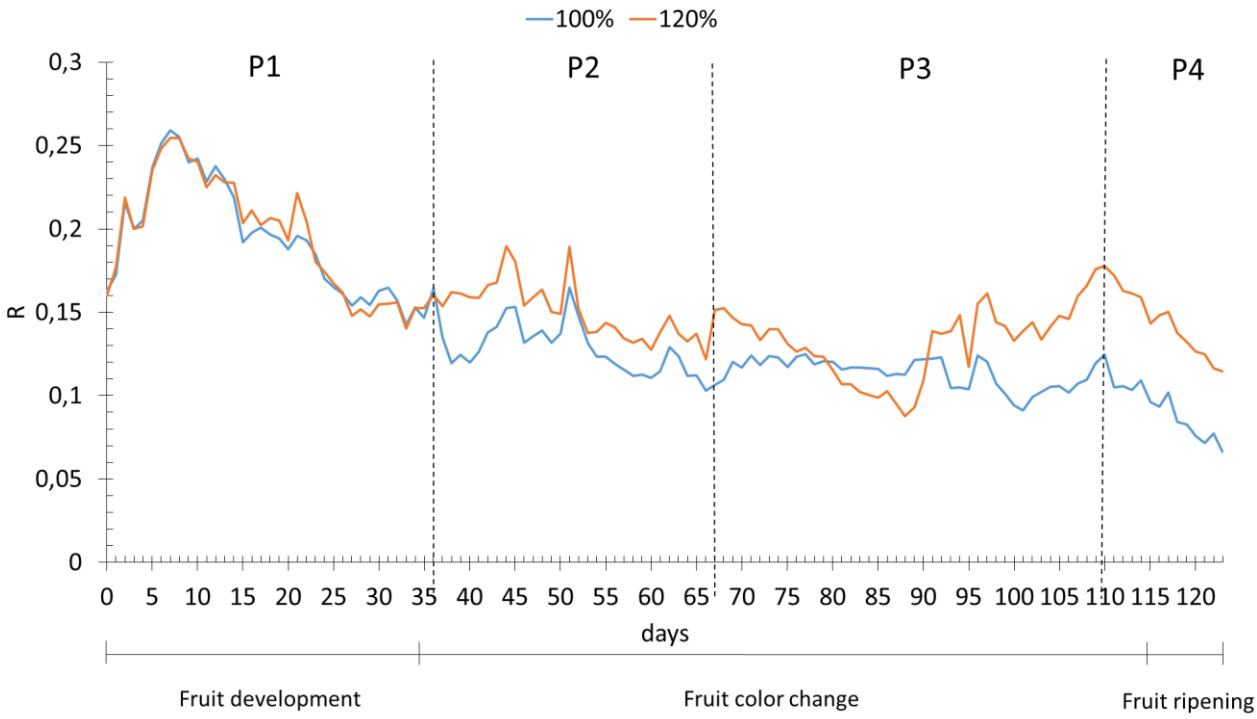

Figure 22: Plot of the daily average of the R measured on 100% thesis (blue line) and 120% thesis (red line) for 123 days of measurements.

Yields have been evaluated for both thesis and no significant differences have been recorded for both theses, leading to hypothesize that the 20% increase was not necessary to enhance kiwi productivity in the 2020 season.

However, further elaborations are needed to better dissect the single physiological components to analyse them with respect to the acquired R data from Bioristor.

5.3 Discussion

The ability to detect drought stress before it causes irreversible physiological and morphological damage is important for crop management and to increase water use efficiency in agriculture. To date crops and livestock already account for 70 percent of all water withdrawals globally, and up to 95 percent in some developing countries (http://www.fao.org/3/i9900en/i9900en.pdf). This water demand is likely to increase as global population growth and economic development drive up food

demand. FAO estimates that more than 40% of the world's rural population in river basins are classified as water scarce (2011) and if current consumption patterns continue, two-thirds of the world population could be living in water-stressed countries by 2025. Sustainable and efficient water management practices in agriculture are key to the success of the 2030 Agenda and offer many climate changes benefits.

In this thesis we considered tomato as key crop in the Italian fresh horticulture products. Tomato (*S. lycopersicum* L.) is one of the largest cultivated vegetable species worldwide, with a production of approximately $182x10^6$ metric tons in 2018 and more than $4x10^6$ ha of area harvested with a total value of approximately $1.67 billion. Tomato is also a higher water demanding crop that requires irrigation throughout the growing season. The irrigation water demand in tomato growth in field conditions can range between 400 and 600 mm depending on climatic condition[128] ensuring a production in terms of dry fruit yield biomass from 4 to 8 t ha^{-1} and fresh fruit yield from 80 to 160 t ha^{-1}. More than 1,340 m^3 of fresh water must be used to produce only 1 Kg of Passata di pomodoro, 370 liters of water consumed to gain 1 Kg of fresh food[129]. In the last year due to water scarcity and the effects of climate change, the production of tomato for industry shrunk of about 15% the total production in the north Italy district. Here the importance to optimize the water consumption through irrigation, firstly to preserve the natural resources and in second place to ensure food security.

Here we consider also as target species Actinidia (kiwi fruit-G3) being Italy the second world producers with 562.00 metric tones produced in 2018 with 25000 ha cultivated. Actinidia species originated in South-East China, are conventionally growth under conditions of high precipitation and relative humidity. *Actinidia deliciosa* (kiwifruit) requires high amounts of irrigation water when cultivated in Mediterranean regions, and can reach seasonal irrigation volumes of about 10–12,000 m^3/ha[125]. In view of the foreseen climate change and reduced water availability for agricultural sector[126], it is important to increase water use efficiency for this crop.

To this end precision agriculture is considered an efficient approach to optimize agriculture management. Usually, proximal sensors (soil probe) and remote sensors (drones and satellites) are nowadays commonly used in precision agriculture although not able to simultaneously provide *in-vivo*, continuously real-time information on physiological changes in plants due to abiotic stress or environmental changes. Based on our experiments, the Bioristor confirmed to be suitable for monitoring in open field changes in the ion uptake and transport in plants during severe drought stress in a proportional manner. Here Bioristor is proposed as additional and fundamental tool to be included in measurement systems used so far in agriculture, considering the higher sensitivity in detecting changes in plant state even compared to conventional physiological tests. Indeed, as well as

confirming its effectiveness in working for the growth cycle in field and detecting water stress even in the open field in different plant species (tomato and kiwi), it can discriminate physiological changes in the plant induced by different levels of water deficiency, from 20% to 120% of regular water irrigation. The percentage of water saving, estimated in the case of tomato as 36% and 34% of the water used in regular irrigation, highlight its efficacy in optimizing water use. Water management and environment sustainability can significantly benefit of Bioristor use, save in tomato cultivation **35% of water means 67 billion of cubic meter of water saved in one season** is equal to a volume of water comparable to 3 times the Lago di Como (22.5 Km^3).

At the onset of water stress kiwi triggers a range defense mechanisms mainly focused on the stomatal control to reduce water losses and to keep its water potential high enough to avoid serious damage[127]. This control of stomatal behavior has been previously observed for other species. Fruit development and the mechanisms leading to growth and dry matter accumulation in the fruit play a pivotal role in defining kiwi water demand. Bioristor proves to be effective in determining water stress in contrast with the soil water humidity measurements and showed that during the last phases of fruit development, an excess of water given through irrigation can triggered a set of responses like those of water deprivation, negatively impacting on fruit development and quality. Our results agree with the general observation that vascular and transpiration flows to/from the fruit showed a decreasing trend during the season reported in Torres et al 2016[127].

Even though kiwi G3 plants were regularly irrigated, the occurrence of severe drought stress was detected by Bioristor in early phases of measurement and might indicate that an alteration of the transpiration regulation occurred altering the the ion concentration and accumulation in the plant vessels.

Another important result achieved through the application of Bioristor both in horticulture and in fruit plants in fields is the ability to detect the conditions that can boost plant diseases, widespread in vineyards. As described in chapter 4, the degree of leaves wetness, and in particular the water droplets on the leaf surface impacts on the ability of pathogen to reach and colonized plant tissues[118,119]. Being Bioristor able to detect and measure directly from the plants the increased amount and exposure time of water on the leaves surface, can enable the identification of the most efficient time window to perform pesticides treatment thus preventing yield losses and preserving food safety.

Taking all together our result, lead to hypothesize that in filed conditions Bioristor can give a concrete support to precision agriculture and towards the achievement of the UN SDG.

Chapter 6

In-vivo monitoring of *Arundo donax* response to salt stress through an OECT-based biosensor

One of the main impacts of climate change on agriculture production is the dramatic increase of saline (Na^+) content in soil, that will impair crop performance and productivity. Soil salinization is a major threat to agriculture in arid and semi-arid regions where water scarcity and inadequate drainage of irrigated lands severely reduce crop yield. Moreover, salt accumulation inhibits plant growth and reduces the ability to uptake water and nutrients, leading to osmotic or water-deficit stress. Globally, the area of saline soil worldwide is as large as 397 million ha, and almost 19.5% of the irrigated soils are today salt-affected[130]. It is well established that a high soil salinity impacts on the survival of many plant species, especially glycophytes[131]. To address growing needs of food production, usable land must be expanded, and plant species (genotypes) resistant to salinity must be identified[132]. Salinity may be tolerated by plants through different strategies involving either 'tissue tolerance', where toxic ions are compartmentalized into specific tissues, cells and subcellular organelles, or 'toxic ion exclusion', where plant survival is maintained by fast translocation of Na^+ out of the plant to avoid excessive accumulation into the shoot apical meristems[133–135].

So far, a wide range of physiological, biochemical, and molecular analyses are employed to detect and study salinity stress and how it adversely affects plant growth and performance[136–142]. However, these methods, that mainly rely on destructive assays or on digital imaging, allow us to assess only indirectly the effects of saline stress on plants performances[82,135,143–146]. Here the ability of the Bioristor to monitor *A. donax* plants challenged with a severe salt stress was proved. *A. donax* is a monocot species responsive to salt treatment[147]and a promising crop for both bioenergy and biomass feedstock[148]. In this chapter the use of the Bioristor as a rapid and non-destructive method of salt stress detection was evaluated, to increase the knowledge on the mechanisms employed by *A. donax* to overcome saline stress. Data and the text in this chapter are taken from a paper submitted to a major journal such as Scientific Report.

6.1 Material and Methods

Plant material and salt (NaCl) stress application

Our experiment was conducted and included in a series of experiments performed by IPSP-CNR. *A. donax* plants were propagated by rhizomes in Sesto Fiorentino (43°81′75″ N, 11°18′88″ E) (Italy). Plants were obtained from rhizomes and growth in 6 L pots containing quartz sand. In two months and then kept growing in a climatic chamber under controlled environmental conditions: maximum and minimum (day/night) temperature of 30°C and 22°C, respectively; maximum and minimum relative air humidity of 60% and 40%, respectively; photosynthetic photon flux density (PPFD) of 700 µmol m^{-2} s^{-1} for 14 hours per day). Plants were watered weekly with full strength Hoagland solution in order to supply mineral nutrients to optimal level until the beginning of the experiment.
The experiment was performed by growing two different groups of 10 *A. donax* plants: a) under optimal nutritional conditions by applying the standard Hoagland solution (control); b) by applying Hoagland solution where 200 mM NaCl (Na^+ salt stress) were added. These solutions were supplied twice a week; the treatment lasted 37 days (Figure 1A).

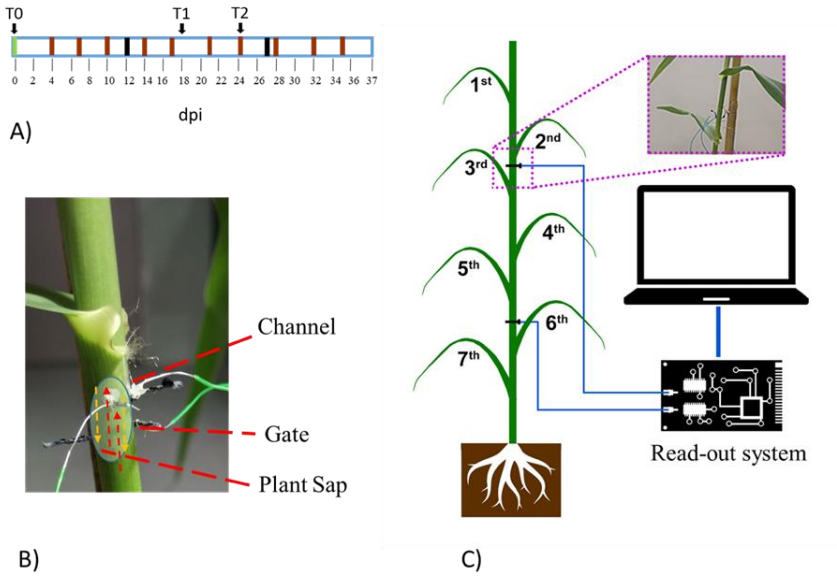

Figure 1. Real-time monitoring of salinity response in *A. donax* with Bioristor. **A)** Experimental set-up: the green block indicates the insertion of sensors into *A. donax* stem; brown lines indicate saline treatments (200 mM NaCl) and the black lines correspond to the sensor maintenance. Destructive measurements were performed at T0 (1 day), T1 (day 18, median phase), T2 (day 24, final phase); **B)** A detailed view of a Biostor inserted into *A. donax* stem. Dashed yellow and red lines represent the sap movement directions. (**C)** Scheme of the Bioristor installation into *A. donax* plants; two sensors were inserted: one between the 2nd and the 3rd leaf (apical sensor, AS), and a second one between the 5th and 6th leaf (basal sensor, BS).

Bioristor measurements

Bioristors were prepared, inserted into the plant stems, and connected to a computer as desribed in Chapter 2. The calculated R parameter at gate voltage of 0.6V (see Chapter 2) was analyzed with MATLAB (https://uk.mathworks.com/) and Microsoft Excel 2016). When monitoring the plant sap concentration over several days it showed to be useful to smooth out the day/night signal oscillations due to plant circadian rhythms that characterize the Bioristor response[39]. Thus, the ratio between the signal recorded form sensors installed in salt-stressed and control plants was expressed as Normalized Response (NR):

$$NR = \frac{R_{stress}}{R_{control}}$$

To investigate the possibility to track the ion transport (in specific of the Na^+ ion) along the plant culms of *A. donax* plants, two Bioristor sensors were integrated at two different heights along the same culm, the apical sensor (AS) between the 2nd and 3rd leaf and the basal sensor (BS) between the 5th and 6th leaf from the apex (Figure 1C) in 3 control and 3 salt-stressed *A. donax* plants (for a total of 12 sensors). From the overall data acquired (37 days), three intervals, defined from the day of installation (days 1-7; days 13-19; days 27-37) have been selected as the most representative of the entire set of measurements due to both their low background noise and accuracy which have been indicated as initial (days 1-7), median (days 13-19) and final (days 27-32) phase. The median and final phases began with a sensor maintenance causing a variation in the recorded values due to the new sensor's part integration. Therefore, these three intervals should be read as independent measurements and therefore the moving average of the NR was evaluated for each of those.
The operability of the Bioristor was validated within the range of sodium (Na^{+}), calcium (Ca^{2+}) and potassium (K^+) concentrations detected in the leaves; the sensor response was measured *in-vitro* by using different solutions at low concentrations of Na^+ (0.01 to 0.19 M), K^+ (0.2 to 0.8 M), and Ca^{2+} (0.01 to 0.1 M).

Physiological analysis

The transpiration flux of H_2O (TR) and the photosynthetic CO_2 assimilation rate (PR) were measured *in-vivo* in the 2nd and 5th leaf (from the shoot apex) of *A. donax* plants by IPSP-CNR. Analysis was performed in leaves sampled at different days post insertion of the sensor: day 1, day 14, day 24.
Moreover, IPSP-CNR group determined the concentrations of Na^+, Ca^{2+} and K^+ (μg g^{-1} DW) accumulated in 1 g of leaves of *A. donax* plants by flame atomic absorption spectrometry (Analyst

200, Perkin Elmer). Analysis of these mineral elements was performed in the same leaves following gas exchange measurements.

Statistical analyses

All data retrieved from the sensors were statistically analysed by applying a multi-comparison approach using the Analysis of Variance (ANOVA) in MatLab 2014a (8.3.0.532). Principal components analyses (PCA) was performed using the R "prcomp" function and represented as a biplot by using the R package factoextra[71]. The first two principal components PC1 and PC2 and the corresponding component loading vectors were visualized and summarized in a biplot, in which component scores (indicated in dots) are colored according to thesis classification. Analysis of variance (ANOVA) was performed to assess the effect of Na^+ supply in *A. donax* plants ($p \leq 0.05$ level).

6.2 Results

In this study, the Bioristor was applied to investigate changes in *A. donax* sap composition to track *in-vivo* and in real-time the plant's response triggered by the application of severe saline stress conditions. The Bioristor confirmed its ability to monitor daily variation of the sensor response (R) in *A. donax* as previously reported in tomato[39], with R values increasing during the night and rapidly decreasing during the day (Figure 2) both in the apical sensor (AS) and in the basal sensor (BS).

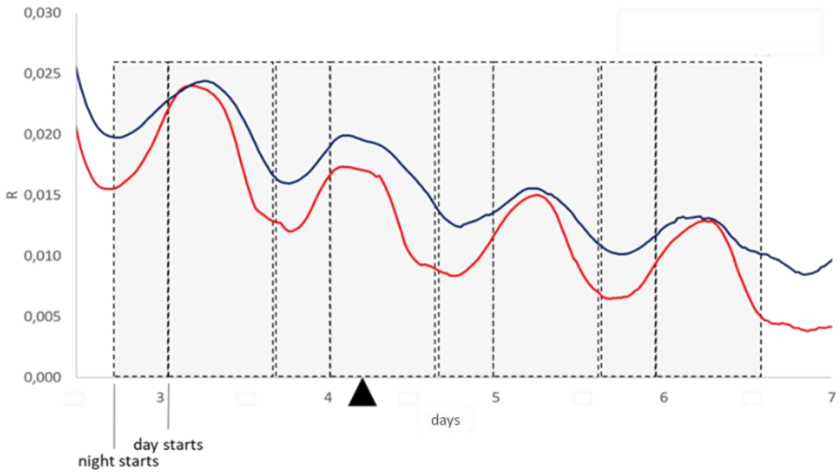

Figure 2. Sensor response (R) calculated as average over a period of 5 days (3-7 days). Grey boxes refer to a day period. Triangle indicates the application of saline treatment. Each line is the mean of data collected in 3 plants.

The ability of Bioristor to reveal changes in the concentration of Ca^{2+}, K^{+}, and Na^{+} during the saline stress was firstly demonstrated *in-vitro*. The transfer characteristics of the sensor response were measured (Figure 3) using concentrations of these ions within the range found in the leaves during the saline stress (see Table 1). The *in-vivo* test on *A. donax* plants confirmed this property of the Bioristor. The linear response of the sensor versus the ions concentration (Figure 4) showed that the Bioristor was able to detect changes in all tested ions.

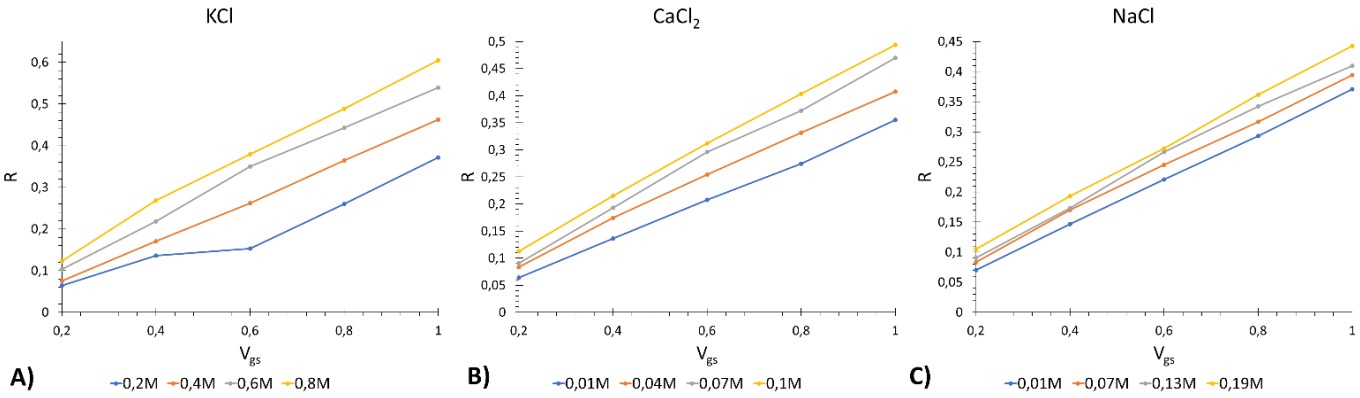

Figure 3: Transfer characteristics of the Sensor Response (R) measured using different concentration of A) K^{+}, B) Ca^{2+} and C) Na^{+} salts, as a function of gate voltage from 0.2 to 1 V with 0.2 V step.

The linear response of the sensor versus the ions concentration (Figure 4) showed that the Bioristor was able to detect changes in all tested ions.

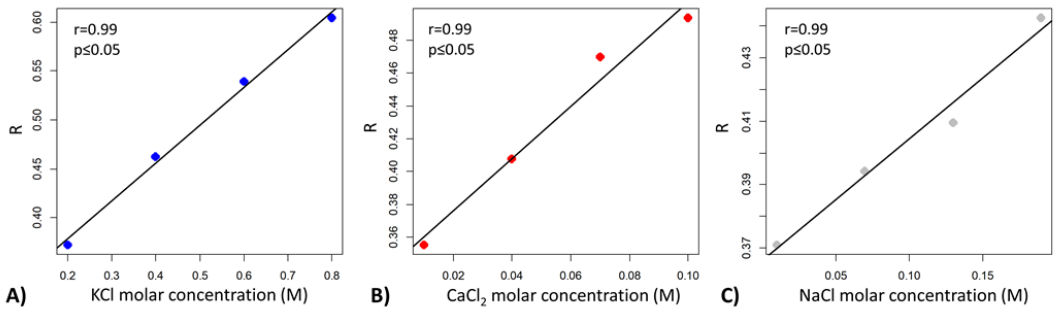

Figure 4. Scatter plots of the correlation between the Sensor Response (R) measured at 1V and the molar concentration of A) K+ (blue dots); B) Ca2+ (red dots); C) Na+ (grey dots).Table 1. Concentration of Na+ (µg g-1), K+ (µg g-1) and Ca2+ (µg g-1) in control and salt stressed. A. donax plants were measured at different sampling times: T0 (initial phase), T1 (median phase), and T2 (final phase). Values are means ± standard errors are shown (n= 4). ANOVA was reported to assess statistical differences between control and salt-stressed plants and between apical and basal leaf level (***, $p \leq 0.001$; **, $p \leq 0.01$; *, $p \leq 0.05$; ns, not significant).

Table 1. Concentration of Na^+ (µg g^{-1}), K^+ (µg g^{-1}) and Ca^{2+} (µg g^{-1}) in control and salt stressed. A. donax plants were measured at different sampling times: T0 (initial phase), T1 (median phase), and T2 (final phase). Values are means ± standard errors are shown (n= 4). ANOVA was reported to assess statistical differences between control and salt-stressed plants and between apical and basal leaf level (***, $p \leq 0.001$; **, $p \leq 0.01$; *, $p \leq 0.05$; ns, not significant).

day		**Na^+ (µg g^{-1})**			**K^+ (µg g^{-1})**			**Na^+/K^+**			**Ca^{2+} (µg g^{-1})**		
		Control	Stress		Control	Stress		Control	Stress		Control	Stress	
0	*apical leaf*	-	-	p-level (control vs stress)	49935.5 ± 3922.2	-	p-level (control vs stress)	-	-	p-level (control vs stress)	2562.4 ± 479.8	-	p-level (control vs stress)
	basal leaf	-	-		44195.7 ± 5828.3	-		-	-		4068.9 ± 610.9	-	
	p-level (apical vs basal)				ns						*		
18	*apical leaf*	0.0 ± 0.0	7338.4 ± 1124.1	***	34108.4 ± 789.7	46975.7 ± 5582.3	*	0.0 ± 0.0	0.48 ± 0.03	***	1581.7 ± 189.8	2770.2 ± 659.7	**
	basal leaf	1070.3 ± 284.4	7033.4 ± 216.6	***	30336.0± 1680.7	33284.7 ± 6036.5	ns	0.11 ± 0.01	0.66 ± 0.04	**	7418.6 ± 358.1	6441.9 ± 1199.0	*
	p-level (apical vs basal)	***	ns		ns	ns		***	*		***	*	
24	*apical leaf*	0.0 ± 0.0	9024.3 ± 0.5	***	42085.8 ± 2140.0	37007.5 ± 0.5	*	0.0 ± 0.0	0.74 ± 0.00	***	2735.7 ± 413.2	6364.3 ± 0.0	***
	basal leaf	3939.4 ± 789.4	8829.3 ± 501.8	***	36123.7 ± 3347.9	44650.0 ± 1475.7	*	0.32 ± 0.01	0.59 ± 0.01	**	8957.4 ± 328.9	5438.0 ± 727.8	**
	p-level (apical vs basal)	***	ns		ns	ns		***	*		***	*	

To gain more accurate results on the trend of the Bioristor response upon saline treatment, the NR parameter allowed us to overcome the disturbance due to day/night oscillation. In the initial phase of the experiment (1-7 days), the NR of the BS showed a rapid and consistent increase (60%) after addition of Na^+ (3 day, Figure 5A) up to a maximum recorded at 6 day ($p \leq 0.001$, Figure 5A, Table 1). Whereas, the AS showed a constant and lower response than BS up to day 4 (Figure 5A). In the median phase of the experiment (13-19 days; Figure 5B, Table 1), the NR value of BS significantly increased up to 15.5 day ($p \leq 0.001$), and then decreased up to 17 day, suggesting first an ongoing accumulation and compartmentalization of Na^+ in the basal leaves. Upon a new addition of Na^+ at day 17 (the fifth salt supply, see Figure 1A), NR of AS showed a new and continuous increase ($p \leq 0.001$) (Figure 5B).

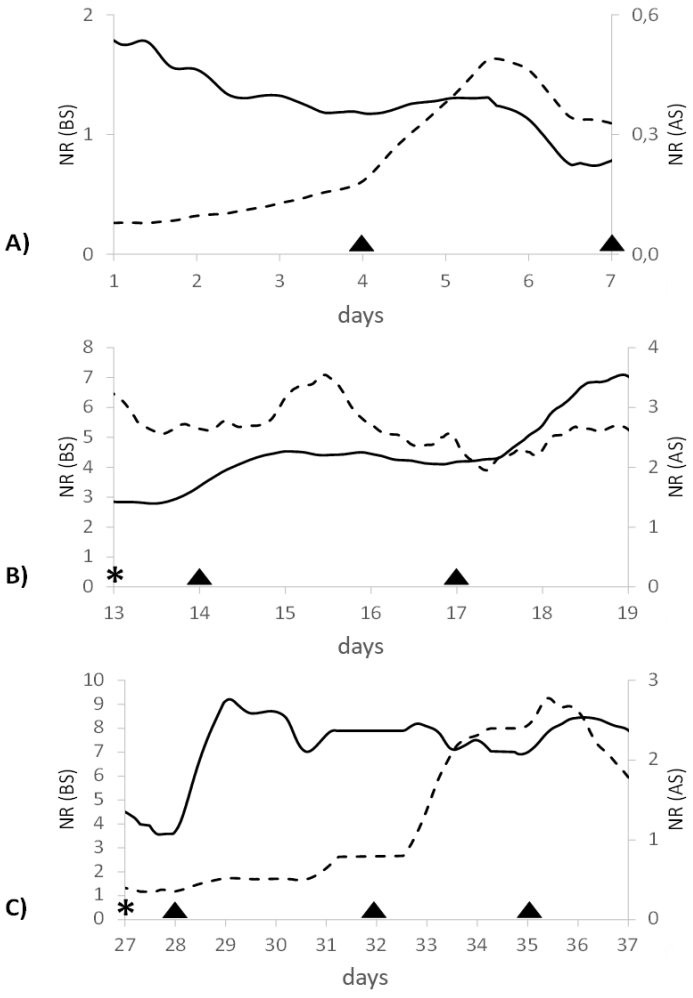

Figure 5: Normalized Sensor Response (NR) of the apical sensor (AS, solid line) and the basal sensor (BS, dashed line) in three different intervals of the experiments: (A) initial phase (1-7 day); (B) median phase (13-19 day); (C) final phase (27-37 day). Solid triangles indicate the application of saline treatments. The asterisk indicates the maintenance of the sensor. These data collected *in-vivo* are consistent with the observed general decrease in the transpiration rate measured in salt-stressed plants (Figure 6).

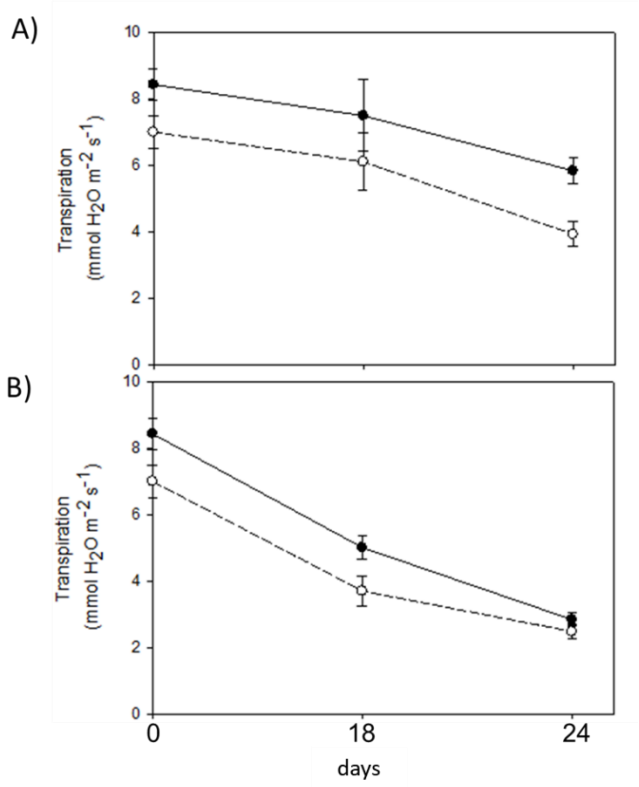

Figure 6: Transpiration rates of control (A) and salt stressed (B) *A. donax* plants measured at different sampling times: 1, 18 and 24 day (see Figure 1). Black circles indicate measurements collected from the 2nd leaf (apical leaf) and white circles indicate measurements collected form the 5th leaf form the top (basal leaf). Values are means ± standard errors (n= 4).

The final phase of the experiment covered day 27-37. Early in this phase, a stable NR signal was observed in BS. However, NR of BS increased rapidly after the addition of salt (Figure. 1A) at 32 day ($p \leq 0.001$, Figure 5C, Table 1). On the other hand, an increase of the NR signal was observed in AS at 28 day, which was not followed by additional increases after subsequent Na^+ treatments.

The transpiration rate (TR) measured in the same time range (1, 18 and 24 day) in salt-stressed plants was lower than in control ones and, in particular, TR was higher in the apical than in basal leaves of salt-stressed plants (Figure 6). Na^+ progressively accumulated in leaves of salt-stressed plants. However, Na^+ concentration did not show any statistical difference between apical and basal leaves in the median and final phases (Table 2).

PCA was performed by considering the measured variables (Na^+, K^+ and Ca^{+2} concentration and the total cations concentration and transpiration rate). Of note, to increase the accuracy of the PCA analyses the Bioristor's response R was here considered to allow for the analyses of stressed and control response. The first two components explain 86.8 % of the variability (Figure 7).

Table 2: Sensor Response (R) of control and salt stressed *A. donax* plants measured at different times: T0 (before the beginning of the experiment), T1 (initial phase), and T2 (median phase). Values are means of the daily R value ± standard errors are shown (n = 3). ANOVA has been used to assess statistical differences between leaves of control and salt-stressed plants (***, $p \leq 0.001$; **, $p \leq 0.01$; *, $p \leq 0.05$)

day		**Sensor Response (R)**		
		Control	Stress	
0	*apical leaf*	$5.24 \times 10^{-2} \pm 1.72 \times 10^{-3}$	$2.81 \times 10^{-2} \pm 6.03 \times 10^{-4}$	p-level (control vs stress) n.s.
	basal leaf	$3.27 \times 10^{-2} \pm 1.72 \times 10^{-3}$	$8.52 \times 10^{-3} \pm 6.24 \times 10^{-4}$	n.s.
	p-level (apical vs basal)	***	***	
18	*apical leaf*	$2.51 \times 10^{-2} \pm 1.17 \times 10^{-3}$	$4.23 \times 10^{-2} \pm 9.32 \times 10^{-4}$	***
	basal leaf	$1.53 \times 10^{-2} \pm 7.02 \times 10^{-4}$	$8.07 \times 10^{-2} \pm 1.44 \times 10^{-3}$	***
	p-level (apical vs basal)	***	***	
24	*apical leaf*	$3.94 \times 10^{-2} \pm 2.70 \times 10^{-3}$	$1.03 \times 10^{-1} \pm 2.56 \times 10^{-3}$	***
	basal leaf	$4.52 \times 10^{-2} \pm 3.51 \times 10^{-3}$	$7.72 \times 10^{-2} \pm 2.1 \times 10^{-3}$	***
	p-level (apical vs basal)	n.s.	***	

The first PC (PC1) explained 54.9 % of the total variability. In particular, the total cations concentration (TCC) and Na^+, K^+ and Ca^{+2} concentrations and R have large positive loading on the PC1 and are positively correlated (Figure 7). The regularly irrigated controls and the salt-stressed plants are well separated in the biplot indicating the efficacy of the saline treatment.

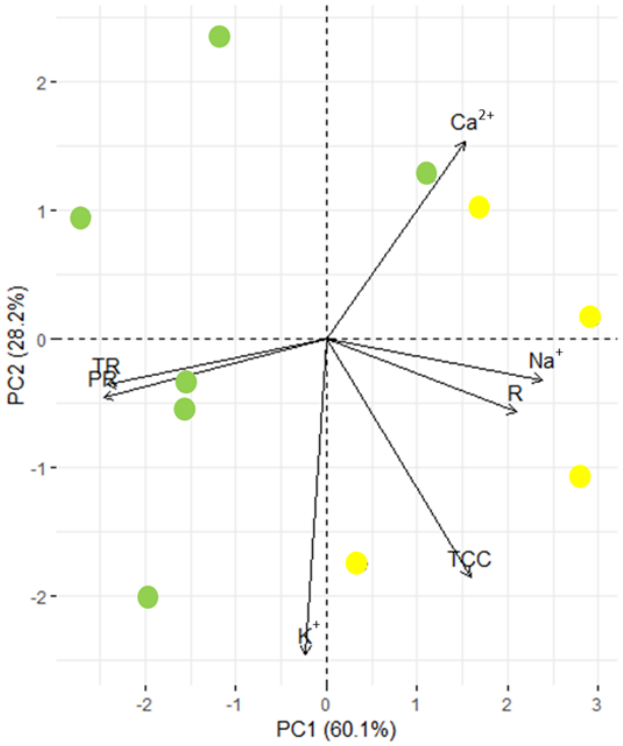

Figure 7: Biplot of the PCA results. The first two PCs display 88.3% of the total physiological variation. The component scores are colored according to the agronomic groups (yellow dots, stressed plants; green dots control plants). The components loading vectors were proportionally superimposed to their contribution, and their direction indicated the influence of variable group. R, Bioristor Response; Na^+, sodium concentration; K^+, potassium concentration; Ca^{2+}, calcium concentration; TCC, total cations concentration; TR, transpiration rate; PR, photosynthetic rate.

The analyses of the PCA loading vectors showed a high correlation between R and Na^+ concentration ($r=0.79$, $p\leq0.05$) and this is confirmed by the multivariate analysis (Figure 7), supporting the efficacy of Bioristor in revealing in real-time changes in the plant sap cation concentration during the stress. Furthermore, the analyses of the correlation between R and TR, showed a high and inverse correlation between R and TR ($r=-0.71$, $p\leq0.05$) that is recognized as strongly affected by the saline stress ($r=-0.89$, $p\leq0.05$).

The time course analyses of the ions in the plant leaves showed that Na^+ increased following the salt treatment and the decreased of Ca^{2+} concentration in salt-stressed basal leaves in comparison to the control ones, both at medial and final stages of the salt treatment. Furthermore, K^+ showed an accumulation in apical leaves only in salt stressed plants in the medial stage, whereas K^+ decreased in apical leaves and increased in basal leaves at the final stage of stress, compared to respective controls (Table 2, Figure 4,8).

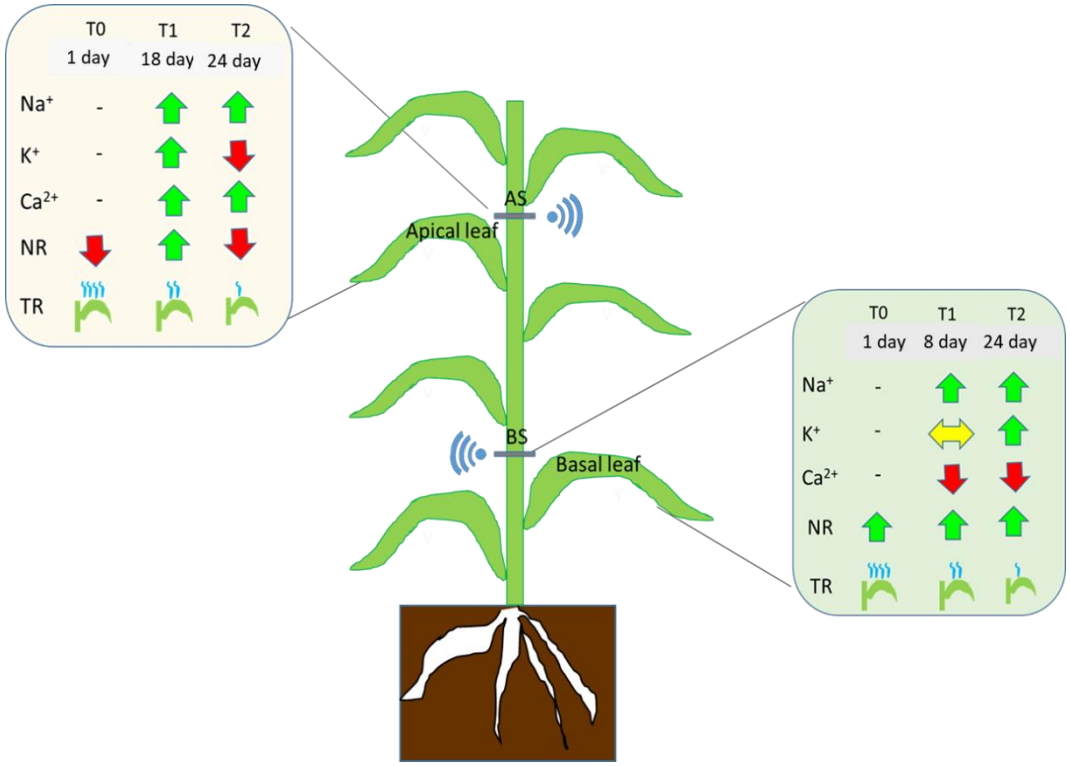

Figure 8: Qualitative visualization of the Bioristor (NR, normalized sensor response; TR, transpiration rate) and plant ions concentration (Na^+, sodium; K^+, potassium; Ca^{2+}, calcium)

6.3 Discussion

Enhancing the ability to investigate plant functions and structure through non-invasive tools and methods with high accuracy has become a major target in phenotyping for plant breeding and precision agriculture[82].

Here we use a bioelectronics approach to investigate the plant defence responses occurring under adverse growing conditions.

Organic bioelectronic devices are based upon organic electronic materials that offer efficient signal transduction from electronic input to ionic output and vice versa, while the toolbox of organic chemistry enables design and tailoring of active materials with desired characteristics, such as functionality, processability, and biocompatibility[15,17]. Organic bioelectronics devices and materials have been applied mainly in the context of light-emitting and photovoltaic devices, stretchable and wearable devices, and biomedical applications. However its usefulness and applicability in plants to monitor and control plant physiology has begun to be explored[17,39,149,150].

Conventionally, to detect the physiological status of plants, a range of technologies and/or their combinations have been applied[151–153], such as chlorophyll fluorescence imaging[154,155], multispectral imaging[156], thermal imaging[157] and electric signals[158].

Here, an OECT based sensor namely Bioristor has been applied to monitor *in-vivo* the physiological effects of salt application in *A. donax* in three intervals and we demonstrated the ability of Bioristor to return a salt stress specific response.

In particular, an increased NR in both BS and AS (Figure 5) and Pearson correlation between R and the concentration of cations clearly indicated that the Bioristor can effectively reveal presence and changes of all cations in the plant sap. Indeed, R is consistent with the daily transpiration trend due to light-driven stomatal opening and the consequent onset of transpirative passive flux from the soil to the air[45]. Plant growth and development relies on the movement of various ions through the plant sap[159]. The observed circadian variation in sap electrical conductivity of *A. donax* was consistent with the long distance transport of solutes through the xylem. In fact, ion concentrations are typically higher during the night than in the day[160] when they are diluted by the higher water transpiration stream[39].

Absence of changes in normalized response (NR) values of apical sensor (AS) during the initial stage of the salt treatments (4-6 days), may indicate that Na^+ mainly accumulate in basal leaves of *A. donax* (and it does reach the apical ones) during the first days upon the treatment (4-6 days), despite these data are not supported by quantitative data on ions concentration in leaves. Overall, our results support a positive ion compartmentalization, namely of Na^+, in the basal portion of the plant during the early phases of the saline stress, following the addition of NaCl to the substrate. The ion transport was differently described by the NR: the basal sensor (BS) continuously detected a different and higher amount of positive ions at lower rate, whereas the upper leaves showed that higher values of ions occurred at a later stage of salinity stress (14 day). When compared with *in-vivo* assessment of leaf transpiration, the Bioristor showed a similar trend of the transpiration stream allowing for the continuously measured of the ion presence in the plant sap and indirectly of the occurrence of the transpiration stream in *A. donax* plants growth under saline stress conditions. High-resolution sensors are powerful tools to investigate promptly plant responses. In this study case, the Bioristor highlighted the potential to synchronize plant functions and environment variations in time series, by providing a continuously monitoring in real-time of the dynamic changes.

The lower transpiration rate (TR) in salt-stressed plants than in control ones and the higher TR in the apical than in basal leaves of salt-stressed plants were expected as root absorption of Na^+ enhanced the synthesis of ABA that causes a prompt stomatal closure and thus limits transpiration[161,162].

However, the toxic accumulation of Na^+ and the enhancement of both K^+ uptake and accumulation imply that Na^+ and K^+ transporters and channels play a major role in salt stress tolerance[163].

The combination of sensors applied in the apical and basal plant parts allowed to hypothesize the trend in time and space of ions or positive electrolytes transport along the culm. The application of the Bioristor to *A. donax* plants revealed an initial compartmentalization of the Na^+, K^+ and Ca^{2+} ions into the basal leaves during the early stages salt stress, whereas Na^+ reaches the apical leaves at later stages of the salt stress. The application of the Bioristor on several plant species and its development for the ion specific detection can significantly improve *in-vivo* plant phenotyping and the real-time monitoring of salt stress for the identification of salt resilient genotypes.

Chapter 7

Conclusions

The present thesis work represents a breakthrough in the use of *in-vivo* sensing technology in plant. The bioristor provides new insights in the dynamic changes of the chemical composition of the sap in the xylem occurring in drought-stressed tomato and kiwi plants in controlled environment. Moreover, its potential to differentiate the response between two cultivars is foreseen, proposition for Bioristor as a tool breeding selection for drought resilient genotypes. Interestingly, Bioristor provides information on the defense response enhanced by the application of biostimulants on drought-stressed plants.

Our experiments performed in controlled and open field conditions, reinforce the characteristic features of Bioristor: i) its ability to continuously monitor plant physiology, ii) its minimal invasiveness, iii) its low cost, and its ease of generating readable and sharable data hypothesizing a future as new sensor in the high-throughput phenotyping scenario as demonstrated in the tomato Bioristor mesurements coupled with image based phenotyping data. Considering that agriculture is currently withdrawing 70% of the fresh water available in the planet, the possibility to early detect the onset of a water deprivation, can represent a concrete step forward the optimization of irrigation and the achievement of UN sustainable development goals. The use of Bioristor to guide the irrigation in both tomato and kiwifruit would reduce of approx. 35% the irrigation volumes.

The use of the Bioristor as a smart sensor in greenhouse conditions to fine tune the regulation of VPD can be used to achieve increased water use efficiency and yield.

Finally, salinity stress, was detected in a specific manner, allowing to hypothesize the ability to define the use of sea water for tomato irrigation and improve fruit quality by constantly monitoring the plant health boosting water reuse and improving quality without compromising yield (**Chapter 6**).

Bibliography

1. Priscoli, J. Water and civilization: using history to reframe water policy debates and to build a new ecological realism. *Water Policy* (2000).

2. Andersson, B. & Larsson, B. Influence of Local Temperature Changes in the Preoptic Area and Rostral Hypothalamus on the Regulation of Food and Water Intake. *Acta Physiol. Scand.* (1961) doi:10.1111/j.1748-1716.1961.tb02203.x.

3. FAO. FAO'S Work on Climate change. United Nations Climate Change Conference 2019. 1–40 (2019).

4. Kohli, A., Frenken, K. & Spottorno, C. Disambiguation of water use statistics. *Fao Aquastat* 1–5 (2010).

5. FAO. How to Feed the World in 2050. *Insights from an Expert Meet. FAO* (2009).

6. Jackson, N., Konar, M. & Hoekstra, A. Y. The water footprint of food aid. *Sustain.* **7**, 6435–6456 (2015).

7. *The World Bank Annual Report 2016*. *The World Bank Annual Report 2016* (2016). doi:10.1596/978-1-4648-0852-4.

8. United Nations. *World Population Prospects 2019: Highlights*. *United Nations Publication* (2019).

9. Bansod, B., Singh, R., Thakur, R. & Singhal, G. A comparision between satellite based and drone based remote sensing technology to achieve sustainable development: A review. *Journal of Agriculture and Environment for International Development* (2017) doi:10.12895/jaeid.20172.690.

10. K. R. Krishna. *PUSH BUTTON AGRICULTURE Robotics, Drones, Satellite-Guided Soil and Crop Management*. *Psychology Applied to Work: An Introduction to Industrial and Organizational Psychology, Tenth Edition Paul* (2012).

11. Dobriyal, P., Qureshi, A., Badola, R. & Hussain, S. A. A review of the methods available for estimating soil moisture and its implications for water resource management. *Journal of Hydrology* (2012) doi:10.1016/j.jhydrol.2012.06.021.

12. Aqeel-Ur-Rehman, Abbasi, A. Z., Islam, N. & Shaikh, Z. A. A review of wireless sensors and

networks' applications in agriculture. *Comput. Stand. Interfaces* (2014) doi:10.1016/j.csi.2011.03.004.

13. Khodagholy, D. *et al.* High transconductance organic electrochemical transistors. *Nat. Commun.* (2013) doi:10.1038/ncomms3133.

14. Rivnay, J. *et al.* High-performance transistors for bioelectronics through tuning of channel thickness. *Sci. Adv.* (2015) doi:10.1126/sciadv.1400251.

15. Rivnay, J. *et al.* Organic electrochemical transistors. *Nature Reviews Materials* (2018) doi:10.1038/natrevmats.2017.86.

16. Liao, J., Si, H., Zhang, X. & Lin, S. Functional sensing interfaces of PEDOT:PSS organic electrochemical transistors for chemical and biological sensors: A mini review. *Sensors (Switzerland)* (2019) doi:10.3390/s19020218.

17. Bernacka-Wojcik, I. *et al.* Implantable Bioelectronics: Implantable Organic Electronic Ion Pump Enables ABA Hormone Delivery for Control of Stomata in an Intact Tobacco Plant (Small 43/2019). *Small* (2019) doi:10.1002/smll.201970233.

18. Rivnay, J., Owens, R. M. & Malliaras, G. G. The rise of organic bioelectronics. *Chemistry of Materials* (2014) doi:10.1021/cm4022003.

19. Berggren, M. & Richter-Dahlfors, A. Organic bioelectronics. *Adv. Mater.* (2007) doi:10.1002/adma.200700419.

20. Owens, R. M. & Malliaras, G. G. Organic electronics at the interface with biology. *MRS Bull.* (2010) doi:10.1557/mrs2010.583.

21. Simon, D. T., Gabrielsson, E. O., Tybrandt, K. & Berggren, M. Organic Bioelectronics: Bridging the Signaling Gap between Biology and Technology. *Chemical Reviews* (2016) doi:10.1021/acs.chemrev.6b00146.

22. Berggren, M. *et al.* Ion Electron–Coupled Functionality in Materials and Devices Based on Conjugated Polymers. *Advanced Materials* (2019) doi:10.1002/adma.201805813.

23. Garrett, C. G. B. & Brattain, W. H. Physical theory of semiconductor surfaces. *Phys. Rev.* (1955) doi:10.1103/PhysRev.99.376.

24. Wikimedia Commons. Band Gap Comparison. *Online* (2015).

25. Groenendaal, L., Jonas, F., Freitag, D., Pielartzik, H. & Reynolds, J. R. Poly(3,4-

ethylenedioxythiophene) and its derivatives: past, present, and future. *Adv. Mater.* (2000) doi:10.1002/(SICI)1521-4095(200004)12:7<481::AID-ADMA481>3.0.CO;2-C.

26. Zhu, Z., Liu, C., Jiang, F., Xu, J. & Liu, E. Effective treatment methods on PEDOT:PSS to enhance its thermoelectric performance. *Synthetic Metals* (2017) doi:10.1016/j.synthmet.2016.11.011.

27. Kumar, S. R. S., Kurra, N. & Alshareef, H. N. Enhanced high temperature thermoelectric response of sulphuric acid treated conducting polymer thin films. *J. Mater. Chem. C* (2015) doi:10.1039/c5tc03145a.

28. Mengistie, D. A., Wang, P.-C. & Chu, C.-W. Highly Conductive PEDOT: PSS Electrode Treated with Polyethylene Glycol for ITO-Free Polymer Solar Cells. *ECS Trans.* (2013) doi:10.1149/05811.0049ecst.

29. Palumbiny, C. M. *et al.* Molecular reorientation and structural changes in cosolvent-treated highly conductive PEDOT:PSS electrodes for flexible indium tin oxide-free organic electronics. *J. Phys. Chem. C* (2014) doi:10.1021/jp501540y.

30. Wang, Y. Research progress on a novel conductive polymer-poly(3,4-ethylenedioxythiophene) (PEDOT). *J. Phys. Conf. Ser.* (2009) doi:10.1088/1742-6596/152/1/012023.

31. Nikolou, M. & Malliaras, G. G. Applications of poly (3,4-ethylenedioxythiophene) doped with poly(styrene sulfonic acid) transistors in chemical and biological sensors. *Chem. Rec.* (2008) doi:10.1002/tcr.20133.

32. Strakosas, X., Bongo, M. & Owens, R. M. The organic electrochemical transistor for biological applications. *Journal of Applied Polymer Science* (2015) doi:10.1002/app.41735.

33. Gründler, P. *Chemical sensors: An introduction for scientists and engineers*. *Chemical Sensors: An Introduction for Scientists and Engineers* (2007). doi:10.1007/978-3-540-45743-5.

34. Dimitriev, O. P., Grinko, D. A., Noskov, Y. V., Ogurtsov, N. A. & Pud, A. A. PEDOT:PSS films-Effect of organic solvent additives and annealing on the film conductivity. *Synth. Met.* (2009) doi:10.1016/j.synthmet.2009.08.022.

35. Krebs, F. C. Fabrication and processing of polymer solar cells: A review of printing and coating techniques. *Solar Energy Materials and Solar Cells* (2009)

doi:10.1016/j.solmat.2008.10.004.

36. Pappa, A. M. *et al.* Organic Transistor Arrays Integrated with Finger-Powered Microfluidics for Multianalyte Saliva Testing. *Adv. Healthc. Mater.* (2016) doi:10.1002/adhm.201600494.

37. Coppedè, N. *et al.* Human stress monitoring through an organic cotton-fiber biosensor. *J. Mater. Chem. B* (2014) doi:10.1039/c4tb00317a.

38. Keene, S. T. *et al.* Wearable Organic Electrochemical Transistor Patch for Multiplexed Sensing of Calcium and Ammonium Ions from Human Perspiration. *Adv. Healthc. Mater.* (2019) doi:10.1002/adhm.201901321.

39. Coppedè, N. *et al.* An in vivo biosensing, biomimetic electrochemical transistor with applications in plant science and precision farming. *Sci. Rep.* (2017) doi:10.1038/s41598-017-16217-4.

40. Friedlein, J. T., McLeod, R. R. & Rivnay, J. Device physics of organic electrochemical transistors. *Organic Electronics* (2018) doi:10.1016/j.orgel.2018.09.010.

41. Bernards, D. A. & Malliaras, G. G. Steady-state and transient behavior of organic electrochemical transistors. *Adv. Funct. Mater.* (2007) doi:10.1002/adfm.200601239.

42. Gentile, F. *et al.* A mathematical model of OECTs with variable internal geometry. *Sensors Actuators, A Phys.* (2020) doi:10.1016/j.sna.2020.111894.

43. Evangelou, E., Tsadilas, C., Tserlikakis, N., Tsitouras, A. & Kyritsis, A. Water footprint of industrial tomato cultivations in the pinios river basin: Soil properties interactions. *Water (Switzerland)* (2016) doi:10.3390/w8110515.

44. Walter, A., Finger, R., Huber, R. & Buchmann, N. Smart farming is key to developing sustainable agriculture. *Proc. Natl. Acad. Sci. U. S. A.* **114**, 6148–6150 (2017).

45. Johnsson, A. Oscillations in plant transpiration. in *Rhythms in Plants: Dynamic Responses in a Dynamic Environment* (2015). doi:10.1007/978-3-319-20517-5_7.

46. Taíz, E. & Zeiger, L. Plant Physiology 5th ed. *SInauer Assoc. Inc.* (2010).

47. Chen, H. & Jiang, J. G. Osmotic adjustment and plant adaptation to environmental changes related to drought and salinity. *Environmental Reviews* (2010) doi:10.1139/A10-014.

48. Study Solutions. Cohesion tension theory. *Study Solutions* https://istudy.pk/cohesion-tension-theory/ (2020).

49. Xiong, L., Schumaker, K. S. & Zhu, J. K. Cell signaling during cold, drought, and salt stress. *Plant Cell* (2002) doi:10.1105/tpc.000596.

50. Tarabella, G. *et al.* A single cotton fiber organic electrochemical transistor for liquid electrolyte saline sensing. *J. Mater. Chem.* (2012) doi:10.1039/c2jm34898e.

51. Mattana, G. *et al.* Organic electronics on natural cotton fibres. *Org. Electron.* (2011) doi:10.1016/j.orgel.2011.09.001.

52. Kim, S. M. *et al.* Influence of PEDOT:PSS crystallinity and composition on electrochemical transistor performance and long-term stability. *Nat. Commun.* (2018) doi:10.1038/s41467-018-06084-6.

53. Ouyang, J. *et al.* On the mechanism of conductivity enhancement in poly(3,4-ethylenedioxythiophene):poly(styrene sulfonate) film through solvent treatment. *Polymer (Guildf).* **45**, 8443–8450 (2004).

54. Crispin, X. *et al.* Conductivity, morphology, interfacial chemistry, and stability of poly(3,4-ethylene dioxythiophene)-poly(styrene sulfonate): A photoelectron spectroscopy study. *J. Polym. Sci. Part B Polym. Phys.* (2003) doi:10.1002/polb.10659.

55. Barrs, H. & Weatherley, P. A RE-EXAMINATION OF THE RELATIVE TURGIDITY TECHNIQUE FOR ESTIMATING WATER DEFICITS IN LEAVES By H. D. BARRs* and P. E. WEATHERLEyt. *Aust.J.Biol.Sci* (1962).

56. Vurro, F. *et al.* Development of an in vivo sensor to monitor the effects of vapour pressure deficit (VPD) changes to improve water productivity in agriculture. *Sensors (Switzerland)* (2019) doi:10.3390/s19214667.

57. Coppedè, N., Villani, M. & Gentile, F. Diffusion driven selectivity in organic electrochemical transistors. *Sci. Rep.* (2014) doi:10.1038/srep04297.

58. Riccardo Manfredi, Filippo Vurro, Michela Janni, Andrea Zappettini, N. C. Study of the stability of textile bioelectronic sensor in smart devices. in *NANO-DAY IV-Book of Abstract* 151 (Univeristà di Parma; Consorzio Interuniversitario Nazionale per le Scienze Ambientali, 2019).

59. Janni, M. *et al.* In Vivo Phenotyping for the Early Detection of Drought Stress in Tomato . *Plant Phenomics* (2019) doi:10.34133/2019/6168209.

60. Petrozza, A. *et al.* Physiological responses to Megafol® treatments in tomato plants under

drought stress: A phenomic and molecular approach. *Sci. Hortic. (Amsterdam).* (2014) doi:10.1016/j.scienta.2014.05.023.

61. Eberius, M. & Lima-Guerra, J. High-throughput plant phenotyping-Data acquisition, transformation, and analysis. in *Bioinformatics: Tools and Applications* (2007). doi:10.1007/978-0-387-92738-1_13.

62. Honsdorf, N., March, T. J., Berger, B., Tester, M. & Pillen, K. High-throughput phenotyping to detect drought tolerance QTL in wild barley introgression lines. *PLoS One* (2014) doi:10.1371/journal.pone.0097047.

63. Casadesús, J. *et al.* Using vegetation indices derived from conventional digital cameras as selection criteria for wheat breeding in water-limited environments. *Ann. Appl. Biol.* (2007) doi:10.1111/j.1744-7348.2007.00116.x.

64. De Assis Gomes, M. D. M., Magalhães Andrade Lagôa, A. M., Medina, C. L., Machado, E. C. & Machado, M. A. Interactions between leaf water potential, stomatal conductance and abscisic acid content of orange trees submitted to drought stress. *Brazilian J. Plant Physiol.* (2004) doi:10.1590/s1677-04202004000300005.

65. Sun, W. H. *et al.* Different mechanisms of photosynthetic response to drought stress in tomato and violet orychophragmus. *Photosynthetica* (2016) doi:10.1007/s11099-015-0177-3.

66. Danzi, D. *et al.* Can high throughput phenotyping help food security in the mediterranean area? *Front. Plant Sci.* (2019) doi:10.3389/fpls.2019.00015.

67. Comai, L. & Henikoff, S. TILLING: Practical single-nucleotide mutation discovery. *Plant Journal* (2006) doi:10.1111/j.1365-313X.2006.02670.x.

68. Wang, T. L., Uauy, C., Robson, F. & Till, B. TILLING in extremis. *Plant Biotechnology Journal* (2012) doi:10.1111/j.1467-7652.2012.00708.x.

69. Minoia, S. *et al.* A new mutant genetic resource for tomato crop improvement by TILLING technology. *BMC Res. Notes* (2010) doi:10.1186/1756-0500-3-69.

70. Dalmais, M. *et al.* UTILLdb, a Pisum sativum in silico forward and reverse genetics tool. *Genome Biol.* (2008) doi:10.1186/gb-2008-9-2-r43.

71. Kassambara, A. & Mundt, F. Extract and visualize the results of multivariate data analyses. *R Packag. version* (2016).

72. D'Ambrosio, C., Stigliani, A. L. & Giorio, G. Overexpression of CrtR-b2 (carotene beta hydroxylase 2) from S. lycopersicum L. differentially affects xanthophyll synthesis and accumulation in transgenic tomato plants. *Transgenic Res.* (2011) doi:10.1007/s11248-010-9387-4.

73. Kim, J., Kim, K. S., Kim, Y. & Chung, Y. S. A short review: Comparisons of high-throughput phenotyping methods for detecting drought tolerance. *Scientia Agricola* (2020) doi:10.1590/1678-992x-2019-0300.

74. Kim, S. L. *et al.* High-throughput phenotyping platform for analyzing drought tolerance in rice. *Planta* (2020) doi:10.1007/s00425-020-03436-9.

75. Ashraf, M. & Foolad, M. R. Roles of glycine betaine and proline in improving plant abiotic stress resistance. *Environ. Exp. Bot.* (2007) doi:10.1016/j.envexpbot.2005.12.006.

76. Kurepin, L. V. *et al.* Stress-related hormones and glycinebetaine interplay in protection of photosynthesis under abiotic stress conditions. *Photosynthesis Research* (2015) doi:10.1007/s11120-015-0125-x.

77. Mäkelä, P., Kontturi, M., Pehu, E. & Somersalo, S. Photosynthetic response of drought- and salt-stressed tomato and turnip rape plants to foliar-applied glycinebetaine. *Physiol. Plant.* (1999) doi:10.1034/j.1399-3054.1999.105108.x.

78. Rezaei, M. A., Jokar, I., Ghorbanli, M., Kaviani, B. & Kharabian-masouleh, A. Morpho-physiological improving effects of exogenous glycine betaine on tomato (Lycopersicum esculentum Mill .) cv . PS under drought stress conditions. *Plant Omi. J.* (2012).

79. Annunziata, M. G., Ciarmiello, L. F., Woodrow, P., Dell'aversana, E. & Carillo, P. Spatial and temporal profile of glycine betaine accumulation in plants under abiotic stresses. *Frontiers in Plant Science* (2019) doi:10.3389/fpls.2019.00230.

80. Chaves, M. M., Flexas, J. & Pinheiro, C. Photosynthesis under drought and salt stress: Regulation mechanisms from whole plant to cell. *Annals of Botany* (2009) doi:10.1093/aob/mcn125.

81. Berger, B., Parent, B. & Tester, M. High-throughput shoot imaging to study drought responses. *Journal of Experimental Botany* (2010) doi:10.1093/jxb/erq201.

82. Tripodi, P., Massa, D., Venezia, A. & Cardi, T. Sensing Technologies for Precision Phenotyping in Vegetable Crops: Current Status and Future Challenges. *Agronomy* (2018)

doi:10.3390/agronomy8040057.

83. Kefauver, S. C. *et al.* Comparative UAV and field phenotyping to assess yield and nitrogen use efficiency in hybrid and conventional barley. *Front. Plant Sci.* (2017) doi:10.3389/fpls.2017.01733.

84. Jackson, M. B., Davies, W. J. & Else, M. A. Pressure-flow relationships, xylem solutes and root hydraulic conductance in flooded tomato plants. *Ann. Bot.* (1996) doi:10.1006/anbo.1996.0003.

85. Hu, Y., Burucs, Z., von Tucher, S. & Schmidhalter, U. Short-term effects of drought and salinity on mineral nutrient distribution along growing leaves of maize seedlings. *Environ. Exp. Bot.* (2007) doi:10.1016/j.envexpbot.2006.11.003.

86. Rodrigues, J., Inzé, D., Nelissen, H. & Saibo, N. J. M. Source–Sink Regulation in Crops under Water Deficit. *Trends in Plant Science* (2019) doi:10.1016/j.tplants.2019.04.005.

87. da Silva, E., Nogueira, R., da Silva, M. & de Albuquerque, M. Drought stress and plant nutrition. *Plant Stress* (2011).

88. Bahrun, A., Jensen, C. R., Asch, F. & Mogensen, V. O. Drought-induced changes in xylem pH, ionic composition, and ABA concentration act as early signals in field-grown maize (Zea mays L.). *J. Exp. Bot.* (2002) doi:10.1093/jexbot/53.367.251.

89. Bista, D. R., Heckathorn, S. A., Jayawardena, D. M., Mishra, S. & Boldt, J. K. Effects of drought on nutrient uptake and the levels of nutrient-uptake proteins in roots of drought-sensitive and -tolerant grasses. *Plants* (2018) doi:10.3390/plants7020028.

90. Hu, Y. & Schmidhalter, U. Drought and salinity: A comparison of their effects on mineral nutrition of plants. *Journal of Plant Nutrition and Soil Science* (2005) doi:10.1002/jpln.200420516.

91. Farooq, M., Wahid, A., Kobayashi, N., Fujita, D. & Basra, S. M. A. Plant drought stress: Effects, mechanisms and management. *Agronomy for Sustainable Development* (2009) doi:10.1051/agro:2008021.

92. Jangid, K. K. & Dwivedi, P. Physiological Responses of Drought stress in Tomato: A Review. *Int. J. Agric. Environ. Biotechnol.* (2016) doi:10.5958/2230-732x.2016.00009.7.

93. Cattivelli, L. *et al.* Drought tolerance improvement in crop plants: An integrated view from breeding to genomics. *Field Crops Research* (2008) doi:10.1016/j.fcr.2007.07.004.

94. Dambrine, E. *et al.* Xylem sap composition: A tool for investigating mineral uptake and cycling in adult spruce. *Plant Soil* (1995) doi:10.1007/BF00029333.

95. Escalona, J., Flexas, J. & Medrano, H. Drought effects on water flow, photosynthesis and growth of potted grapevines. *Vitis* (2002).

96. Easlon, H. M. & Richards, J. H. Drought response in self-compatible species of tomato (Solanaceae). *Am. J. Bot.* (2009) doi:10.3732/ajb.0800189.

97. Mills, T. M., Li, J. & Behboudian, M. H. Physiological responses of gold kiwifruit (Actinidia chinensis) to reduced irrigation. *J. Am. Soc. Hortic. Sci.* (2009) doi:10.21273/jashs.134.6.677.

98. Mahouachi, J., Argamasilla, R. & Gómez-Cadenas, A. Influence of Exogenous Glycine Betaine and Abscisic Acid on Papaya in Responses to Water-deficit Stress. *J. Plant Growth Regul.* (2012) doi:10.1007/s00344-011-9214-z.

99. Massmann, A., Gentine, P. & Lin, C. When does vapor pressure deficit drive or reduce evapotranspiration? *arXiv* (2018) doi:10.5194/hess-2018-553.

100. Abou Hadid, A. F. *Good Agricultural Practices for Greenhouse Vegetable Crops: Principles for Mediterranean Climate Areas*. *Fao* (2013).

101. Pesce, M. *et al.* Research for AGRI Committee - Impacts of the digital economy on the food chain and the CAP. *Eur. Parliam. Policy Dep. Struct. Cohes. Policies,* (2019).

102. Jalilvand, E., Tajrishy, M., Ghazi Zadeh Hashemi, S. A. & Brocca, L. Quantification of irrigation water using remote sensing of soil moisture in a semi-arid region. *Remote Sens. Environ.* (2019) doi:10.1016/j.rse.2019.111226.

103. Fricke, W. Water transport and energy. *Plant Cell and Environment* (2017) doi:10.1111/pce.12848.

104. Roderick, M. L., Greve, P. & Farquhar, G. D. On the assessment of aridity with changes in atmospheric CO2. *Water Resour. Res.* (2015) doi:10.1002/2015WR017031.

105. Wang, P., Li, D., Liao, W., Rigden, A. & Wang, W. Contrasting Evaporative Responses of Ecosystems to Heatwaves Traced to the Opposing Roles of Vapor Pressure Deficit and Surface Resistance. *Water Resour. Res.* (2019) doi:10.1029/2019WR024771.

106. Medina, S. *et al.* The plant-transpiration response to vapor pressure deficit (VPD) in durum wheat is associated with differential yield performance and specific expression of genes

involved in primary metabolism and water transport. *Front. Plant Sci.* (2019) doi:10.3389/fpls.2018.01994.

107. Devi, M. J. & Reddy, V. R. Transpiration response of cotton to vapor pressure deficit and its relationship with stomatal traits. *Front. Plant Sci.* (2018) doi:10.3389/fpls.2018.01572.

108. Devi, M. J., Sinclair, T. R., Jain, M. & Gallo, M. Leaf aquaporin transcript abundance in peanut genotypes diverging in expression of the limited-transpiration trait when subjected to differing vapor pressure deficits and aquaporin inhibitors. *Physiol. Plant.* (2016) doi:10.1111/ppl.12378.

109. Shamshiri, R. R. *et al.* Review of optimum temperature, humidity, and vapour pressure deficit for microclimate evaluation and control in greenhouse cultivation of tomato: A review. *International Agrophysics* (2018) doi:10.1515/intag-2017-0005.

110. Ramos-Fernández, J. C. *et al.* Fuzzy Modeling Vapor Pressure Deficit to Monitoring Microclimate in Greenhouses. *IFAC-PapersOnLine* (2016) doi:10.1016/j.ifacol.2016.10.068.

111. Zhang, D. *et al.* Vapour pressure deficit control in relation to water transport and water productivity in greenhouse tomato production during summer. *Sci. Rep.* (2017) doi:10.1038/srep43461.

112. Millan-Almaraz, J. R. *et al.* FPGA-based fused smart sensor for real-time plant-transpiration dynamic estimation. *Sensors* (2010) doi:10.3390/s100908316.

113. Murray, F. W. On the Computation of Saturation Vapor Pressure. *J. Appl. Meteorol.* (1967) doi:10.1175/1520-0450(1967)006<0203:otcosv>2.0.co;2.

114. Monteith, J. & Unsworth, M. *Principles of Environmental Physics: Plants, Animals, and the Atmosphere: Fourth Edition*. *Principles of Environmental Physics: Plants, Animals, and the Atmosphere: Fourth Edition* (2013). doi:10.1016/C2010-0-66393-0.

115. Finkelstein, R. Abscisic Acid Synthesis and Response. *Arab. B.* (2013) doi:10.1199/tab.0166.

116. Ishikawa, T., Cuin, T. A., Bazihizina, N. & Shabala, S. Xylem Ion Loading and Its Implications for Plant Abiotic Stress Tolerance. in *Advances in Botanical Research* (2018). doi:10.1016/bs.abr.2018.09.006.

117. Merilo, E. *et al.* Stomatal VPD response: There is more to the story than ABA. *Plant Physiol.* (2018) doi:10.1104/pp.17.00912.

118. Kumar, N., Pandey, S., Bhattacharya, A. & Ahuja, P. S. Do leaf surface characteristics affect

Agrobacterium infection in tea [Camellia sinensis (L.) O Kuntze]? *J. Biosci.* (2004) doi:10.1007/BF02702613.

119. Wang, H., Shi, H. & Wang, Y. The Wetting of Leaf Surfaces and Its Ecological Significances. in *Wetting and Wettability* (2015). doi:10.5772/61205.

120. Rouse, J. W., Haas, R. H., Schell, J. A. & Deering, D. W. Monitoring the vernal advancement and retrogradation (green wave effect) of natural vegetation. *Prog. Rep. RSC 1978-1* (1973).

121. Xue, J. & Su, B. Significant remote sensing vegetation indices: A review of developments and applications. *Journal of Sensors* (2017) doi:10.1155/2017/1353691.

122. Zarco-Tejada, P. J., González-Dugo, V. & Berni, J. A. J. Fluorescence, temperature and narrow-band indices acquired from a UAV platform for water stress detection using a micro-hyperspectral imager and a thermal camera. *Remote Sens. Environ.* (2012) doi:10.1016/j.rse.2011.10.007.

123. Mundim, F. M. & Pringle, E. G. Whole-plant metabolic allocation under water stress. *Front. Plant Sci.* (2018) doi:10.3389/fpls.2018.00852.

124. Johnston, R. B. Arsenic and the 2030 Agenda for sustainable development. *Arsen. Res. Glob. Sustain. - Proc. 6th Int. Congr. Arsen. Environ. AS 2016* 12–14 (2016) doi:10.1201/b20466-7.

125. Holzapfel, E. A., Merino, R., Mariño, M. A. & Matta, R. Water production functions in kiwi. *Irrig. Sci.* (2000) doi:10.1007/s002710050003.

126. Döll, P. Impact of climate change and variability on irrigation requirements: A global perspective. *Clim. Change* (2002) doi:10.1023/A:1016124032231.

127. Torres-Ruiz, J. M. *et al.* Time of irrigation affects vine water relations and the daily patterns of leaf gas exchanges and vascular flows to kiwifruit (Actinidia deliciosa Chev.). *Agric. Water Manag.* (2016) doi:10.1016/j.agwat.2015.12.012.

128. Rana, G., Rinaldi, M., Introna, M., Ciciretti, L. Determinazione sperimentale dei consumi idrici del pomodoro da industria in Capitanata. in *Atti Convegno POM B19* (ed. Ed. Gutenberg) 99–106 (2000).

129. Hannah Ritchie, M. R. Environmental impacts of food production. (2020).

130. Fao. Fao soils portal. http://www.fao.org/soils-portal/en/ (2018).

131. Hanin, M., Ebel, C., Ngom, M., Laplaze, L. & Masmoudi, K. New insights on plant salt

tolerance mechanisms and their potential use for breeding. *Frontiers in Plant Science* (2016) doi:10.3389/fpls.2016.01787.

132. FAO. *Handbook for saline soil management*. *Published by the Food and Agriculture Organization of the United Nations and Lomonosov Moscow State University* (2018).

133. Munns, R. & Tester, M. Mechanisms of salinity tolerance. *Annual Review of Plant Biology* (2008) doi:10.1146/annurev.arplant.59.032607.092911.

134. Munns, R., Passioura, J. B., Colmer, T. D. & Byrt, C. S. Osmotic adjustment and energy limitations to plant growth in saline soil. *New Phytol.* (2020) doi:10.1111/nph.15862.

135. Negrão, S., Schmöckel, S. M. & Tester, M. Evaluating physiological responses of plants to salinity stress. *Ann. Bot.* (2017) doi:10.1093/aob/mcw191.

136. Yang, Y. & Guo, Y. Elucidating the molecular mechanisms mediating plant salt-stress responses. *New Phytologist* (2018) doi:10.1111/nph.14920.

137. Hairmansis, A., Berger, B., Tester, M. & Roy, S. J. Image-based phenotyping for non-destructive screening of different salinity tolerance traits in rice. *Rice* (2014) doi:10.1186/s12284-014-0016-3.

138. Nackley, L. L. & Kim, S. H. A salt on the bioenergy and biological invasions debate: Salinity tolerance of the invasive biomass feedstock Arundo donax. *GCB Bioenergy* (2015) doi:10.1111/gcbb.12184.

139. Romero-Aranda, R., Soria, T. & Cuartero, J. Tomato plant-water uptake and plant-water relationships under saline growth conditions. *Plant Sci.* (2001) doi:10.1016/S0168-9452(00)00388-5.

140. Munns, R. *et al.* Energy costs of salt tolerance in crop plants. *New Phytologist* (2020) doi:10.1111/nph.15864.

141. Zhou, R. *et al.* Drought stress had a predominant effect over heat stress on three tomato cultivars subjected to combined stress. *BMC Plant Biol.* (2017) doi:10.1186/s12870-017-0974-x.

142. Cocozza, C. *et al.* The excess of phosphorus in soil reduces physiological performances over time but enhances prompt recovery of salt-stressed Arundo donax plants. *Plant Physiol. Biochem.* (2020) doi:10.1016/j.plaphy.2020.04.011.

143. Berger, B., De Regt, B. & Tester, M. Trait dissection of salinity tolerance with plant phenomics. *Methods Mol. Biol.* (2012) doi:10.1007/978-1-61779-986-0_27.

144. Costa, C., Schurr, U., Loreto, F., Menesatti, P. & Carpentier, S. Plant phenotyping research trends, a science mapping approach. *Frontiers in Plant Science* (2019) doi:10.3389/fpls.2018.01933.

145. Fahlgren, N., Gehan, M. A. & Baxter, I. Lights, camera, action: High-throughput plant phenotyping is ready for a close-up. *Current Opinion in Plant Biology* (2015) doi:10.1016/j.pbi.2015.02.006.

146. Pieruschka, R. & Schurr, U. Plant Phenotyping: Past, Present, and Future. *Plant Phenomics* (2019) doi:10.34133/2019/7507131.

147. Cocozza, C. *et al.* Impact of high or low levels of phosphorus and high sodium in soils on productivity and stress tolerance of Arundo donax plants. *Plant Sci.* (2019) doi:10.1016/j.plantsci.2019.110260.

148. Roberto Pilu. Giant reed (Arundo donax L.): A weed plant or a promising energy crop? *African J. Biotechnol.* **11**, 9163–9174 (2012).

149. Brotchie, A. Plant physiology: Organic electronics take root. *Nature Reviews Materials* (2017) doi:10.1038/natrevmats.2017.32.

150. Poxson, D. J. *et al.* Regulating plant physiology with organic electronics. *Proc. Natl. Acad. Sci. U. S. A.* (2017) doi:10.1073/pnas.1617758114.

151. Zhao, C. *et al.* Crop phenomics: Current status and perspectives. *Frontiers in Plant Science* (2019) doi:10.3389/fpls.2019.00714.

152. Li, L., Zhang, Q. & Huang, D. A review of imaging techniques for plant phenotyping. *Sensors (Switzerland)* (2014) doi:10.3390/s141120078.

153. Atkinson, J. A., Jackson, R. J., Bentley, A. R., Ober, E. & Wells, D. M. Field Phenotyping for the Future. *Annu. Plant Rev. online* **1**, 719–736 (2018).

154. Barbagallo, R. P., Oxborough, K., Pallett, K. E. & Baker, N. R. Rapid, noninvasive screening for perturbations of metabolism and plant growth using chlorophyll fluorescence imaging. *Plant Physiol.* (2003) doi:10.1104/pp.102.018093.

155. Rosenqvist, E., Großkinsky, D. K., Ottosen, C. O. & van de Zedde, R. The phenotyping

dilemma—the challenges of a diversified phenotyping community. *Frontiers in Plant Science* (2019) doi:10.3389/fpls.2019.00163.

156. Lowe, A., Harrison, N. & French, A. P. Hyperspectral image analysis techniques for the detection and classification of the early onset of plant disease and stress. *Plant Methods* (2017) doi:10.1186/s13007-017-0233-z.

157. Still, C. *et al.* Thermal imaging in plant and ecosystem ecology: applications and challenges. *Ecosphere* (2019) doi:10.1002/ecs2.2768.

158. Tran, D. *et al.* Electrophysiological assessment of plant status outside a Faraday cage using supervised machine learning. *Sci. Rep.* (2019) doi:10.1038/s41598-019-53675-4.

159. Herdel, K., Schmidt, P., Feil, R., Mohr, A. & Schurr, U. Dynamics of concentrations and nutrient fluxes in the xylem of Ricinus communis - Diurnal course, impact of nutrient availability and nutrient uptake. *Plant, Cell Environ.* (2001) doi:10.1046/j.1365-3040.2001.00655.x.

160. Mengel, K. & Kirkby, E. A. *Principles of plant nutrition.International Potash Institute, Bern, Switzerland*. *International Potash Institute, Bern, Switzerland* (1987).

161. Wilkinson, S. & Davies, W. J. Manipulation of the apoplastic pH of intact plants mimics stomatal and growth responses to water availability and microclimatic variation. *J. Exp. Bot.* (2008) doi:10.1093/jxb/erm338.

162. Seiler, C. *et al.* Abscisic acid flux alterations result in differential abscisic acid signaling responses and impact assimilation efficiency in barley under terminal drought stress. *Plant Physiol.* (2014) doi:10.1104/pp.113.229062.

163. Assaha, D. V. M., Ueda, A., Saneoka, H., Al-Yahyai, R. & Yaish, M. W. The role of Na+ and K+ transporters in salt stress adaptation in glycophytes. *Frontiers in Physiology* (2017) doi:10.3389/fphys.2017.00509.